Unclassified
SECURITY CLASSIFICATION OF THIS PAGE

DTIC ELECTE JUN 0 1989 S B D

AD-A208 268

Approved
OMB No. 0704-0188

REPORT DOCUMENTATION

1a. REPORT SECURITY CLASSIFICATION: Unclassified	1b. RESTRICTIVE MARKINGS
2a. SECURITY CLASSIFICATION AUTHORITY	3. DISTRIBUTION/AVAILABILITY OF REPORT: Approved for public release; distribution is unlimited.
2b. DECLASSIFICATION/DOWNGRADING SCHEDULE	
4. PERFORMING ORGANIZATION REPORT NUMBER(S): Astron Final Report Number 7151-001	5. MONITORING ORGANIZATION REPORT NUMBER(S): AFOSR-TR- 89-0659
6a. NAME OF PERFORMING ORGANIZATION: Astron Research and Engineering	6b. OFFICE SYMBOL (If applicable):
6c. ADDRESS (City, State, and ZIP Code): Sunnyvale California 94086	7a. NAME OF MONITORING ORGANIZATION: AFOSR/NA
	7b. ADDRESS (City, State, and ZIP Code): Building 410, Bolling AFB DC 20332-6448
8a. NAME OF FUNDING/SPONSORING ORGANIZATION: AFOSR/NA	8b. OFFICE SYMBOL (If applicable): NA
	9. PROCUREMENT INSTRUMENT IDENTIFICATION NUMBER: F49620-88-C-0130
8c. ADDRESS (City, State, and ZIP Code): Building 410, Bolling AFB DC 20332-6448	10. SOURCE OF FUNDING NUMBERS: PROGRAM ELEMENT NO. 65502F; PROJECT NO. 3005; TASK NO. A1; WORK UNIT ACCESSION NO.

11. TITLE (Include Security Classification)

(U) Demonstration of Oblique Detonation Wave for Hypersonic Propulsion

12. PERSONAL AUTHOR(S)
Takashi Nakamura, Michael J Schuh, Donald S Randall, Thomas J Dahm, David T Pratt

13a. TYPE OF REPORT	13b. TIME COVERED	14. DATE OF REPORT (Year, Month, Day)	15. PAGE COUNT
Final Technical	FROM 8/1/88 TO 1/31/89	1989, March, 30	115

16. SUPPLEMENTARY NOTATION

17. COSATI CODES			18. SUBJECT TERMS (Continue on reverse if necessary and identify by block number)
FIELD	GROUP	SUB-GROUP	oblique detonation wave, detonation, hypersonic propulsion, hypervelocity launcher, ram accelerator

19. ABSTRACT (Continue on reverse if necessary and identify by block number)

The Oblique Detonation Wave Engine (ODWE) offers a number of advantages over the Supersonic Combustor Ramjet (SCRAMJET) for hypersonic aeropropulsion. The objective of this program is to obtain data on the stability of the Oblique Detonation Wave (ODW) and to assess the applicability of the ODW to hypersonic propulsion. The program consists of the basic study of the ODW phenomenon and the design study of the test facility (Phase I), and an indepth experimental study of the ODW in a ram cannon-type combustion tube with a hypervelocity projectile launched into the tube by a two-stage light-gas gun (Phase II). This Phase I report summarizes the results pertaining to the stability of the ODW and the experimental facility designs. It is concluded that the ODW will be initiated and sustained in the test facility configuration and that the tests will generate data concerning key issues for the application of the ODW to hypersonic propulsion.

20 DISTRIBUTION/AVAILABILITY OF ABSTRACT	21. ABSTRACT SECURITY CLASSIFICATION
☒ UNCLASSIFIED/UNLIMITED ☒ SAME AS RPT ☒ DTIC USERS	Unclassified
22a. NAME OF RESPONSIBLE INDIVIDUAL: Julian M Tishkoff	22b. TELEPHONE (Include Area Code): (202) 767-[illegible] 22c. OFFICE SYMBOL: AFOSR/NA

DD Form 1473, JUN 86 Previous editions are obsolete. SECURITY CLASSIFICATION OF THIS PAGE

89 6 01 042 Unclassified

Preface

This is the final report for the SBIR Phase I contract F49620-88-C-0130, "Demonstration of the Oblique Detonation Wave (ODW) for Hypersonic Propulsion," sponsored by the Air Force Office of Scientific Research (AFOSR). The program manager of AFOSR was Dr. Julian Tishkoff, Directorate of Aerospace Science. This work was performed during the period August 1988 to January 1989 by Astron Research and Engineering, Sunnyvale, CA. The personnel actively involved in this program were: Dr. Takashi Nakamura (Principal Investigator), Dr. Michael J. Schuh, Mr. Donald S. Randall, and Mr. Thomas J. Dahm. Professor David T. Pratt, University of Washington, conducted the computational fluid dynamic (CFD) work discussed in this report and supported the Astron team in conducting the basic analysis of the ODW.

An informal progress review of this program was held on 24 January 1989 at NASA Lewis Research Center (LeRC) in which T. Nakamura and D.T. Pratt gave briefings on the program's progress. Dr. Edward J. Mularz, Propulsion Directorate at NASA LeRC, hosted the meeting with Dr. Julian Tishkoff, who was visiting LeRC for this occasion. Dr. Erwin Lezberg, Dr. Peter Sockol, and other members of LeRC who are actively involved in hypersonic propulsion attended the meeting and provided us with valuable input in analytical and experimental aspects of the program.

We are indebted to members of the Combustion Research Facility, Sandia National Laboratory, for their participation in developing concepts for diagnostics and instrumentation. Our special thanks go to Dr. Robert W. Dibble, Dr. Robert J. Cattolica, Dr. William L. Flower, and Dr. Robert S. Barlow for much valuable discussion.

It is our great sorrow to have lost our colleague Mr. Thomas J. Dahm on 22 February 1989. Mr. Dahm, co-founder and Chairman of Astron, was the inventor of the Wave Gun and an active participant in this program. We miss his deep engineering insights and his amicable nature which have been an encouragement and an inspiration to all of us. Although we feel deep sadness and a great sense of loss, we are determined to move forward to undertake the tasks left to us.

Contents

SECTION 1 - INTRODUCTION

The Oblique Detonation Wave Engine (ODWE) has been proposed as an alternative to the Supersonic Combustion ramjet (scramjet) for propulsion of hypersonic aircraft [1.1,1.2]. For the ODWE, schematically described in Figure 1-1, the fuel is injected at a location where the air temperature is below the fuel ignition condition. The fuel/air mixture is heated as it goes through subsequent shocks until the last oblique shock ignites the mixture. Rapid chemical reactions behind the last shock wave form a standing Oblique Detonation Wave (ODW). The chemical energy is released rapidly into the flow and the expansion of the flow begins a short distance downstream of the detonation wave.

The advantages of the ODWE over the scramjet include the fact that the diffuser pressure and the temperature in the ODWE are much lower than those for the scramjet, and, therefore, the losses involved in flow deceleration are less than those for the scramjet. Also, as the release of the chemical energy in the ODWE is accomplished by a steady detonation wave instead of by diffusive burning, the engine area exposed to high-temperature, high-pressure combustion gas is much smaller for the ODWE than for the scramjet.

There has been a long-standing interest in harnessing detonation waves for propulsion of hypersonic aircraft [1.1, 1.2,1.3] and hypervelocity projectile launchers [1.4,1.5]. Approximate performance calculations show that normal (as opposed to oblique) detonations are unsuitable for propulsion, due to the difficulty of wave stabilization and the exceedingly high loss of total pressure. Standing oblique detonation waves appear to be satisfactory from a total pressure loss standpoint, but historical attempts to stabilize oblique detonation waves in combustion tunnels [1.6] were inconclusive, due in part to limited approach Mach numbers, but also due to a fundamental lack of understanding of detonation wave mechanics. Recent theoretical work [1.7, 1.8] has clarified the conditions under which standing oblique detonation waves can be stabilized with acceptable propulsive efficiency. Specifically, it is shown [1.7] that only overdriven weak oblique waves are suitable for propulsion, and that, for any given approach Mach number and reactant gas thermodynamic state, there are minimum and maximum flow deflection angles outside of which an ODW cannot be stabilized.

To date, there has been limited experimental work pertaining to the stability of the ODW for propulsion. Hertzberg et al. [1.5] have proposed the use of stabilized detonation waves, either normal or oblique, as one of many alternative combustion modes for a 'ram accelerator,' a device in which a shaped projectile is accelerated by combustion through a tube filled with a reactive mixture.

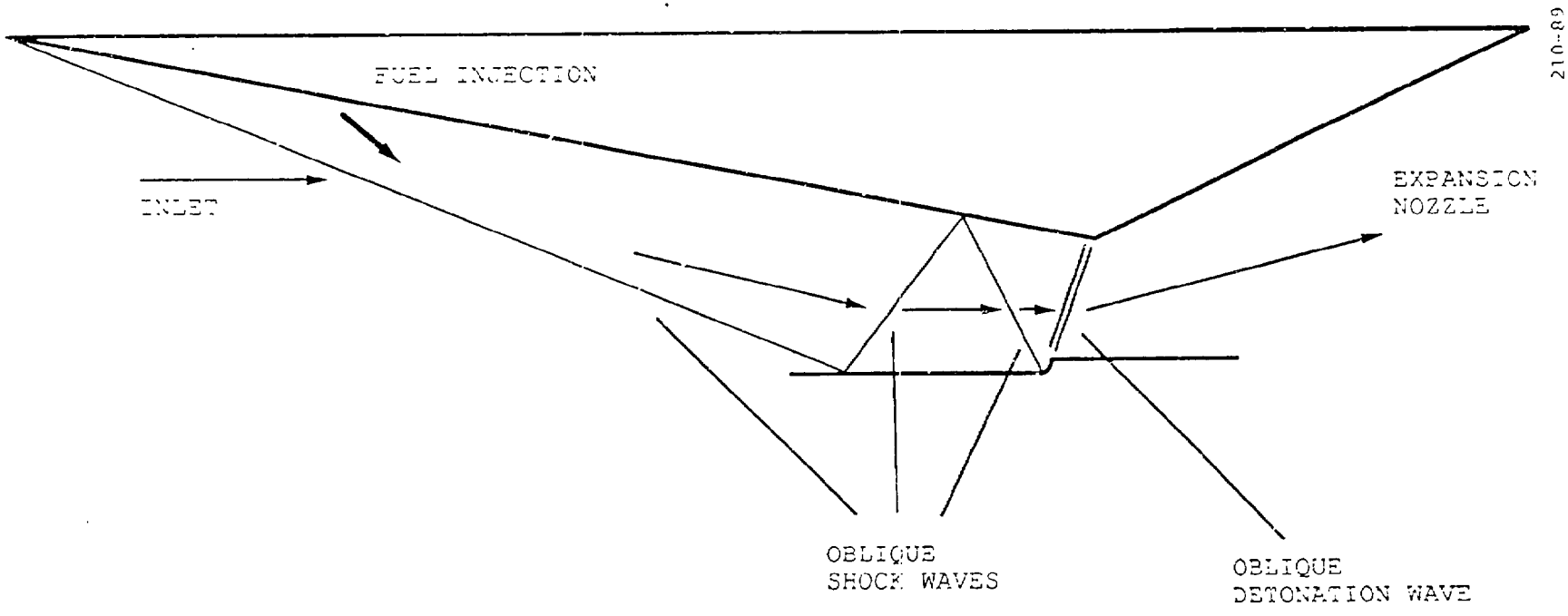

Figure 1-1 Schematic of Oblique Detonation Wave Engine (ODWE)

In a series of experiments using methane-oxygen mixtures, they have demonstrated the acceleration of projectiles (60 to 75 gram) from initial injection velocities in the range of 900 m/s to 1200 m/s to final velocities of 1500 m/s to 1900 m/s.

The propulsion mechanism of this acceleration, however, was thermally choked subsonic combustion and not stabilized detonation [1.9]. Recently, they were able to achieve acceleration of projectiles beyond this velocity range [1.10]. Since this velocity range is above the Chapman-Jouguet velocity, the propulsion mechanism is considered to be superdetonative, which involves oblique shock and associated combustion phenomena. In the case of their results it is not clear whether the combustion process is shock-induced combustion or the oblique detonation wave. Hertzberg and Bruckner stated that their test projectile forebody was a 10° half-angle cone [1.10] which, according to the analysis of Pratt et al. [1.7], is too small to stabilize an ODW. Consequently, it is most likely that their observed superdetonative acceleration was due to shock-induced combustion. Unfortunately, the diagnostic methods used in their experiment do not provide sufficient data to determine the shock structure and the combustion wave structure.

To gain better understanding of this important phenomena, Astron Research and Engineering proposed to conduct a theoretical and experimental study to investigate ODW phenomena and to assess the applicability of the ODW to hypersonic propulsion. To achieve these goals in a direct and unambiguous way, we proposed to conduct the experiment in a ram cannon configuration using the Wave Gun, a hypervelocity two-stage light-gas gun developed by Astron, to achieve the initial projectile velocity 2.5 km/s necessary to initiate the ODW.

Figure 1-2 shows a projectile launched by the Wave Gun being injected into the combustion tube. The tube is initially filled with premixed fuel, oxygen, and diluent. Compression of the reactant gases is accomplished by a single conical weak oblique shock. The reflected wave off the cylinder wall causes detonation to occur in the compressed reactant gas flowing through the annular area between the projectile body and the cylinder wall. Expansion from the annulus to the full tube area in the projectile wake occurs through an isentropic, supersonic nozzle defined by the projectile afterbody shape. The static pressure on the projectile afterbody is considerably greater than that on the conical forebody, so that net thrust is produced. In the proposed study, this acceleration is not the primary objective but, rather, a proof of the successful stabilization of the ODW.

Wave Gun is a concept conceived at Astron in 1981; it is a modification of two-stage light-gas gun technology utilizing a very light piston. Like a conventional, laboratory light-gas gun, the Wave Gun consists of a first-stage propellant (typically a cannon powder), a piston, and a compressed, low-molecular-weight

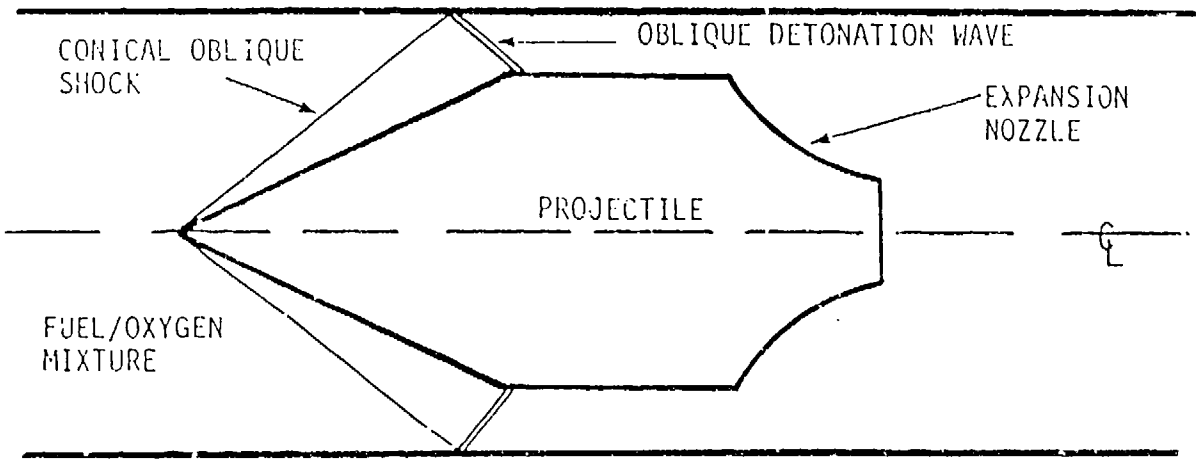

Figure 1-2 Schematic of a Hypervelocity Projectile Injected by the Wave Gun into a Combustion Tube Filled with Premixed Fuel, Oxygen and Diluent

gas. Unlike a more conventional design, however, the Wave Gun piston is as light as it can be and still serve as an effective separation between the propellant combustion products and the second-stage light gas. In Figure 1-3 a typical wave gun cycle is illustrated.

The Wave Gun was first demonstrated in a 20-mm bore gun in a privately funded program. Subsequently, under combined DARPA and ARDEC funding, a 30-mm bore gun was designed and built to demonstrate a range of operating conditions. In the course of this development program, projectiles with masses to 85 grams have been routinely accelerated to velocities in excess of 2.5 km/s, velocities suitable as injection velocities to an ODW diagnostic tube.

Schematic of the experimental facility for the proposed experiment is given in Figure 1-4. The first element of the system is a Wave Gun. The 30-mm gun constructed for the DARPA/ARDC program will be used as presently configured [1.11]. The muzzle of the Wave Gun will extend into a unit that will

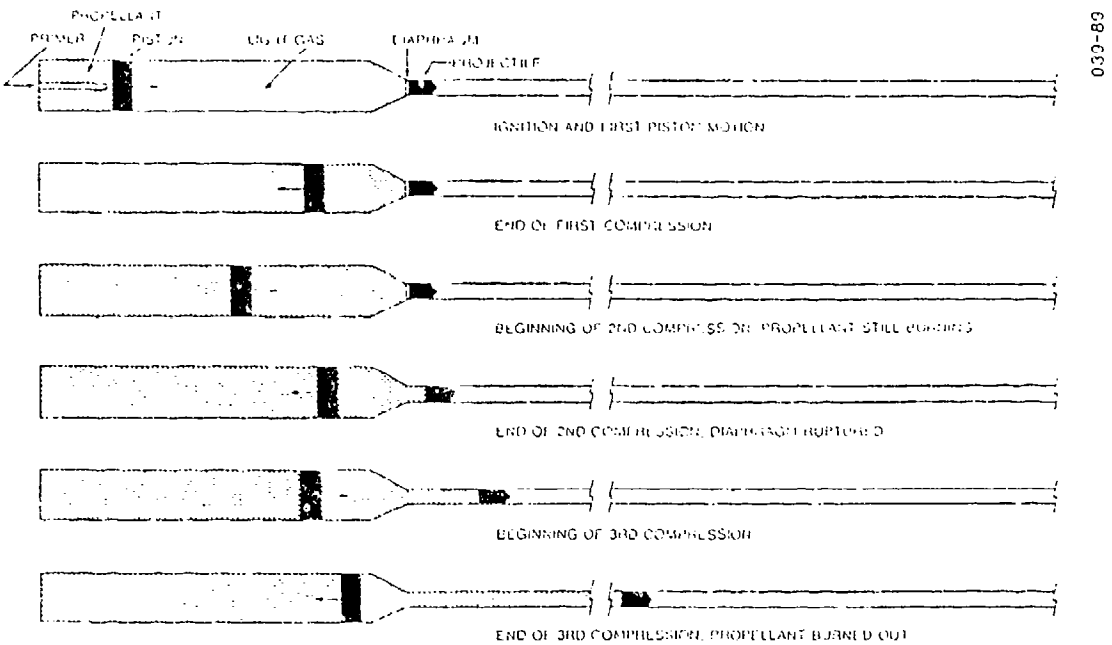

Figure 1-3 Typical Wave Gun Cycle

permit free Wave Gun recoil while anchoring the downstream hardware. Within this unit the projectile passes through a diaphragm separating the evacuated barrel from an atmospheric tube, which serves the dual functions of venting the driving gas and axially separating the projectile from its obturating sabot.

The projectile, stripped of its sabot, enters the ODW section through another diaphragm that separates the combustible test gas from the stripping gas. After passage of the projectile, the gases from this section will also exhaust through the stripping section into the dump tank. At the downstream end of the ODW section, yet another diaphragm will serve to isolate the reactive gas mixture. After passing through this barrier, the projectile will be decelerated by passing through a series of containers holding materials with increasing densities.

Diagnostics and instrumentation are the key elements of the proposed experimental program. The objective of the diagnostic effort is to determine the formation and stability of the oblique detonation waves by measuring the projectile velocity, shock structures, gas pressures and temperatures, and optical signature

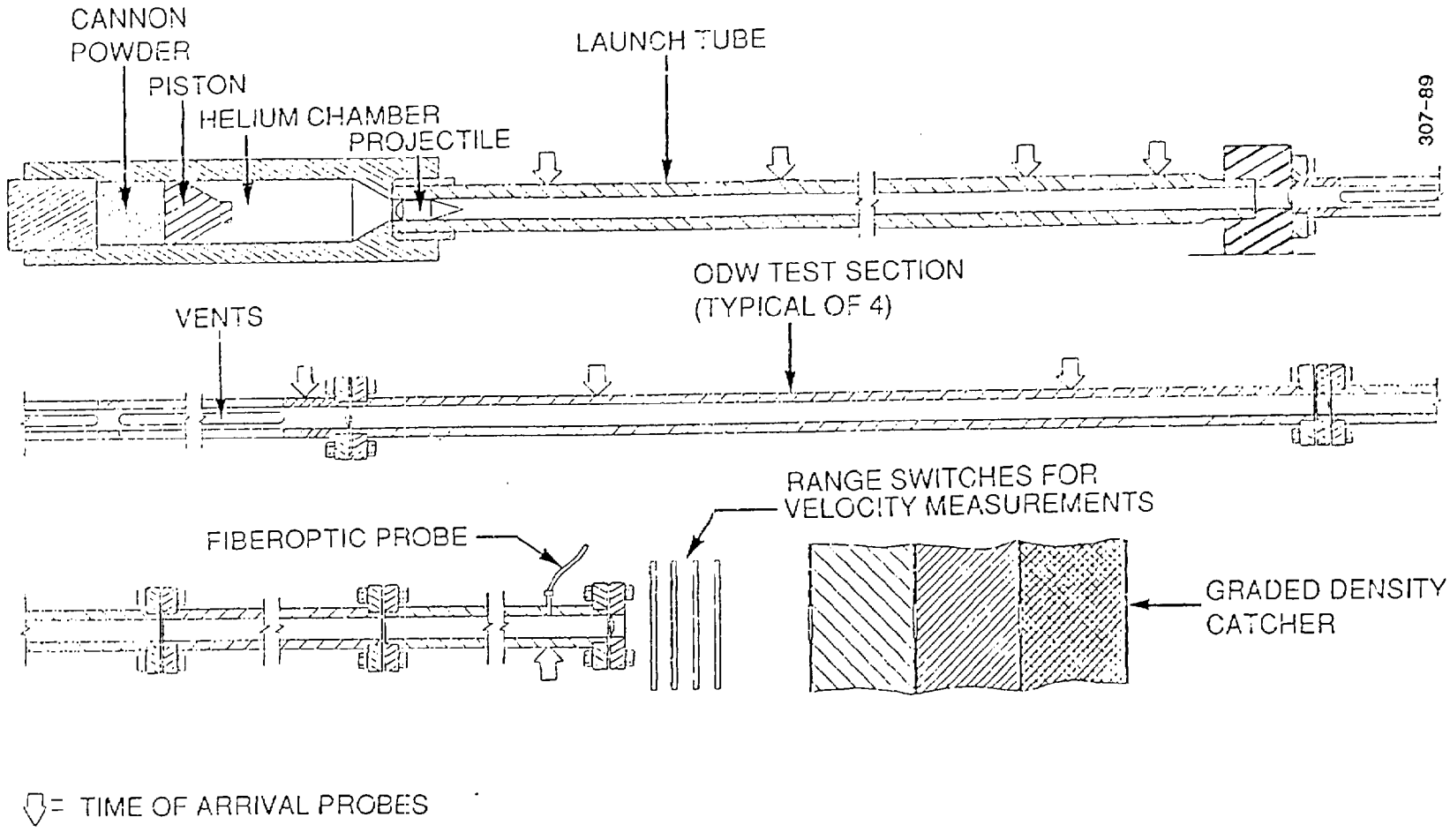

Figure 1-4 Schematic of ODW Test Apparatus

of chemical species created by reactions. The diagnostic methods to be employed for the proposed experiments include gas pressure measurements, spectrally resolved optical measurements, shock structure visualization and flash x-radiography.

This report summarizes the results of the Phase 1 effort conducted in the period of 6 months from August 1988 to January 1989. The purpose of the Phase 1 program was to conduct basic studies of the proposed concept to assess its feasibility. The objectives of the Phase 1 program were to:

1. Conduct thermodynamic/computational fluid dynamic analyses of the ODW for a hypervelocity projectile in a combustion tube.

2. Define optimum operating conditions for the proposed experiment.

3. Select and establish diagnostic methods and instrumentation.

4. Design and analyze key components.

5. Formulate experimental procedure.

6. Evaluate effectiveness of the proposed experiment.

This report consists of eight sections. In Section 2, results of the analyses of the hypervelocity projectile are given. This section includes the discussion of the ODW and analyses of the basic thermodynamic and fluid dynamic phenomena associated with the hypervelocity projectile in the combustion tube. A discussion of the design of hypervelocity projectiles, including stress analysis, heat load analysis, material selection, and fabrication method, is given in Section 3. CFD analyses of the ODW are presented in Section 4. This section includes discussion of the code used for the analyses of the flowfield around the hypervelocity projectile, the ODW, and the shock-induced combustion phenomena. In Section 5, a discussion of the test facility design, functions of each component, and design parameters is given. A summary of the work on the diagnostic methods and instrumentation is given in Section 6. Detailed discussions on each diagnostic method pertinent to the proposed experiment, including instrumentation and methods of implementation, are given in this section. The experimental procedure and test simulation are discussed in Section 7. The purpose of the discussion presented in this section is to simulate the actual experimental conditions so that we can have a realistic awareness of what is to be done in the proposed experiment. In the final section, Section 8, we summarize the results obtained in this study and present our assessment of the effectiveness of the proposed experiment.

References

[1.1] O'Brien, C.J., and Kobayashi, "Advanced Earth-to-Orbit Propulsion Concepts," AIAA/SAE/ASME/ASEE 23rd Joint Propulsion Conference, AIAA-86-1386, Huntsville, AL, June 1986.

[1.2] Ostrander, M.J., J.C. Hyde, M.F. Young, R.D. Kissinger, and D.T. Pratt, "Standing Oblique Detonation Wave Engine Performance," 23rd AIAA/ASME/SAE/ASEE Joint Propulsion Conference, San Diego, CA, 29 June - 2 July 1987.

[1.3] Adamson, T.C., and R.B. Morrison, "On The Classification of Normal Detonation Waves," Jet Propulsion, August 1955.

[1.4] Lehr, H.F., "Experiments on Shock-Induced Combustion," Astronautica Acta, Vol. 17, Nos. 4 and 5, 1972.

[1.5] Hertzberg, A., A.P. Bruckner, and D.W. Bogdanoff, "The Ram Accelerator: A New Chemical Method of Achieving Ultrahigh Velocities," 37th Meeting of the Aeroballistic Range Association, Quebec, Canada, 9-12 September 1986.

[1.6] Gross, R.A. and W. Chinitz, "A Study of Supersonic Combustion," J. of Aerospace Sciences, July 1960.

[1.7] Pratt, D.T., J.W. Humphrey, and D.L. Kors, "Morphology of a Standing Oblique Detonation Wave," 23rd AIAA/ASME/SAE/ASEE Joint Propulsion Conference, San Dieço, CA, 29 June - 2 July 1987.

[1.8] Pratt, D.T., and D.E. Glenn, "Numerical Simulation of a Standing Oblique Hydrogen-Air Detonation Wave," SIAM Conference on Numerical Combustion, San Francisco, CA, 9-11 March 1987.

[1.9] Bruckner, A.P., and A. Hertzberg, "Development of the Ram Accelerator Hypervelocity Launcher," 38th Meeting of the Aeroballistic Range Association, Tokyo, Japan, October 6-9, 1987.

[1.10] Bruckner, A., "Laboratory Scale Ram Accelerator Experiments" presented at 1988 Aerospace Engineering Conference and Show, Los Angeles, CA, 14-16 February 1989.

[1.11] Dahm, T.J., and D.S. Randall, "The Wave Gun Concept for a Hypervelocity Rapid-Fire Weapon," presented at the 1984 JANNAF Propulsion Meeting, New Orleans, LA, 8 February 1984.

SECTION 2 - ANALYSIS OF HYPERVELOCITY PROJECTILE TEST FLIGHT

In this section a description is given of the flowfield surrounding the projectile in the tube followed by a theoretical overview of the oblique detonation phenomena. Finally, results of parametric studies pertaining to projectile design, working fluid, boundary layer, and heat transfer are presented.

2.1 FLOWFIELD SURROUNDING THE PROJECTILE

As discussed in Section 1, the projectile will be launched into the combustion tube filled with a fuel and oxidizer mixture by the Wave Gun at approximately Mach 6. A conical bow shock will be formed on the nose of the projectile as shown in Figure 1-2. The pressure and temperature will increase in the fluid as it passes through the bow shock. The conical bow shock will reflect off the tube wall and form an oblique detonation wave, which substantially increases the temperature and pressure of the fluid. The flow will then proceed past the projectile to the nozzle. The fluid will expand through the nozzle to propel and accelerate the projectile down the tube.

2.2 THEORETICAL OVERVIEW

The oblique detonation wave phenomena is described in detail by Pratt, Humphrey, and Glenn [2.1, 2.2]. Figure 2-1 shows a schematic of an oblique detonation wave. The supersonic flow is turned through an angle θ and an oblique detonation wave is formed at the angle β. The addition of heat in the oblique detonation wave is what differentiates the oblique detonation wave from an oblique shock wave. *Detonation* occurs when a shock-induced combustion wave follows so closely on the igniting shock wave that the two waves are fully pressure-coupled. By contrast, a *shock-induced combustion* wave results whenever the igniting shock wave is uncoupled followed by a distinct, temporally or spatially resolvable combustion wave. More detailed discussion on this matter is given elsewhere [2.2]. Detonation waves are classified as overdriven, Chapman-Jouguet, or underdriven, depending on whether the normal component of the flow velocity following the wave is subsonic, sonic, or supersonic respectively.

The governing equations pertinent to the oblique detonation wave are

Conservation of mass

$$\rho_1 u_{1n} = \rho_2 u_{2n} \qquad (2.1)$$

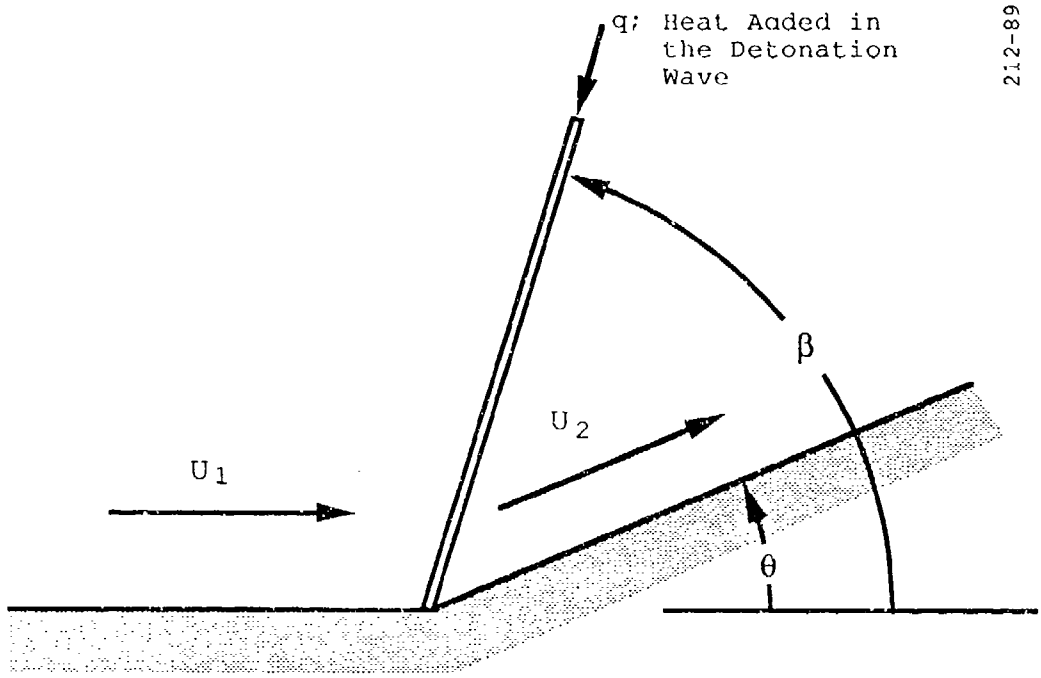

Figure 2-1 Schematic of Oblique Detonation Wave Phenomena

Conservation of normal momentum

$$p_1 + \rho_1 u_{1n}^2 = p_2 + \rho_2 u_{2n}^2 \qquad (2.2)$$

Conservation of tangential momentum

$$(\rho_1 u_{1n}) u_{1t} = (\rho_2 u_{2n}) u_{2t} \qquad (2.3)$$

Conservation of energy

$$h_1 + \frac{u_{1n}^2}{2} = h_2 + \frac{u_{2n}^2}{2} \qquad (2.4)$$

With the assumption of heat released implicitly due to chemical reaction, Equation 2.4 may be used as is, provided the enthalpies h_1 and h_2 include both the sensible enthalpy and the chemical enthalpy (enthalpy of formation). Accurate analysis of performance at high temperature and pressure requires the use of variable specific heats and complex chemical equilibrium and kinetics calculations. For simplification purposes, it is assumed that the q units of heat per unit mass are added to the fluid to represent the sensible heat release due to combustion. It is also

assumed that the fluid has a constant specific heat capacity and does not change composition when the heat is added. This results in the modification of Equation 2.4 to

$$h_1 + q + \frac{u_{1n}^2}{2} = h_2 + \frac{u_{2n}^2}{2} \tag{2.5}$$

The Mach number is defined as

$$M \equiv \frac{u}{\sqrt{\gamma R T}} \tag{2.6}$$

Combination of the conservation equations (Equations 2.1 to 2.3 and 2.5), the definition of the Mach number, and the description of the geometry from Figure 2-1 result in

$$\tilde{q} = -\frac{\gamma + 1}{2}\chi^2 M_1^2 \sin^2\beta + \left(1 + \gamma M_1^2 \sin^2\beta\right)\chi - \left(1 + \frac{\gamma - 1}{2} M_1^2 \sin^2\beta\right) \tag{2.7}$$

where

$$\tilde{q} \equiv \frac{q}{C_p T_1} \qquad \text{and} \qquad \chi \equiv \frac{\rho_1}{\rho_2} = \frac{u_{2n}}{u_{1n}} = \frac{\tan(\beta - \theta)}{\tan\beta} \tag{2.8}$$

A plot of the solution of Equation 2.7 for several values of $\tilde{q}$ and constant M_1 is shown in Figure 2-2. The figure shows the classifications of the different flowfields predicted in the solution. The first classification is that of strong and weak shocks. The solution of Equation 2.7 gives two values of β for each value of θ. The smaller value corresponds to the weak shock and the larger to the strong shock. For all solutions where $\tilde{q} > 0$, the minimum value of β corresponds to the Chapman-Jouguet detonation wave with $M_{2n} = 1$. Points on the constant $\tilde{q}$ lines to the left of the Chapman-Jouguet point on the lower branch of the solution are underdriven waves with $M_{2n} > 1$. Points on the constant $\tilde{q}$ lines to the right of the Chapman-Jouguet point on the lower branch and all of the points on the upper branch of the solution have $M_{2n} < 1$ and are thus overdriven. Points on the lower, weak-wave branch will be referred to as weak overdriven, and on the upper branch, as strong overdriven. However, since all strong oblique shock waves are overdriven, they will be called simply strong oblique detonation waves to avoid redundancy.

Weak underdriven oblique detonation waves will not occur in nature because the detonation wave cannot be maintained at the shock if the normal component of the flow velocity following the wave is supersonic [2.2]. Weak overdriven and Chapman-Jouguet oblique detonation waves can occur in nature and are the desired operating condition for the oblique detonation wave experiment.

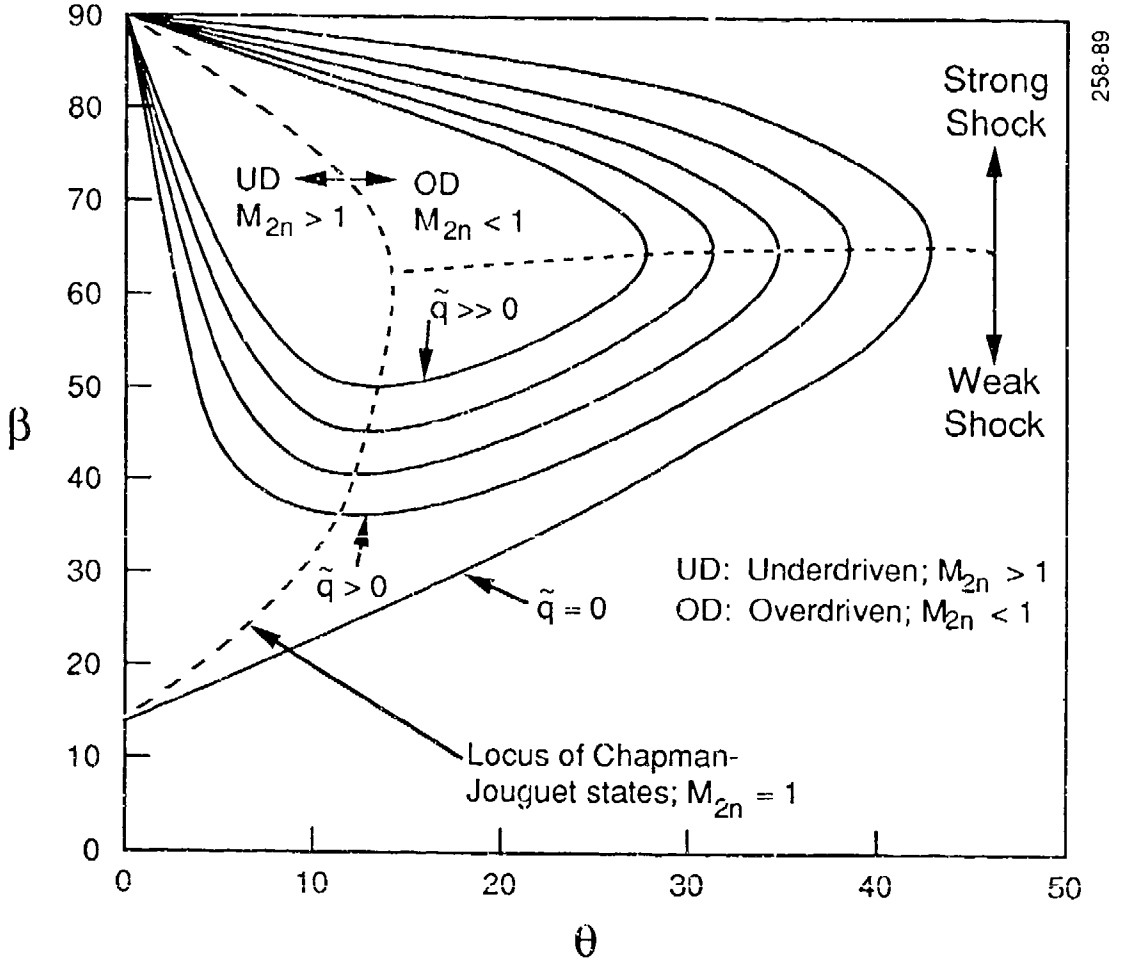

Figure 2-2 Variation of Oblique Shock Wave Angle (β) with Turning Angle (θ) for Variable Specific Heat Addition and Constant Freestream Mach Number and Temperature

Just as with strong oblique shocks, strong oblique detonation waves will not occur unless there is a strong back pressure downstream. If the turning angle is too great, the oblique detonation wave will detach. Figure 2-2 shows that as the energy release is increased the maximum turning angle decreases. It also shows that as more energy is released, the Chapman-Jouguet angle increases. The operational turning angles are bounded by the detachment angle and the Chapman-Jouguet angle. As the energy release is increased, the operating range decreases. On the other hand, as the Mach number of the incoming flow is increased, the detachment angle increases which increases the operating range. The minimum projectile velocity required to establish an overdriven weak oblique detonation wave is called the takeover velocity.

2.3 ONE-DIMENSIONAL FLOW ANALYSIS

The analysis pertaining to optimization of the projectile shape, dimension, and operating conditions were calculated by one-dimensional code ODRAM by Pratt [2.3]. The code assumes that viscous effects and thermal effects (other than the fuel combustion) are small. It also assumes that all of the fuel and oxidizer will burn completely in the oblique detonation wave. The code can treat any combination of fuel and oxidizer correctly. Real fluid properties and equilibrium states are calculated in the code by using a set of combustion reaction equilibrium and kinetics (CREK) subroutines from Pratt and Wormeck [2.4]. The code calculates the conditions through a conical shock wave, oblique detonation wave, and an isentropic expansion behind the projectile. More detailed descriptions of these three processes follow.

Flow conditions through the conical shock wave are calculated by using a modified Taylor-Maccoll method, based on locally constant C_p's, and integrated from the conical shock wave to the cone surface. An option in the code allows the conditions directly behind the shock, on the surface of the cone, or some average of the two to be used as input to the oblique detonation wave section of the code. Then flow is calculated through an oblique detonation wave for crossflow of reactants (air-fuel mixture, ideal gas, variable specific heats, and chemical equilibrium) for prescribed fuel/air equivalence ratio. Equations 2.1, 2.3, and 2.4 are solved iteratively with the assumption that the flow is steady and uniform with no heat transfer. Zero prescribed equivalence ratio simply recovers weak oblique-shock solutions without combustion. Detonation in the oblique shock wave can be turned off in the code. This allows calculation of the conditions downstream of the oblique shock formed at the wall due to the reflected conical bow shock. These conditions are then used as input to a one-dimensional chemical kinetics code CREK1D from Radhakrishnan and Pratt [2.5] to determine if the fuel will ignite and if so, what the induction time is. If the fuel does

ignite and the distance over which the fluid travels during the induction time is short relative to the projectile length, then the flame front will travel back up to the oblique shock wave and form an oblique detonation wave. Otherwise, shock-induced combustion, with heat release occurring in the annulus, is treated as Rayleigh flow, i.e., constant area flow with heat release.

The fluid is compressed in both the conical bow shock and in the oblique detonation wave. The code calculates a projectile diameter that will allow the fluid from the oblique detonation wave to exactly fill the annulus between the projectile and the tube wall. The code then calculates the properties downstream of the projectile by assuming an isentropic nozzle expansion from the annular area to the full bore area following the projectile. The thrust is calculated by using an integral analysis of a control volume which extends from the front of the bow shock to the location where the fluid flow has fully expanded to fill the tube. This integral analysis simplifies to the following equation to determine the thrust

$$Thrust = \left(\rho_{exp} u_{exp}^2 - \rho_{in} u_{in}^2 + p_{exp} - p_{in}\right) A_{bore} \qquad (2.9)$$

where subscripts *in* and *exp* represent fluid conditions in front of the conical bow shock and after the fluid has fully expanded, respectively. The velocities are relative to a frame of reference attached to the projectile, and A_{bore} is the cross-sectional area of the test facility bore. The ballistic efficiency is the ratio of the increase in the projectile kinetic energy to the energy released through the combustion process. It is given by

$$\eta_{ballistic} = \frac{Thrust \cdot V_{projectile}}{\dot{m}_{fluid} \cdot h_{react}} \qquad (2.10)$$

where h_{react} is the heat of combustion and $\dot{m}_{fluid}$ is the mass flowrate of the fluid past the projectile. Upon completion of a calculation, the code returns the projectile performance information and the states of the fluid five regions: 1) in the freestream, 2) directly behind the conical bow shock, 3) on the projectile cone surface, 4) directly behind the oblique detonation wave, and 5) in the fully expanded region downstream of the projectile. The code does not take into account all viscous losses and assumes a uniform flow through the annulus between the projectile and the tube wall.

2.4 PARAMETRIC CALCULATIONS TO OBTAIN OPTIMUM CONDITIONS

The one-dimensional flow code as described in Section 2.3 was used to conduct a parametric study to determine the optimum conditions for the proposed test. The parameters varied were: gas composition, equivalence ratio, gas temperature and pressure, projectile cone half angle, and projectile injection velocity.

The results of the parametric study on the effects of changing the cone half angle from 15° to 22.5° for air and hydrogen are shown in Figure 2-3. The fill pressure is 10 atm and the temperature is 300 K. The equivalence ratio and projectile velocity were varied to determine where the flow regime for the oblique detonation wave will be weak underdriven, weak overdriven, or detached. The weak overdriven oblique detonation wave is desired for the test because it is predicted to be stable. The weak underdriven oblique detonation wave is not theoretically possible because the normal component of the fluid velocity downstream of the oblique detonation wave is supersonic, which prevents the stabilization of the detonation wave. A detached wave will not occur because, as the flow is unable to turn as much as required by the configuration, it will force an overdriven normal shock to form in front of the projectile resulting in negative thrust. This parametric study shows that increasing the cone angle increases the stability of the oblique detonation wave. It also shows that decreasing the equivalence ratio decreases the required projectile injection (takeover) velocity.

The next parametric investigation presented in detail shows the relationship between the takeover velocity, equivalence ratio, and gas composition. The takeover velocity is the minimum required velocity for a projectile to support an oblique detonation wave. Figure 2-4 shows that as the fraction of the inert gas is increased, the takeover velocity decreases. Again, as shown in Figure 2-3, the takeover velocity decreases as the equivalence ratio is decreased. The following conclusions can be drawn from the parametric studies performed: the takeover velocity decreases as the temperature is increased and as the equivalence ratio is decreased. The takeover velocity is unaffected by the gas pressure; however, the thrust and acceleration are directly proportional to the pressure.

As a result of the parametric study, the following test conditions were selected for the proposed experiment. Table 2-1 summarizes the selected test conditions while Figure 2-5 shows a scale view of the projectile in flight within the combustion tube. A gas fill temperature of 300 K was selected because the very weak temperature dependence of the takeover velocity is less beneficial than the added expense and difficulty that would be incurred by performing the experiment at a lower temperature. A gas fill pressure of 10 atm was chosen because higher pressures would result in additional costs for the tube to withstand the higher than 600 atm of pressure downstream of the oblique detonation wave. The heat transfer to the projectile wall is directly proportional to the fill pressure and higher pressures will further complicate the thermal protection of the projectile surface. Parametric runs investigating different working fluid compositions confirmed that the takeover velocity decreases when the fraction of nitrogen is increased or the equivalence ratio is decreased. However, lowering the concentration of hydrogen might inhibit the establishment and stability of detonation in the

Oblique Detonation Wave Parametric Study

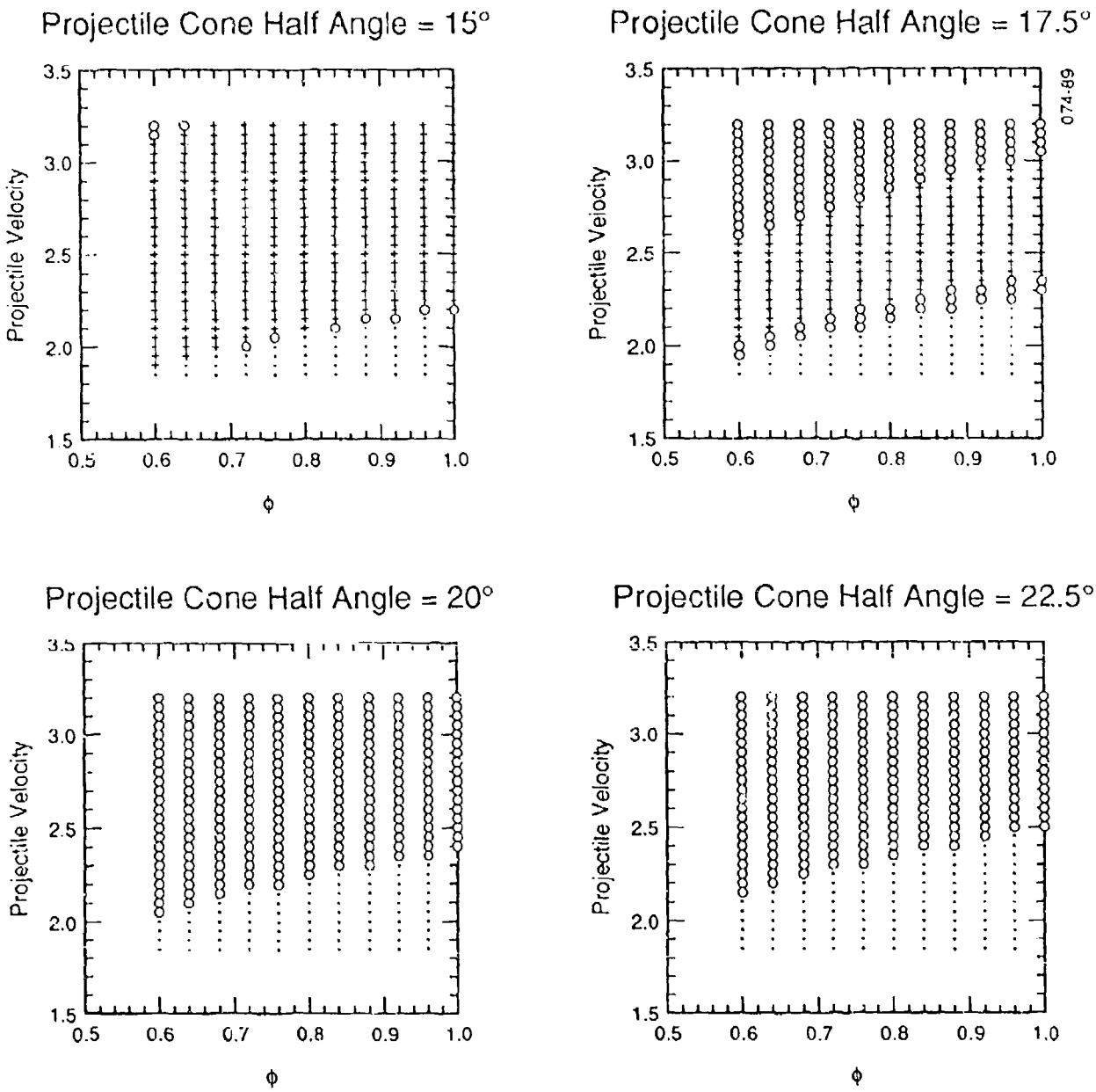

$4\phi H_2 + 2O_2 + 7.52N_2$

\+ Weak Underdriven

O Weak Overdriven (Possible)

· Detached

Figure 2-3 Parametric Study on the equivalence ratios and cone half angle for constant fill pressure of 10 atm and temperature of 300K.

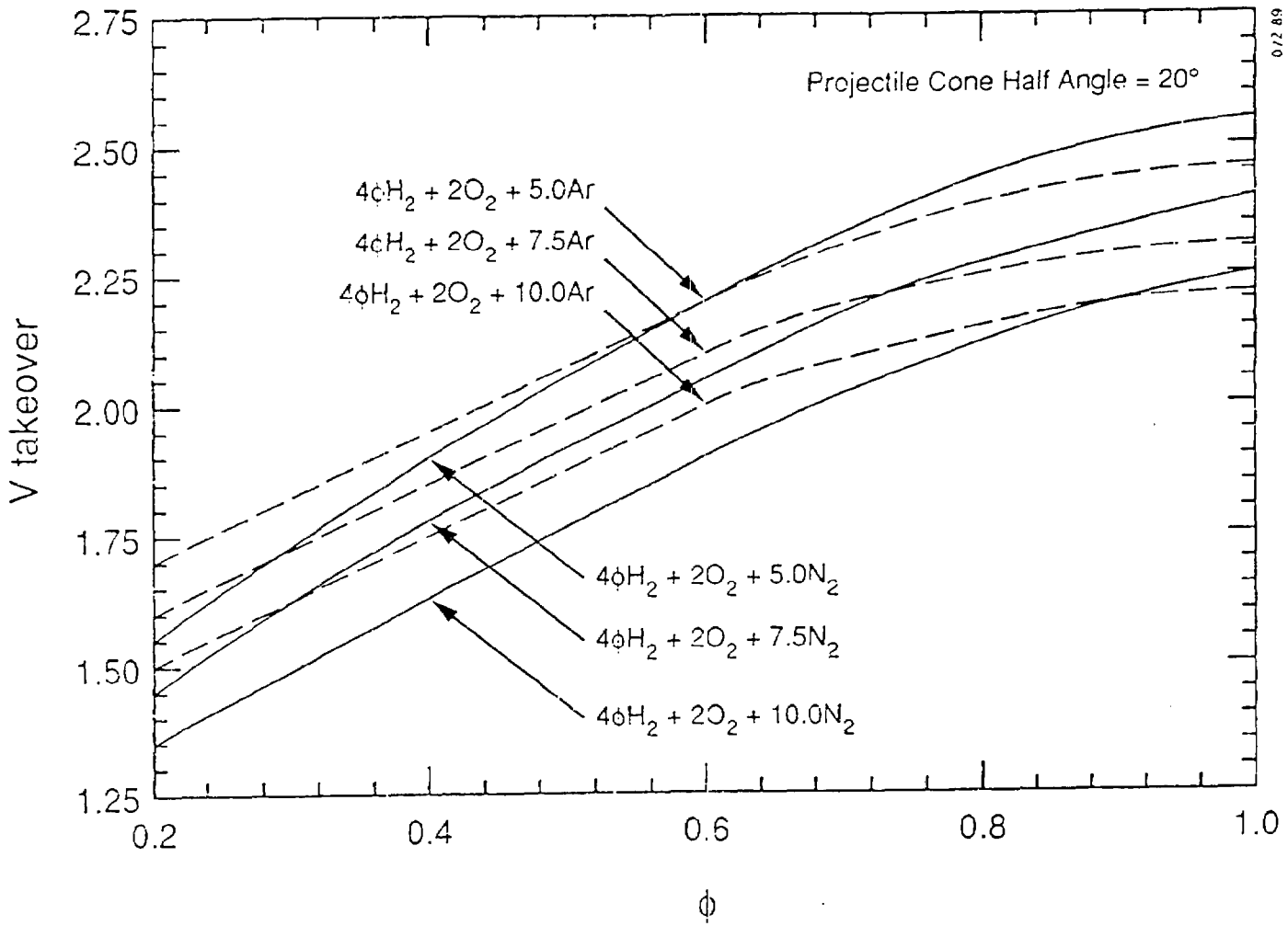

Figure 2-4 Takeover Velocity vs Equivalence Ratio for Constant Fill Pressure of 10 atm and Temperature of 300 K.

Table 2-1 Selected Test Conditions

GAS MIXTURE:	H_2 + AIR
PRESSURE:	10 atm
TEMPERATURE:	300 K
INJECTION VELOCITY:	2500 m/s
THRUST:	4900N
ACCELERATION:	10,000 g
TEST SECTION LENGTH:	10m
FINAL VELOCITY:	2870 m/s

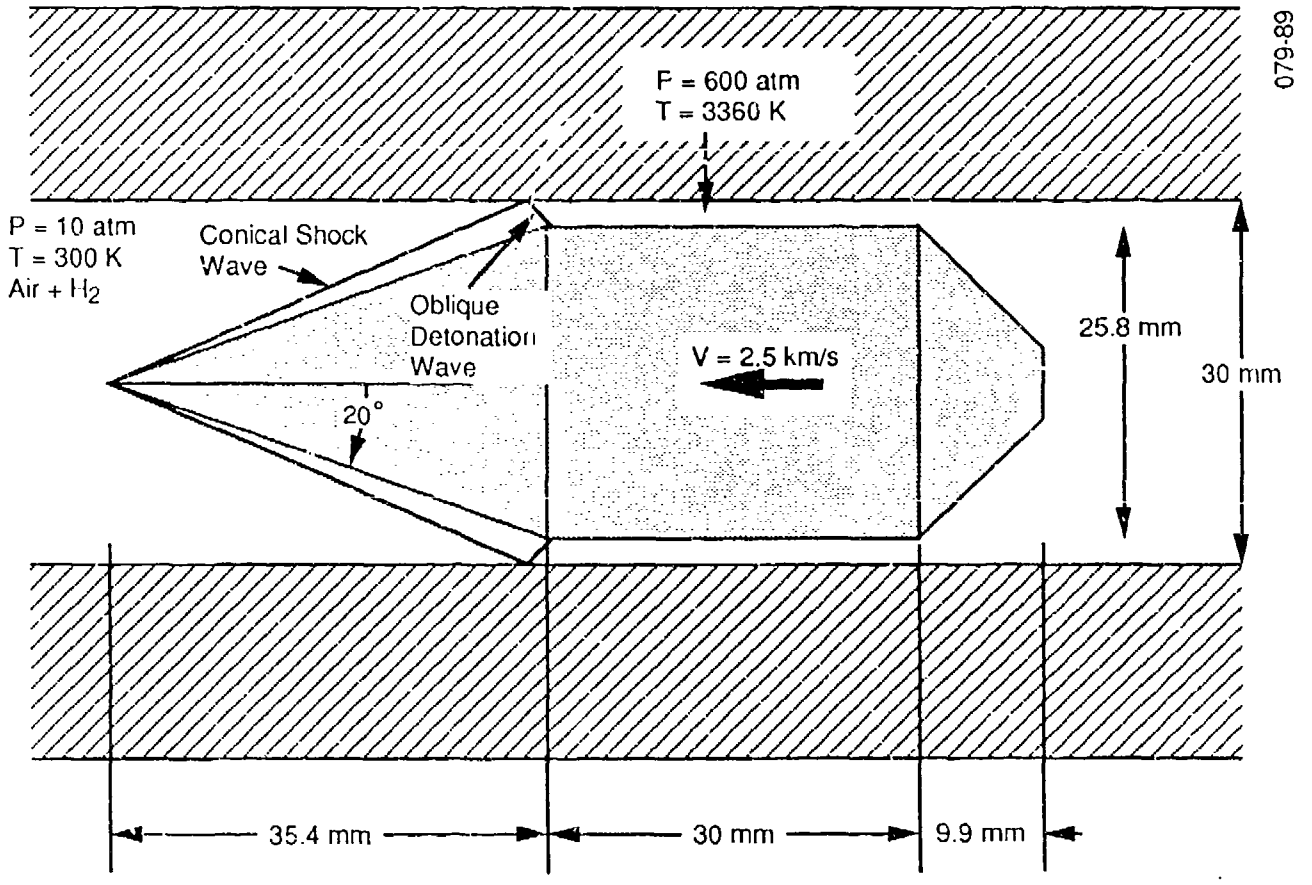

Figure 2-5 Scale View of the Projectile in Flight with the Conical Bow Shock and Oblique Detonation Wave

oblique detonation wave and decrease the performance. A stoichiometric mixture of air and hydrogen was chosen as a good compromise between a lower injection velocity and performance. A cone half angle of 20° and an injection velocity of 2.5 km/s were chosen by trading off the performance benefits of a higher injection velocity against the Wave Gun's ability to propel the projectile and sabot at higher velocities. These test conditions will provide 10,000 g of acceleration to a 50g projectile and a 15 percent increase in the projectile velocity as it is propelled through a 10m-long test section.

2.5 BOUNDARY LAYER THICKNESS PREDICTIONS

Calculations have been performed to estimate the boundary layer thickness on the projectile and on the tube wall for the proposed test conditions. The purpose of the calculation was to estimate the boundary layer thicknesses to determine what fraction of the annulus between the projectile and the tube wall will be filled by the boundary layer. For this analysis, the flow was assumed to have constant properties and a constant freestream velocity near the wall. The constant property flow assumption is not true, but it should lead to a reasonable approximation of the boundary layer thickness. The constant velocity assumption for flow over projectile conical forebody at first hand appears to be an oversimplification of the actual flowfield, but it is theoretically correct because the similarity solution for flow over a cone yields a constant velocity on the cone surface.

To derive theoretical relations for the boundary layer growth on the conical forebody and the projectile body surface, the development in Kays and Crawford [2.6] is followed. A turbulent velocity profile of

$$u^+ = 8.75y^{+1/7} \tag{2.11}$$

is assumed for the flow. An integral boundary layer technique is used to obtain

$$\delta_2 = \frac{0.036\nu^{0.2}}{R\,u_\infty^{3.29}}\left(\int_0^x R^{5/4}u_\infty^{3.86}dx\right)^{0.8} \tag{2.12}$$

which describes the momentum thickness as a function of the fluid properties and R, the radius of the surface along the flow direction. This is integrated to give

$$\delta_2 = 0.0188\,x\,Re_x^{-0.2} \tag{2.13}$$

where x is distance from the nose of the cone along the centerline. The displacement and boundary layer thicknesses are related to the momentum thickness by

$$\delta_1 = 1.29\,\delta_2 \qquad \text{and} \qquad \delta = 10.3\,\delta_2 \tag{2.14}$$

It is likely that in the real flowfield there will be a separated region where the oblique detonation wave meets the projectile surface. It is assumed in this approximation that this will not substantially change the boundary layer thickness downstream of this separated region. In this approximate analysis, the boundary layer is compressed by the oblique detonation wave by the relation

$$\rho u \delta_2 \Big|_{\substack{\text{Before} \\ \text{ODW}}} = \rho u \delta_2 \Big|_{\substack{\text{After} \\ \text{ODW}}} \tag{2.15}$$

The flow on the body of the projectile is assumed to be steady and uniform which results in

$$\delta_2 = 0.036\, x\, Re_x^{-0.2} \tag{2.16}$$

after integrating Equation 2.12 for constant R and u_∞. A relative origin is determined for Equation 2.16 by taking δ_2 from Equation 2.15 and solving Equation 2.16 for x. The relative origin is necessary because the boundary layer is not zero at the beginning of the body, but has already been established. The momentum thickness at the end of the projectile body is determined by adding the distance to the relative origin to the length of the body and using this sum for x in Equation 2.16.

The boundary layer profile on the tube wall is approximated by

$$\delta_2 = 0.037\, x \left(1 - \frac{u_f}{u_w}\right)^{0.8} \left(\frac{(u_w - u_f)x}{\nu}\right)^{-0.2} \left(0.3 + \frac{u_f}{u_w}\right)^{0.8} \tag{2.17}$$

which is from Derbidge and Dahm [2.7]. In this relation, u_f and u_w are the fluid and wall velocities relative to the projectile. For a worst-case condition, the wall temperature can be taken to be the same as the freestream temperature. With this boundary condition, Dahm et al. [2.8] gives

$$\delta_1 = 1.44\,\delta_2 \qquad \delta = 10.4\,\delta_2 \tag{2.18}$$

for the displacement and momentum thicknesses respectively for Equation 2.17. The viscosity of a gas is a weak function of pressure and increases with temperature. An empirical relation for the viscosity of air is given by

$$\mu = 29.6\times10^{-6} \left(\frac{T}{583\ \text{K}}\right)^{0.659} \text{Pa·s} \tag{2.19}$$

from Anderson and Clark [2.9]. The viscosity of air is used since it is a good estimate of the viscosity for the mixture of air and

hydrogen upstream of the oblique detonation wave and for the mixture of nitrogen and water vapor downstream of the oblique detonation wave.

Using the results from the one-dimensional code and Equations 2.11 to 2.19, the estimates of the boundary layer profiles in Table 2-2 were calculated.

Table 2-2 Boundary Layer Profile Estimates

	Boundary Layer Thickness (mm)	Displacement Thickness (mm)	Momentum Thickness (mm)
Before ODW	0.18	0.022	0.017
After ODW	0.14	0.018	0.014
End of Projectile Body	0.46	0.057	0.044
Tube Wall at End of Projectile Body	0.21	0.028	0.020

The boundary layer and momentum thicknesses on the projectile and tube walls are drawn to scale in Figure 2-6. This figure shows that the boundary layer should not cause any significant blockage in the flowfield. The figure shows two velocity profiles drawn relative to a frame of reference attached to the projectile. The first profile is located at the beginning of the annulus and the second profile is located at the end of the annulus. These velocity profiles show that the boundary layer on the projectile wall prevents fluid from moving past the projectile while the boundary layer on the tube wall drags fluid past the projectile. The displacement thickness on the projectile surface is only 2.1 percent of the gap between the tube wall and the projectile. The displacement thickness on the tube wall is 1 percent of the gap between the tube wall and the projectile.

2.6 HEAT TRANSFER PREDICTIONS

Calculations have been performed to estimate the heat transfer rates to the projectile and the tube wall for the proposed test conditions. There are two objectives in this section. The first is to determine if the detonation will be quenched by radiation from the combustion process to the tube and projectile surfaces. The second is to determine the magnitude of the convective and radiative heating of the projectile and wall surfaces.

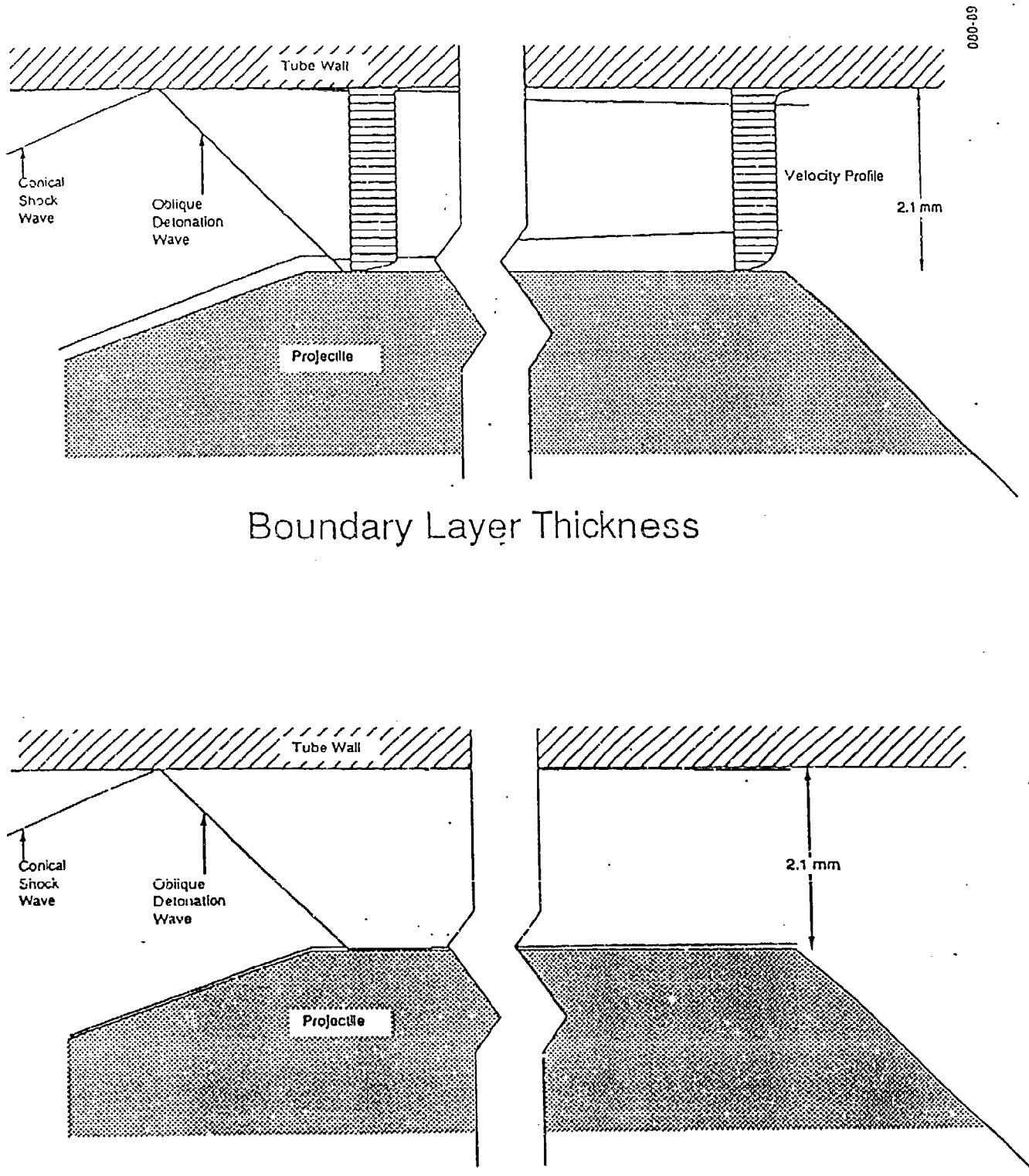

Figure 2-6 Scaled Drawing of Boundary Layer and Displacement Thicknesses on the Projectile

The energy released by burning the fuel in the oblique detonation wave is

$$Q_{comb} = h_{react}\,\dot{m} \tag{2.20}$$

The radiation heat flux is given by

$$Q_{rad} = \sigma A\left(T_f^4 - T_w^4\right) \tag{2.21}$$

where σ = 5.67x10^{-8} W/(m^{2}K^4), T_f is the fluid temperature, and T_w is the wall temperature. The convective heat flux is determined by

$$Q_{conv} = \bar{h}_{conv} A \left(T_{aw} - T_w\right) \tag{2.22}$$

where the adiabatic wall temperature i : given by

$$T_{aw} = T_f + \frac{u^2}{2C_p} \tag{2.23}$$

The average convective heat transfer coefficient, h_{conv}, is calculated from the Stanton number by

$$\overline{St} = \frac{\bar{h}_{conv}}{\rho u C_p} \tag{2.24}$$

The Stanton number as given by Dahm et al. [2.8] for compressible flow over a flat plate can be averaged by integrating from the beginning of the boundary layer and dividing by the length to yield

$$\overline{St} = 0.037F\,Re^{-0.2}Pr^{-0.4} \tag{2.25}$$

where F is a correction factor for the property variations through the boundary layer given by

$$F = \left(\frac{T_f}{0.353T_f + 0.197T_{aw} + 0.45T_w}\right)^{0.66} \tag{2.26}$$

and

$$Re = \frac{\rho\, u\, x}{\mu} \tag{2.27}$$

For a first estimate at calculating the heat transfer to the wall, the thermal boundary layer is assumed to start on the body of the projectile after the oblique detonation wave. It is also assumed that Equations 2.25 and 2.26 will give adequate estimates of the Stanton number for the tube and projectile walls even though it was derived for momentum and thermal boundary layers that start on the beginning of a flat plate with a 1/7 power law velocity profile. For the proposed test conditions, these

equations give a heat transfer coefficient of 279 kW/m^2K on the 933 K projectile body. This yields a heat flux of 864 MW/m^2 or a total of 2.1 MW for the total surface area of the projectile body. They also give a heat transfer coefficient of 209 kW/m^2K on the 300 K tube wall. This yields a heat flux of 691 MW/m^2 or a total of 2.0 MW for the total surface area of the tube above the projectile body.

A schematic for the heat fluxes showing radiation and convective heat transfer is shown in Figure 2-7. The radiation heat transfer from the flame was calculated by using a view factor of 1 for radiation from one side of the flame to the projectile and to tube surfaces at their initial temperature of 300 K. The emissivity of the gas is assumed to be unity. This would be a worst-case condition. Less heat should be lost from the detonation wave than is shown because some of the radiation will be to a hot gas and not the cold surfaces. Only 0.004 percent of the heat released in the combustion process is lost by radiation to the projectile and tube surfaces. This means that the detonation will not be quenched by radiative heat losses.

The projectile will be heated by the fluid on the conical forebody as well as on the body. Equations 2.24 to 2.25 can be used for determining the heat transfer to the projectile body. However, to analyze the heat transfer on the conical forebody, a relation for the Stanton number is required. From Kays and Crawford [2.6],

$$St \propto C_f \propto \delta_2^{-0.25} \tag{2.28}$$

which can be combined with Equations 2.13, 2.16, and 2.25 to give

$$\overline{St} = 0.045F\,Re^{-0.2}Pr^{-0.4} \tag{2.29}$$

for the average Stanton number on the cone surface. As a check of this equation, consider the case of a 20° cone flying at 2.5 km/s through air at 10 atm and 300 K. The use of Equation 2.29 gives heat fluxes within 12 percent of the heat flux predicted by the Abres Shape Change Code (ASCC) from Lee et al. [2.10]. ASCC is used for predicting the flowfield and shape change of a projectile due to ablation while traveling through air. For the proposed test conditions, a heat transfer coefficient of 77 kW/m^2K is predicted by using Equation 2.29. This gives a heat flux of 103 MW/m^2 or a total of 166 kW for the total surface area of the cone at 933 K. This is also shown in Figure 2-7.

2.7 PROJECTILE THERMAL LOAD

As shown in the preceding section, the thermal load on the projectile is substantial. The Biot and Fourier numbers are

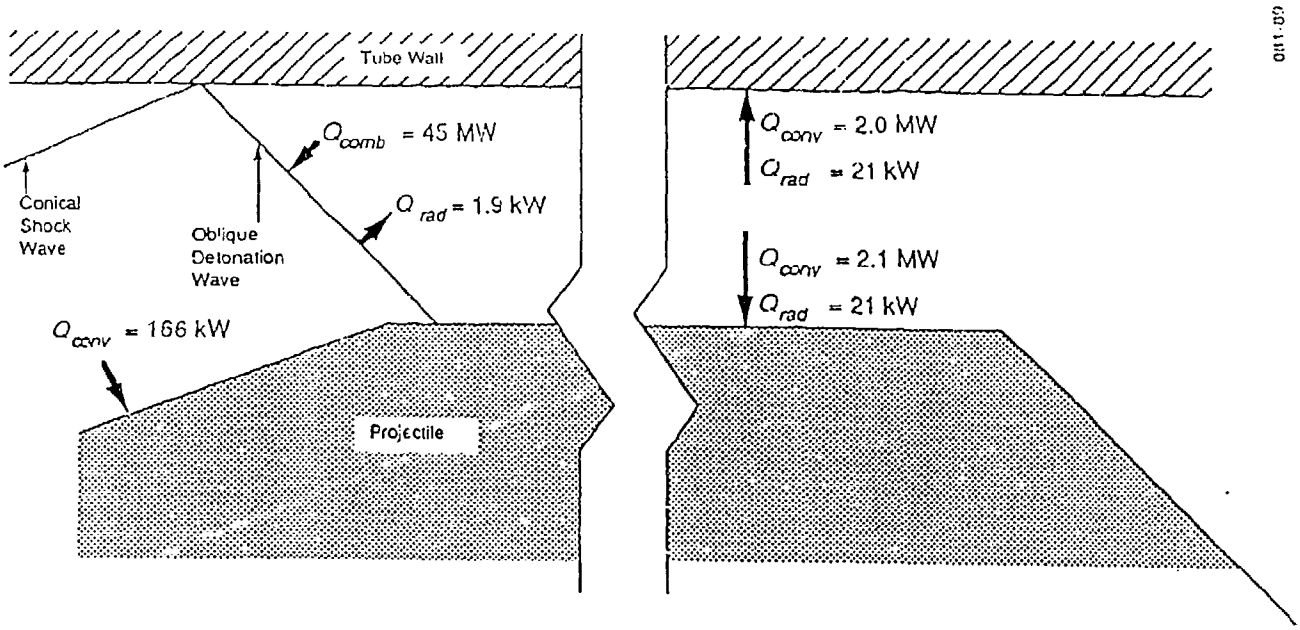

Figure 2-7 Schematic of the Heat Flux for Flow Over the Projectile and the Tube Wall

useful in determining which analytical method is appropriate for determining the thermal response of the projectile. The Biot number is the nondimensional parameter that gives the ratio of the projectile thermal resistance to the fluid thermal resistance. If Bi << 1, then a lumped capacitance model can be used. A lumped capacitance model assumes that the projectile is at a uniform temperature and the convective heat transferred to the projectile will uniformly increase the temperature of the projectile. The Biot number is given by

$$\mathrm{Bi} \equiv \frac{\bar{h}_{conv} L}{k_{solid}} \tag{2.30}$$

The Fourier number is the nondimensional parameter that gives the ratio of the conduction of heat into the projectile to the storage of heat in the projectile. If Fo << 1, then the projectile can be treated as a semi-infinite solid. As a semi-infinite solid, the projectile surface can support a temperature gradient as it is heated up. The Fourier number is given by

$$\mathrm{Fo} \equiv \frac{\alpha t}{L^2} = \frac{k\, t}{\rho\, C_p\, L^2} \tag{2.31}$$

As an illustration of this analysis, assume the projectile body with a heat transfer coefficient of 223 W/m^{2}K has a surface of unprotected aluminum. For an aluminum projectile, the Biot number is 17.7 and the Fourier number is 0.0017. Therefore, the projectile cannot be analyzed with a lumped capacitance method but can be treated as a semi-infinite solid. From Kreith & Black [2.11], the temperature profile for a semi-infinite solid at an initial temperature of T_O exposed to a constant ambient temperature of T_f and an average convective-heat-transfer coefficient of $\bar{h}^2_{conv}$ is

$$\frac{T(x,t) - T_o}{T_\infty - T_o} = 1 - \mathrm{erf}\xi - \left[1 - \mathrm{erf}\left(\xi + \sqrt{\eta}\right)\right] e^{\mathrm{Bi}+\eta} \tag{2.32}$$

where

$$\xi = \sqrt{\frac{x^2}{4\alpha t}} \tag{2.33}$$

$$\eta = \frac{\bar{h}^2_{conv}\,\alpha\, t}{k^2_{solid}} \tag{2.34}$$

and

$$\mathrm{Bi} \equiv \frac{\bar{h}_{conv}\, x}{k_{solid}} \tag{2.35}$$

In this solution x is the distance from the surface in the semi-infinite solid. Using a 10m-long test section, a heat transfer coefficient of 279 MW/m^{2}K from Equations 2.24 and 2.25, a melt temperature of 933 K for aluminum, and an initial projectile temperature of 300 K, a semi-infinite calculation predicts that the projectile will start to melt 0.53m down the test section. Assuming that while traveling down the remainder of the tube all of the heating is used to heat the aluminum from its initial temperature to its melt temperature and then transform from solid to liquid, 5.5g of the 51g projectile will melt during the test. This is not acceptable and, therefore, thermal protection must be provided for the projectile.

For the proposed test case in Table 2-1 and in Figure 2-5 for a surface temperature of 933 K, Equations 2.25 and 2.29 give heat transfer coefficients of 77 kW/m^{2}K and 279 kW/m^{2}K for the projectile cone and body, respectively. For all cases of interest in the test design, the Fourier number will be much less than 1. Therefore, the semi-infinite analysis will be appropriate for determining the temperature profile for the projectile cone and body. The projectile tip temperature will quickly rise to the fluid total temperature it is passing through because of the higher heating rates near the tip and the small nose radius. The

boundary layer on the cone grows as the fluid moves down the cone which results in the largest heat transfer located at the nose of the projectile. The ASCC predictions for flow through air can be used to estimate the increase in the heat transfer rates at the projectile nose due to the thinner boundary layer at the nose. The ASCC results show heat transfer rates that are 8 times as high on the tip of a cone as at the end of the cone. The ASCC calculations also show that the heat transfer is 1.5 times as high or higher on the first 7 percent of the projectile cone. It is here that the nose of the projectile should be required to withstand the total temperature of the fluid.

The surface temperature of the cone and body of the projectile can be calculated by using Equation 2.32 and estimates of the heat transfer coefficients. For the cone, the ASCC results suggest that a multiplier of 1.55 is appropriate for determining the heat transfer coefficient near the tip of the cone. This results in a heat transfer coefficient of 120 kW/m^2K. For the projectile body, the heat transfer coefficient was calculated to be 279 kW/m^2K by using the beginning of the body as the origin of the thermal boundary layer. This is a conservative estimate as was previously described, so this value will be used without modification.

Figures 2-8 and 2-10 show the surface temperature of the projectile cone and body for several materials as a function of location in the test section. Figures 2-9 and 2-11 show the temperature of the cone and body for several materials as a function of distance into the surface when the projectile reaches the end of the test section. These temperatures were calculated by using Equation 2.32 and a constant velocity equal to the injection velocity of 2500 m/s to determine the time as a function of location. These plots show the severity of the thermal protection problem and the dependance of the surface temperature on the material. These results will be used to select the material for the projectile as discussed in Section 3.

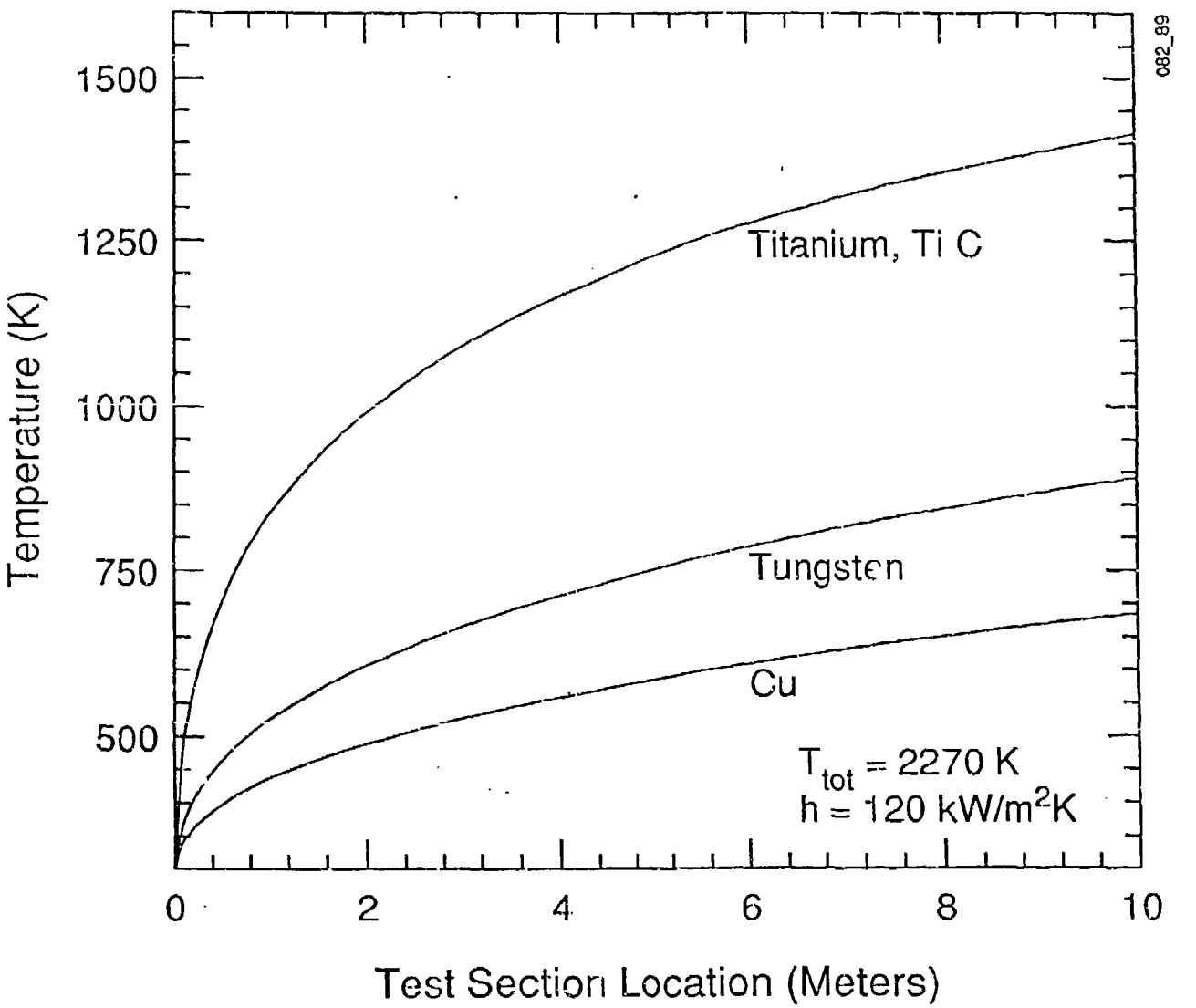

Figure 2-8 Projectile Conical Forebody Surface Temperature for the Proposed Test Conditions

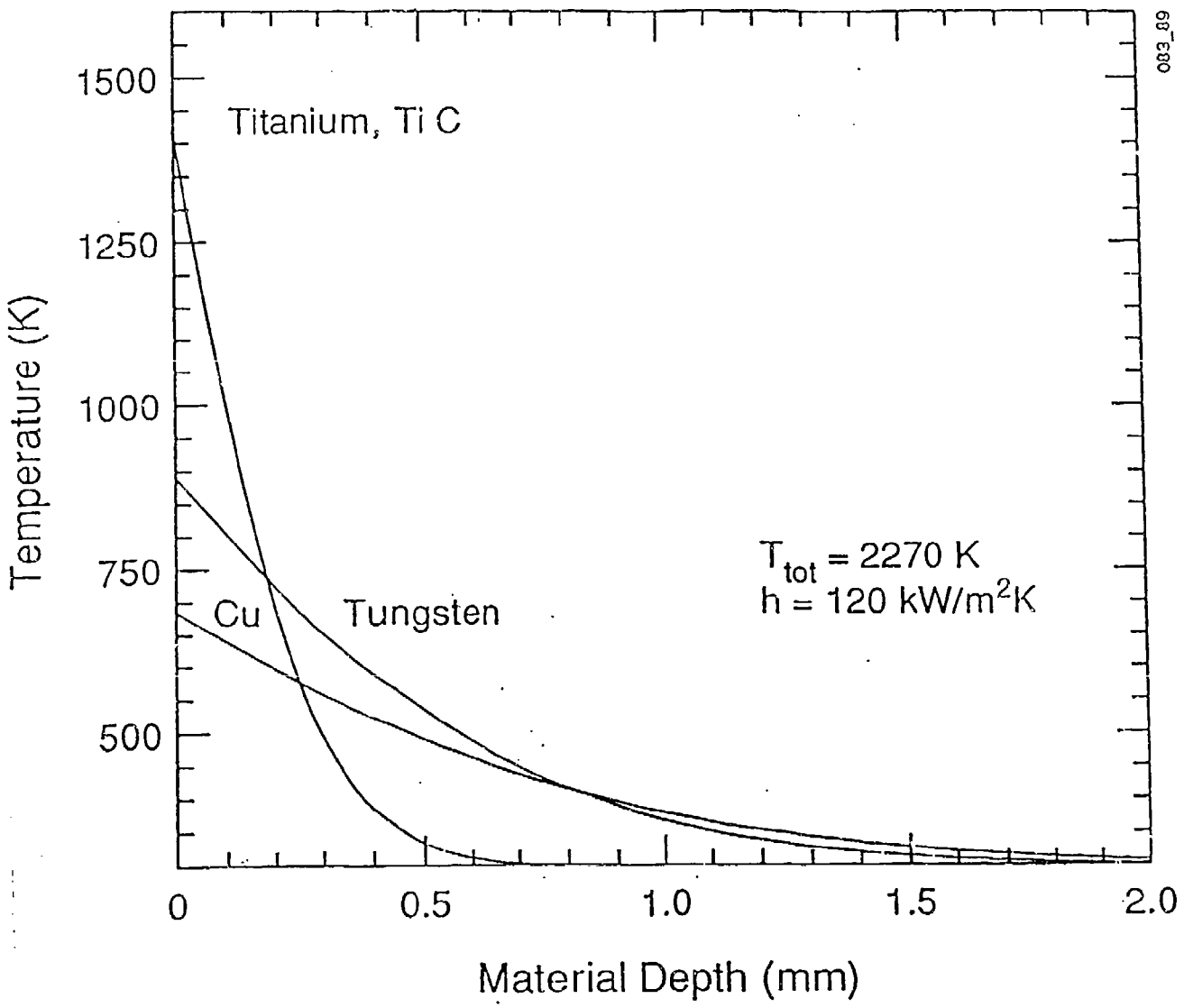

Figure 2-9 Projectile Conical Forebody Temperature at the End of the Test Section as a Function of Depth in the Material for the Proposed Test Conditions

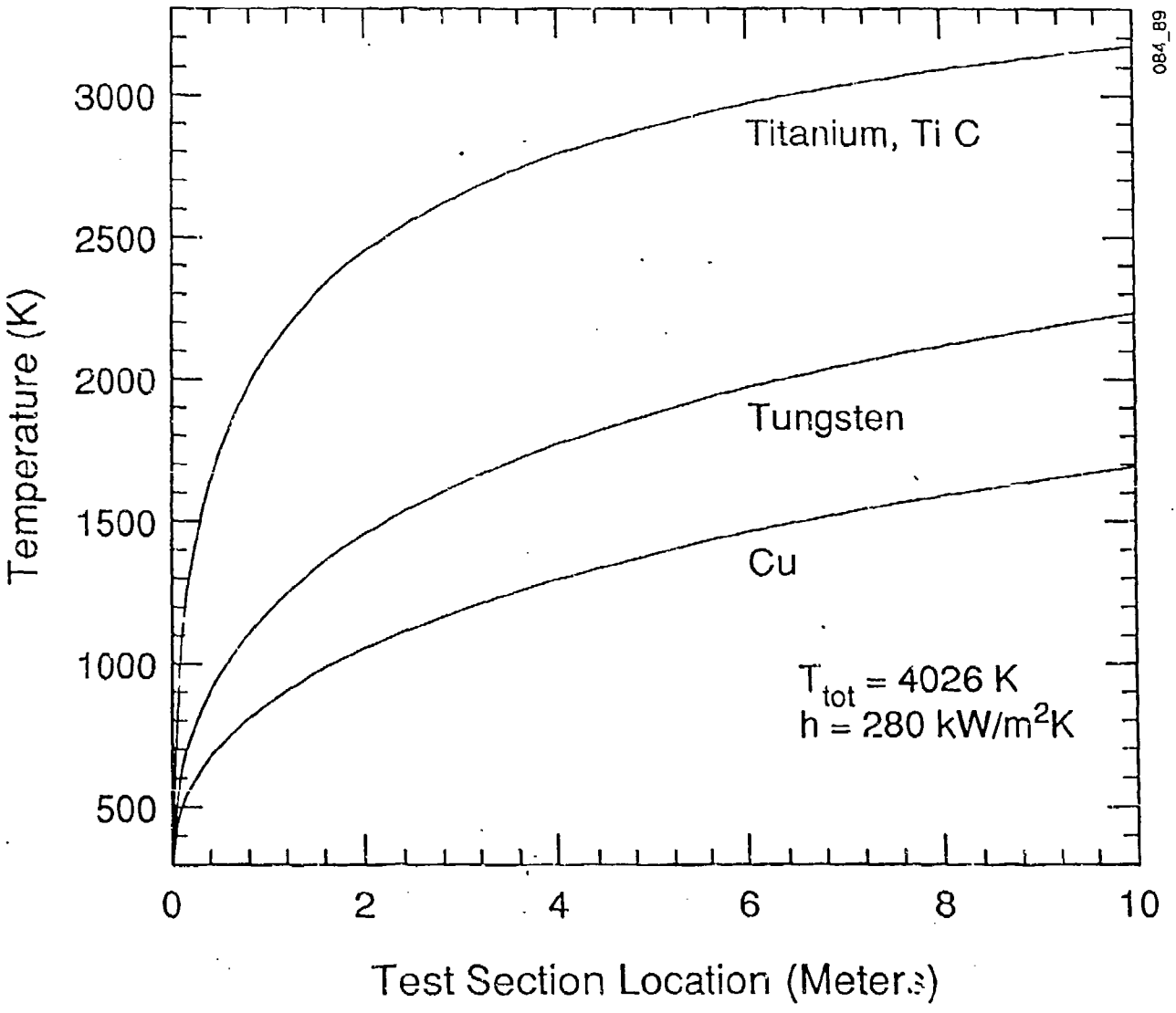

Figure 2-10 Projectile Body Surface Temperature for the Proposed Test Conditions

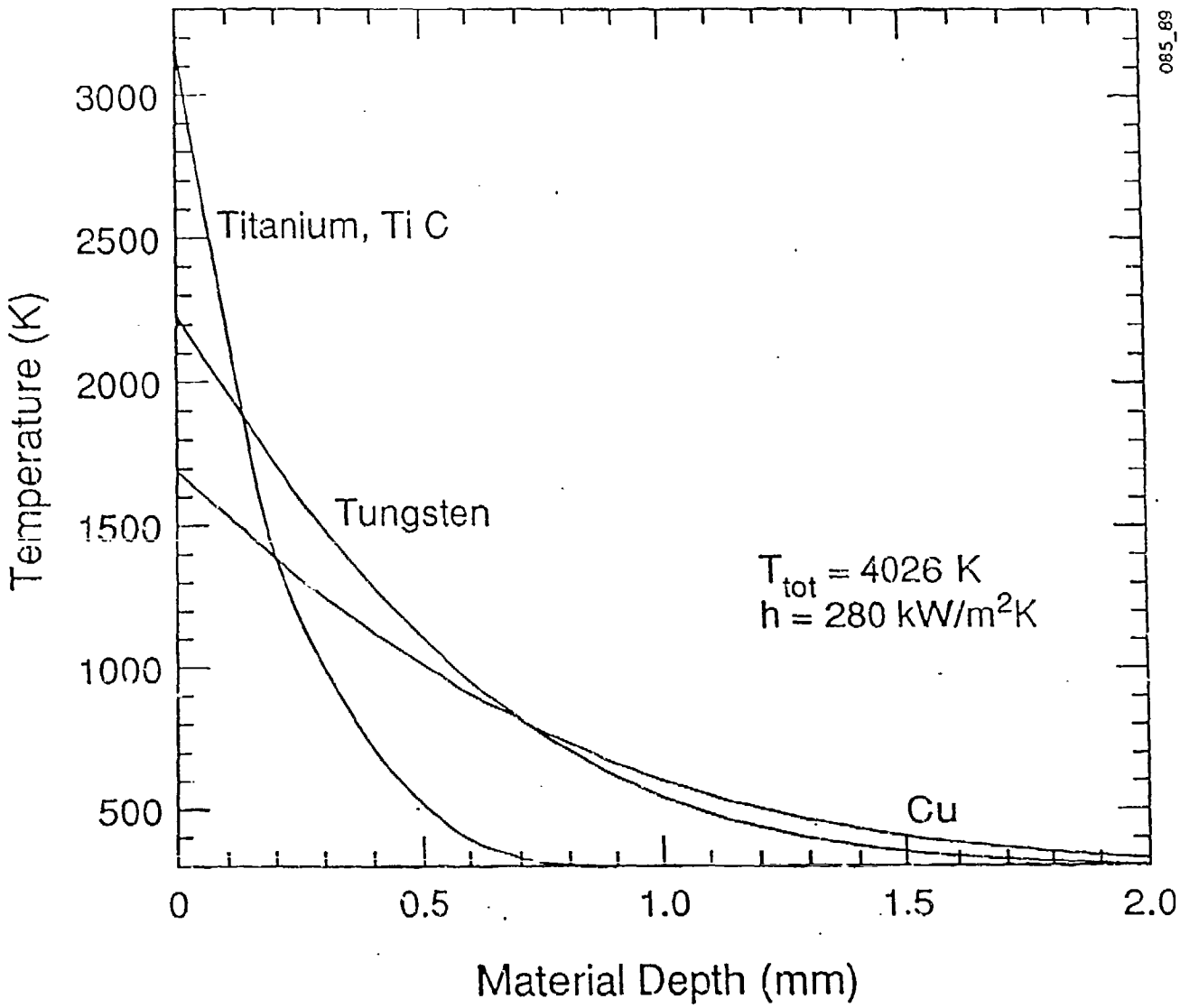

Figure 2-11 Projectile Body Temperature at the End of the Test Section as a Function of Depth in the Material for the Proposed Test Conditions

References

[2.1] Pratt, David T., Joseph W. Humphrey, and Dennis E. Glenn, "Morphology of Standing Oblique Detonation Waves," Paper No. AIAA-87-1785 at the AIAA/ASME/SAE/ASEE 23ed Joint Propulsion Conference, San Diego, CA, 29 June - 2 July 1987.

[2.2] Pratt, David T., Joseph W. Humphrey, and Dennis E. Glenn, "Morphology of Standing Oblique Detonation Waves," to appear in the *AIAA Journal of Propulsion and Power* 1989.

[2.3] Pratt, David T., "ODRAM: A One-Dimensional Performance and Design Code for ODW-Driven Ram Accelerator," personal communication, 1987.

[2.4] Pratt, David T., and John J. Wormeck, "CREK, A Computer Program for Calculation of Combustion Reaction Equilibrium and Kinetics in Laminar or Turbulent Flow," Report WSU-ME-TEL-76-1, Thermal Energy Laboratory, Dept. of Mech. Engineering, Washington State University, March 1976.

[2.5] Radhakrishnan, Krishnan, and David T. Pratt, "Fast Algorithm for Calculating Chemical Kinetics in Turbulent Reacting Flow," Combustion Science and Technology, Volume 58, pages 155-176, 1988.

[2.6] Kays, William M., and Michael E. Crawford, *Convective Heat and Mass Transfer*, Second Edition, McGraw-Hill Book Company, New York, 1980.

[2.7] Derbidge, T. C., and T. J. Dahm, "Recovery Tub Trade-Off Study for Reentry Ground Test Facility," Report Aerotherm TR-76-196, Acurex Corporation/Aerotherm Division, Mountain View, CA 1 May 1976.

[2.8] Dahm, T. J., and L. Cooper, D. Rafinejad, S. B. Youngblood, and J. T. Kelly, "Passive Nosetip Technology (PART II) Program," Report SAMSO-TR-77-11, Acurex Corporation/Aerotherm Division, Mountain View, CA, 30 November 1976.

[2.9] Anderson and Clark, "Correlation for the Viscosity of Air Including the Effects of Dissociation," Internal Memo, Acurex Corporation/Aerotherm Division, Mountain View, CA, 1975.

[2.10] Lee, E. M., and C. L. Minell, G. L. Tice, and G. A. Wallace, "Abres Shape Change Code (ASCC 85Q): Technical Report and User's Manual," Report BMO TR-86-42, Acurex Corporation, Aerotherm Division, Mountain View, CA, 7 November 1986.

[2.11] Kreith, Frank, and William Z. Black, *Basic Heat Transfer*, Harper & Row, New York, 1980.

SECTION 3 - DESIGN OF HYPERVELOCITY PROJECTILE

3.1 REQUIREMENTS FOR PROJECTILE

For a projectile to perform satisfactorily in a ram accelerator geometry, it must survive several severe environments without significant deformation or deterioration. The first of these is the stress loading caused by the Wave Gun injector. The acceleration process subjects the base of the projectile to stress levels of as much as 500 MPa (72,500 psi) imparting accelerations of 4 x 10^6 m/s^2 (400,000 g) or more to projectiles. The stress levels imposed on the projectile exceed the yield strength of many materials, so material selection is limited to those with very high strength-to-mass ratios. It is necessary to consider the stress levels throughout the projectile to ensure that strengths are not exceeded at any point during the acceleration process. When the launch package includes a sabot, the problem of avoiding excessive stresses becomes even more complex.

As the projectile enters the ODW test section it will be subjected to conditions that are very different, but no less extreme. As discussed in the previous section, the tip of the conical nose will be immersed in stagnant gas behind the normal shock at that point, and refractory materials must be used there to avoid melting and the resultant ablation. The remainder of the leading cone will be subjected to hot gas flowing across its surface behind the conical shock. It is desirable to keep this surface and the gas in its proximity below the ignition temperature of the gaseous mixture to prevent premature ignition of the gas mixture in front of the projectile. Therefore, materials with a high thermal diffusivity are required. The "body" or cylindrical section of the projectile also experiences a very hostile thermal environment. This surface faces the detonated gas at 600 atm and 3360 K. The energy added by the detonation reaction does increase the temperature and pressure of the products greatly. Melting and the resulting ablation must still be prevented in this extremely severe atmosphere.

3.2 PROJECTILE DESIGNS

As discussed in Section 7 below, the proposed program has two series of test activities - a preliminary test series called Stage I and a subsequent main test series called Stage II. The purpose of the Stage I tests is to conduct proof-of-principle testing pertaining to the validity of the projectile thermodynamics and the effectiveness of the facility and instrumentation. The purpose of the Stage II tests is to conduct a more detailed and indepth study

pertaining to characterization and quantification of the ODW phenomena.

We will use two different projectile designs for the proposed test program: 1) a simple polycarbonate projectile for Stage I tests; and 2) a more complex titanium alloy projectile for Stage II tests. Specific features of each projectile design are discussed in the following sections.

3.2.1 Stage I Projectile Design

The projectile for Stage I study should be designed to meet the proof-of-principle objective discussed in detail in Section 7.

To meet the Stage I objective of simplicity with quick, simple turnaround, we have chosen to fabricate the projectile as a solid, single piece of polycarbonate plastic machined to the shape shown in Figure 3-1. We will make the outside diameter of the projectile equal to that of the Wave Gun bore and thus avoid the use of a sabot. This will eliminate design complexity and the requirement for sabot discard techniques. Polycarbonate is frequently referred to by one of its trade names, Lexan. It has low density, is extremely

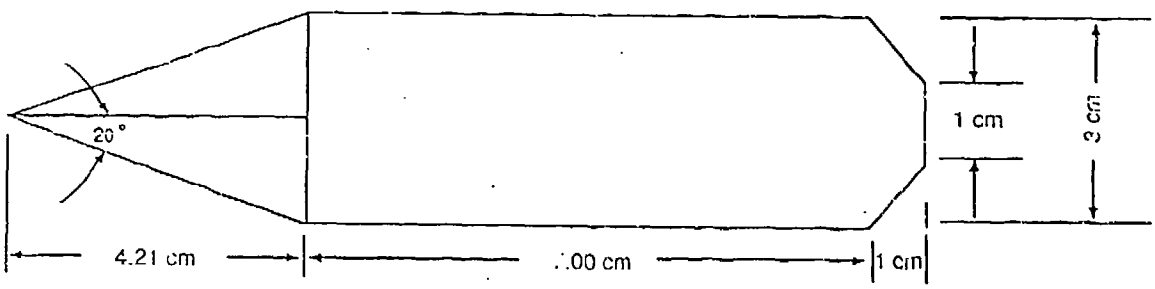

Figure 3-1 Stage I Projectile Design

tough in response to impulsive stresses, and has an extensive history of success as projectile and sabot material [3.1, 3.2, and 3.3]. This choice of design and material virtually eliminates any concern over projectile survival during the Wave Gun launch phase. The low density of polycarbonate (1.2 g/cm^3) permits the projectile to have a long cylindrical body without exceeding the mass that promotes in-bore stability. Because the projectiles are solid and machined from a single piece of rod stock, the shape can be easily and quickly modified in response to experimental results.

The dimensions for the Stage I projectile design are shown in Figure 3-1; they reflect the longer body possible as a result of the lower density of the polycarbonate material. The mass of this projectile will be 75g. This mass is well below that which the Wave Gun can accelerate to the design injection velocity.

3.2.2 Stage II Projectile Design

The projectile for Stage II study should be designed to withstand extreme test conditions discussed in Section 3.2. In contrast to the polycarbonate projectile for Stage I, the projectile for Stage II study must complete the flight along a 10m-long combustion tube keeping its structural integrity. The external shape of the projectile is dictated by the nature of the ODW phenomenon as given in Figure 2-5 in the preceding section. The design is illustrated in Figure 3-2, together with the obturating sabot. This figure defines the terminology to be used in the remainder of this discussion. The centralizers mechanically hold the projectile at the center of the combustion tube. The centralizer is designed so as to leave a small clearance between the centralizer edge and the tube wall. As the projectile travels along the tube, the edge of the centralizer glides over a thin film of gas between the centralizer edge and the tube wall, which acts as a lubricant. The angle of the conical nose (20° half-angle) was selected on the presumption that the injection velocity would be close to 2.5 km/s. The calculations on which this choice is based have been discussed in Section 2. In this situation the conditions behind the bow shock should not induce detonation, but such conditions should be achieved upon reflection from the wall. Similar considerations dictated the choice of body diameter. The choice of shape in the boat-tail expansion region is somewhat arbitrary based on the expectation that the effectiveness of this region, from the standpoint of its function as an expansion nozzle, will be quite high independent of details of its shape. Centralizers are shown as an integral part of the projectile, although the determination of whether or not they are required will depend on an estimate regarding the stability of an uncentralized projectile in the geometry required for

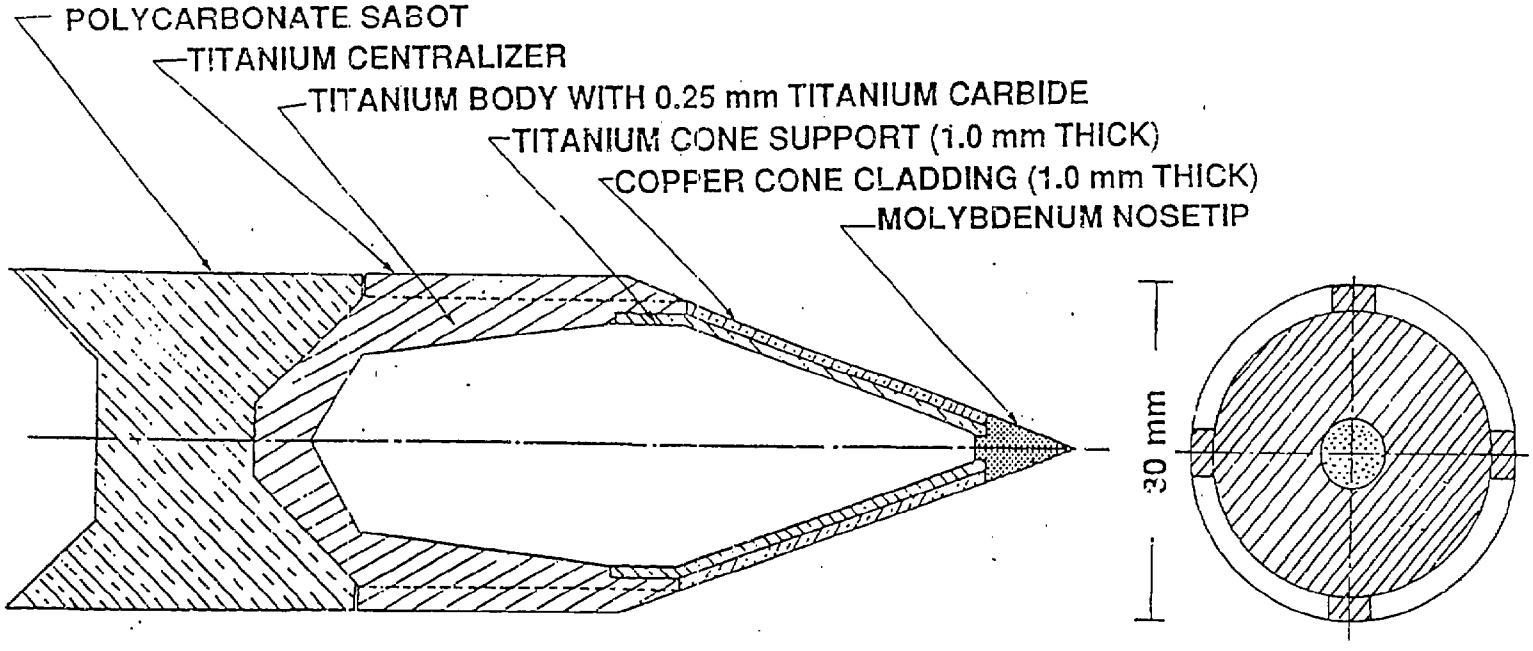

PROJECTILE MASS 50g

SABOT MASS 20g

Figure 3-2 Stage II Projectile and Sabot

ODW demonstration. We have designed the length of the body region to be as long as mass limitations will permit to decrease the likelihood of problems resulting from a tendency for the projectile to tumble within the bore.

The bore of the Wave Gun to be used in the proposed experiment is 30 mm. In this caliber, our experience is that we can accelerate an 85g launch package (including projectile and sabot) to a velocity slightly in excess of the injection velocity (2.5 km/s) required for ODW function. To avoid Wave Gun development efforts, we have designed the launch package to stay within that mass limit.

In the region where the very high stagnation temperatures will be achieved, the design includes a tip of molybdenum alloy. The melting point of molybdenum is 2883 K, high enough to avoid melting at this critical location. Except for this region, the cone consists of a substrate of titanium alloy clad with copper. We have chosen copper for its very high thermal diffusivity. The importance of thermal diffusivity to this application is that it will allow the surface to remain relatively cool and thus avoid surface ignition as described in Section 2.7. Figure 2-8 shows the results of a set of one-dimensional calculations that calculated temperature as a function of depth into semi-infinite blocks of several materials immersed in air at the conditions calculated to exist behind the conical shock wave. It can be seen that of these, only copper keeps the surface below the ignition temperature for the expected duration of the experiment. It can also be seen that the temperature 1 mm into the copper is only slightly above ambient. For these reasons, we have chosen to design a projectile with its conical nose clad with 1 mm of copper despite the undesirable structural properties of low strength and high density.

The exterior surface of the body of the projectile presents a different thermal problem. The energy added to the gas by the detonation process brings the temperature of the freestream gas around the body to more than 3000 K. Computed temperatures at the surface as a function of the distance along the combustion tube and the temperature as a function of depth at the end of the tube are shown for several materials in Figures 2-10 and 2-11. Of these, titanium carbide was chosen because of its high melting point, low density, and appropriate diffusivity. A 0.25-mm (0.01-inch) layer will be applied to the projectile body.

To keep the overall mass of the projectile below the 85g limit imposed by the characteristics of the Wave Gun, we require a material with a low density for the major portion of the projectile. Further, in order to support the materials described in the preceding paragraphs against the very large forces produced at the peak acceleration of the Wave Gun, we need a material with very high strength. The

family of materials for high ratios of strength to weight are titanium and its alloys. These materials appear to be ideal for this application. We have made a preliminary choice of an alloy designated Ti-6Al-4V (6 percent aluminum, 4 percent vanadium, and the balance titanium) for the major structural material of the projectile. With appropriate heat treatment, this material exhibits yield strengths in excess of 10^9 Pa (145 kpsi) with a specific gravity of only 4.52. The thicknesses of the section have been chosen on the basis of fabricability and on the ability to support the stresses resulting from the acceleration. We have given the conical section supporting the molybdenum nose tip and the copper cladding a thickness of 1.0 mm on the presumption that this is about the thinnest section that could be reliably machined.

The mean acceleration stresses computed along the base of the molybdenum tip, 3×10^8 Pa (44 kpsi), and at the junction of the cone with the body, 6.54×10^8 Pa (95 kpsi), are well below yield strength of the titanium alloy. The computed mean stresses at these and other sections are shown on Figure 3-3. It can be seen that in all cases these stress levels are well below yield. It must be said that the above mean stresses have been computed by dividing the total force required to accelerate the mass ahead of a given section by the area of the section. This simple methodology is adequate for the preliminary design that is being given here. Before the design is experimentally applied, however, it should be subjected to a finite-element stress analysis. Such an analysis is beyond the scope of this Phase I program.

3.3 PROJECTILE FABRICATION

The fabrication of the the projectile according to the design shown in Figure 3-2 will require a combination of several manufacturing processes. All of these are developed conventional processes, however; no innovation or process development will be required. The nose cone is small and has some quite thin sections, so some finesse will be required and no doubt some special fixtures will be needed to support the piece for some of the final turning operations, but such precision turning is routinely accomplished by quality shops.

When the form of the titanium cone is completed, the copper cladding will be applied by electroforming to a thickness in excess of the 1-mm final thickness so that the the final shape can be produced by lathe turning. We plan to produce the projectile body as an investment casting of the titanium alloy with the external shape having the cruciform cross section. The casting will be made as a rod long enough to make several projectile bodies. The internal contours

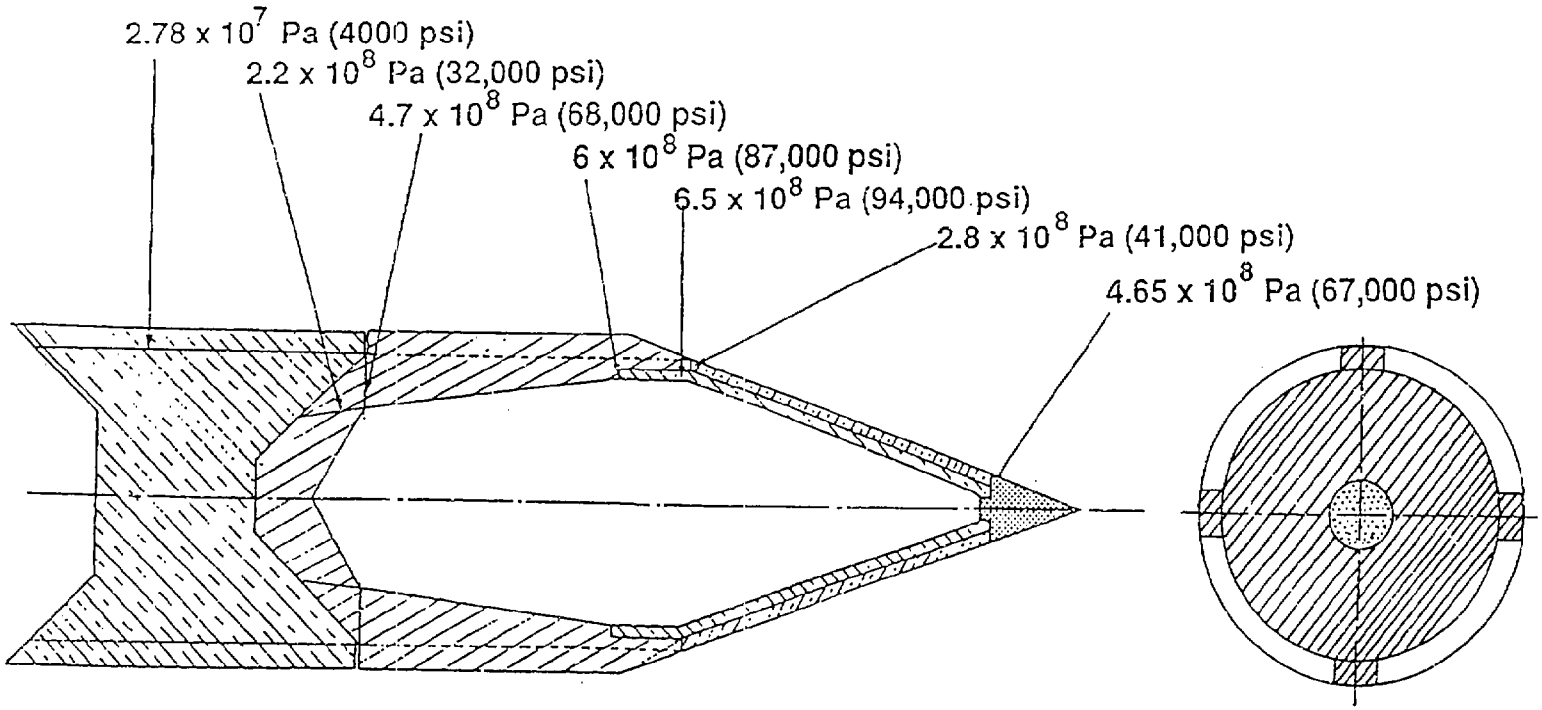

YIELD STRENGTHS

MATERIAL	YIELD
Ti-6Al-4V (Compress)	1 x 10^9 Pa (145,000 psi)
Ti-6Al-4V (Shear)	5 x 10^8 Pa (73,000 psi)
Copper (Compression)	2.8 x 10^8 Pa (41,000 psi)
Polycarbonate (Shear)	3.0 x 10^7 Pa (4,300 psi)

Figure 3-3 Mean Stress at Critical Surfaces at Peak Accelerations

will be produced by machining. The external coating of titanium carbide will be applied by plasma spray and the external surfaces of the centralizers will be produced by lathe turning. The sabot can be produced by simple turning of polycarbonate rod stock.

References

[3.1] Swift, H. F., and D. E. Strange, "Sabot Discard Technology," 38th Meeting of the Aeroballistic Range Association, Tokyo, Japan, October 1987.

[3.2] Barker, L. M., T. G. Trucano, and A. R. Susoeff, "Gun Barrel Gouging by Sliding Metal Contact at Very High Velocities," 39th Meeting of the Aeroballistic Range Association, Albuquerque, NM, October 1988.

[3.3] Personal Communication with L. M. Barker, Sandia National Laboratories, Albuquerque, NM, January 1989.

SECTION 4 - COMPUTATIONAL FLUID DYNAMIC (CFD) ANALYSIS OF THE ODW STABILIZATION EXPERIMENT

4.1 INTRODUCTION

As described in Section 2, Analysis of Hypervelocity Projectile Test Flight, the design of the projectile for generation of (and propulsion by) a weak, overdriven ODW can be achieved by a combination of quasi-one-dimensional control volume analysis, finite-rate chemical kinetics, and boundary layer wall heat flux calculations. Therefore, a major CFD effort was not required to meet the design-of-experiment goal of Phase I.

However, the ultimate research goal is to understand the physics of stabilized detonation waves, in order to assess the benefits which they may offer, or the danger which they may present, to hypersonic flight propulsion systems. While a "tour de force" computational modeling of the entire ram accelerator flowfield is both challenging and interesting -- and has in fact been done by Bogdanoff and Brackett [4.1], by Glenn and Pratt [4.2], and by Yungster, Eberhardt, and Bruckner [4.3] -- the CFD effort must be focused on the gasdynamic and combustion processes which occur in the annulus between projectile body and launch tube wall, the region where the ODW is to be stabilized and investigated.

Specifically, a key question which this research seeks to answer by diagnostic measurement, guided and interpreted by CFD analysis, is under what conditions the reflected oblique shock wave from the launch tube wall may result in one of the following phenomena:

a) No ignition within the annulus (no thrust)

b) Shock-induced combustion: the reactant mixture is ignited by compression ignition, but the induction (chemical ignition delay) time is long compared to convective transit time through the reflected shock wave, so that the compression wave and subsequent combustion wave are decoupled.

c) Weak, overdriven detonation, partial or complete: the induction time is comparable to or less than the convective transit time through the reflected shock, so that some or all of the chemical heat release occurs within the shock wave, thereby altering its structure and strength.

d) Chapman-Jouguet (C-J) detonation, partial: under conditions which would require a complete ODW to be underdriven, and thus unstable, only partial post-induction heat release would occur, of just

sufficient heat release to permit an oblique C-J wave to occur. As the C-J wave is only neutrally stable, possibly severe periodic transient waves (detonation "cells") will laterally traverse the wave front.

While the control volume analysis of Chapter 2 establishes the necessary conditions for stabilization of an ODW, sufficient conditions for the occurrence of cases a, b, c, or d above depend on the complex, coupled interaction of time-dependent gasdynamic, chemical-kinetic, and viscous processes of the reacting gases, thus necessitating analysis by CFD.

4.2 COMPUTATIONAL APPROACH

Two parallel computational modeling strategies have been adopted for the CFD effort. Since the planned initial experiments have been conservatively designed to ensure that a weak overdriven, complete or near-complete ODW will result (Case c above), a computationally efficient, time-steady CFD code with modest spatial resolution should be adequate for interpretation and guidance of these experiments. For future experiments, where test conditions will be chosen to allow investigation of underdriven and/or C-J ODWs to occur (Case d above), a temporal- and spatial-accurate solution of the full, transient Reynolds/Navier-Stokes equation will be required.

4.2.1 Development of a Time-Accurate Transient CFD Code: E2D

If molecular and turbulent viscous stresses are ignored, the Reynolds/Navier-Stokes equations reduce to the Euler equations. A two-dimensional, transient, axial symmetry Euler code E2D is being developed for investigation of oblique C-J detonations [4.4]. In its present form, E2D is limited to a nonreacting flow. A reactive flow version of this code is in the development stage.

Because of the hyperbolic character of the Euler equations for everywhere-supersonic flows, the axial component of flow of information from boundaries is in one direction only, from the inflow to the outflow boundary (that is, the eigenvalues of the Euler equations are all positive.) The hyperbolic character allows the flowfield to be decomposed into streamwise zones as shown in Figure 4-1, where solutions in successive zones depend only on the solution at the outflow boundary of the upstream zone. Such a zonal approach has benefits beyond allowing a large problem to be divided up into more manageable smaller problems. As is shown in Reference [4.4], this approach allows the selective use of special solutions (analytical) for a given zone. The result is improved computational efficiency and accuracy in the solution.

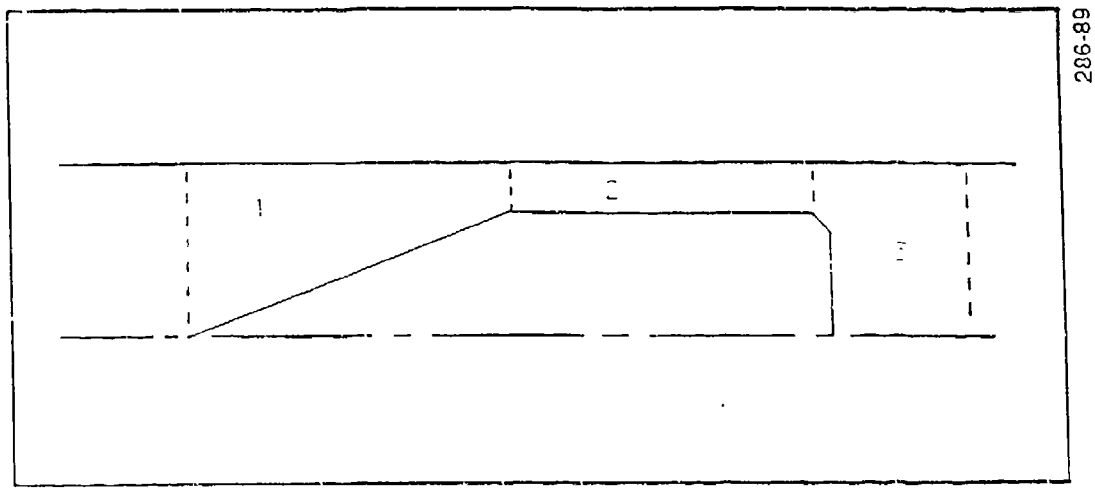

Figure 4-1 Initial Solution Zones

It is reasonable to assume inviscid flow in the forebody and annular zones since the boundary layers (both on the projectile and on the duct wall) are estimated to be vanishingly thin, as was shown in Section 2. The expanding flow over the tail of the projectile is also well described by the inviscid equations: since the flow is supersonic at the outflow of the annulus, the axially increasing flow area causes the gas to accelerate, resulting in a favorable axial pressure gradient. Strong viscous effects occurring after the recompression shock will not influence the net thrust on the projectile, which depends only on surface pressure forces.

Further assumptions include that of ideal gas behavior, a valid assumption for the operating conditions considered. Without chemical reaction, this assumption together with that of inviscid flow allows the use of the classical, "numerically exact" gasdynamic solution for the bow shock over a cone (Taylor-Maccoll solution). Also, since the annular width is small relative to the projectile radius, two-dimensional planar flow in the annulus can be assumed. This additional assumption allows the use of oblique shock theory to verify the predicted angle of the reflected bow shock, and the Prandtl-Meyer solution for the expansion over the cone-cylinder shoulder.

However, once the shoulder expansion wave interacts with the reflected shock, a numerical solution of the governing equations is the only practical way to predict the resulting flowfield. The actual case will of course involve chemical reaction, but by design the reaction must not occur upstream of the first reflected shock. Thus, the solution for the forebody and shoulder expansion wave apply equally well to both the reacting and nonreacting cases.

For computational simplicity the special case is considered where the bow shock reflection is axially coincident with the cone-cylinder interface. The first zone can then be treated entirely with the Taylor-Maccoll solution for inviscid, supersonic, axisymmetric flow over a cone, as described in Section 2.

The solution in the annulus (Zone 2) requires a numerical solution of the complete Euler equations. The axisymmetric form of the equations was used even though the cylindrical effects are small in this zone. Central differencing was used for all interior points, in combination with first-order TVD correction terms [4.4]. Taken together with first-order time differencing, the solution method is overall of first-order accuracy. The Taylor-Maccoll solution was used as the inflow boundary condition and the interior solution was extrapolated for the supersonic outflow boundary. Reflective boundary conditions were used for both walls.

The Prandtl-Meyer solution was initially used as a check on the shoulder expansion in the annular zone. But due to poor conservation of total pressure in the first-order approximated strong expansion, the Prandtl-Meyer solution was eventually imposed as an additional zone in the solution, as is discussed in Section 4.3.1 below. Oblique shock equations were used as a check on the angle of the reflected bow shock.

4.2.2 Efficient Steady-State CFD Code: RPLUS2D

An existing NASA Lewis Research Center CFD code, RPLUS2D [4.5,4.6], has been selected as the "workhorse" for guidance and interpretation of diagnostic experiments. The RPLUS2D program is one of the RPLUS family of CFD codes developed at NASA LeRC. This code has been made available to all NASP (National Aero-Space Plane) contractors and similar permission for its use and required modification has been granted to the University of Washington. The RPLUS codes have been tested on a wide variety of reacting and nonreacting flows and comparisons with experimental data have shown good agreement [4.5,4.6].

The RPLUS2D solution algorithm is computationally efficient. In its vectorized form, only tens of minutes are required to achieve converged solutions on a Cray XMP/48

supercomputer. In its non-vectorized form, RPLUS2D executes in a relatively few hours on VAX class minicomputers. As in all practical implicit schemes, the equations are factored, in this case using the "LU" factorization scheme of Jameson and Turkel [4.7]. Further simplification is achieved by taking the limit as the timestep approaches infinity, so that the converged solution can be achieved by diagonalized Newton iteration. Because of the latter feature, RPLUS2D can be used only for steady-state solutions.

RPLUS2D models all of the basic physics important to the ram accelerator. It solves the two-dimensional Navier-Stokes equations for a reacting gas mixture. Closure of the Reynolds stress term is accomplished with a Baldwin-Lomax algebraic eddy viscosity model with a constant turbulent Prandtl number of 0.9. Turbulence-chemistry interaction effects are not accounted for. The present version is specialized to hydrogen-air mixtures and ideal gas equations of state, and considers a 13-reaction mechanism with 8 species. However, the code is being modified to admit arbitrarily specified gaseous mixtures.

Modifications were made to the as-received code to incorporate the inflow boundary condition as described in Reference [4.4]. This inflow boundary condition results from an inviscid solution and therefore does not give the proper inflow conditions for the viscous simulations that will be described below. This modification will be correctly treated in future work. Also note that axisymmetric terms are not included in the RPLUS2D algorithm and thus the solution is for the 2-D planar case. However, as described previously, this is a good approximation to the annular flowfield. Later solutions for the forebody and plug nozzle flowfield will require that these terms be added.

4.3 COMPUTATIONAL RESULTS

Results using both codes are presented for a single test case, that of inviscid, nonreactive flow with parameters given in Table 4-1. (Note that the Mach number included in Table 4-1 is not an independent parameter as it is calculated from the preceding two parameters.) All results are presented in their dimensionless form. Nondimensionalizing parameters are described in Reference [4.4].

Table 4-1. Assumptions and Parameter Values Used in Solution

Assumptions	Ideal Gas (k=1.4) Inviscid Flow
Freestream temperature (C)	25.0
Projectile velocity (km/s)	2.5
Freestream Mach number	7.3
Cone half angle (degrees)	20.0

4.3.1 Results with F2D

To minimize computer time, initial test cases were run with an annular aspect ratio (annular length:annular width) of 1:1 and a grid density of 61 x 51 points. The grid is shown in Figure 4-2. A plot of Mach number contours for the converged solution is shown in Figure 4-3. The reflected bow shock is clearly defined in the upper portion of the grid. A drawn-in line representing the angle from an oblique shock wave chart agrees well with the computed result. However, the expansion fan shown at the bottom of Figure 4-3 is smeared downstream and poorly simulated. The true expansion wave would be fan-like in appearance and emanate from the cone cylinder interface (the bottom left corner of Figure 4-3). Using the Prandtl-Meyer solution, the flow should be expanded to a Mach number of 6.4. Figure 4-3 shows an expansion to only Mach 5.4. The results for the expansion wave were improved only slightly when the grid density was doubled.

This difficulty in treating a shoulder expansion wave is due to at least two things. First, the shoulder represents a singular point in the flow, and representing such a point with a finite difference grid will always give problems. The obvious remedy is to increase the grid density, perhaps locally, but this is very inefficient since a vastly refined grid would be required. The second reason for the poor resolution is that the numerical algorithm treats the

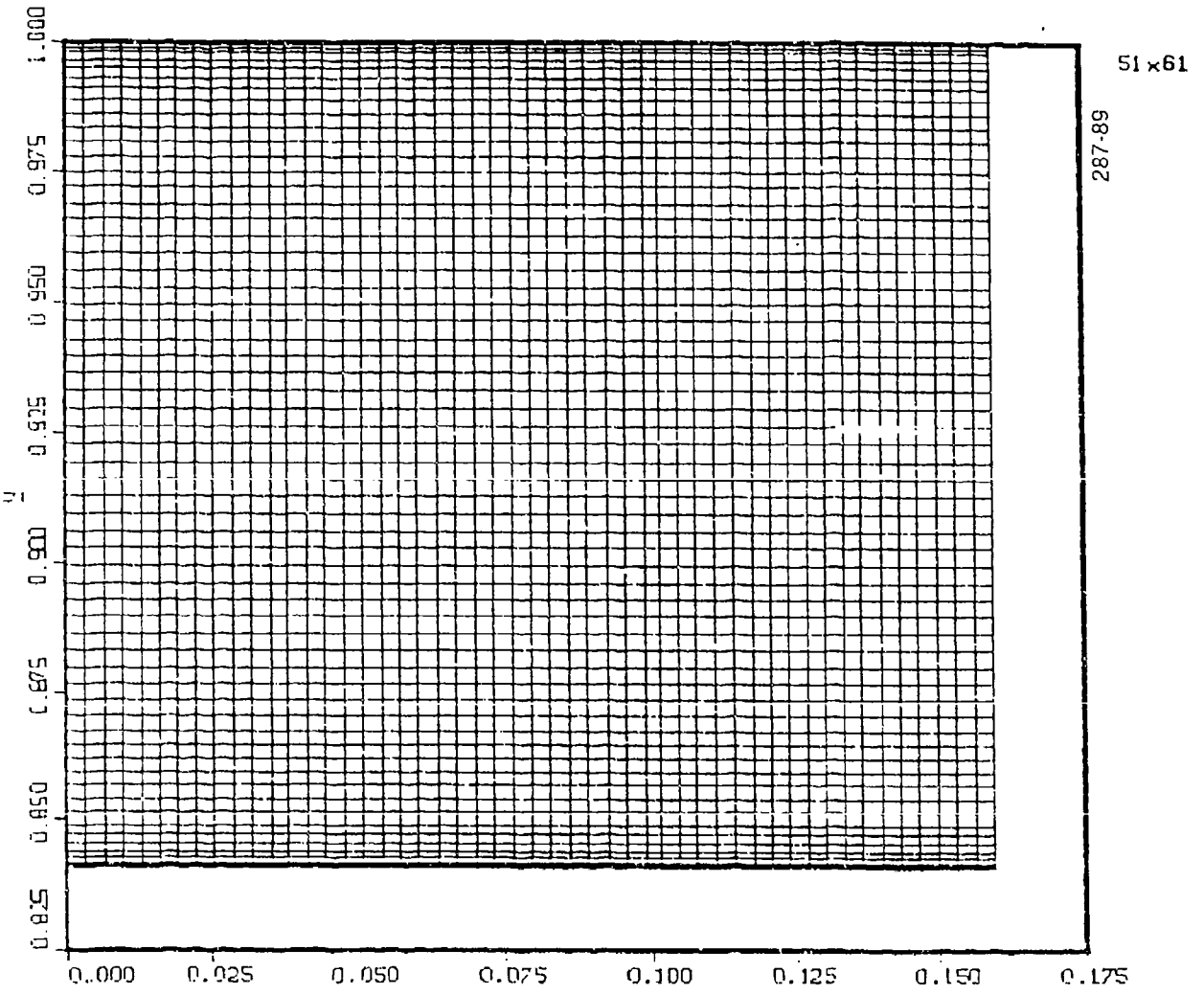

Figure 4-2 Grid Used for Test Case

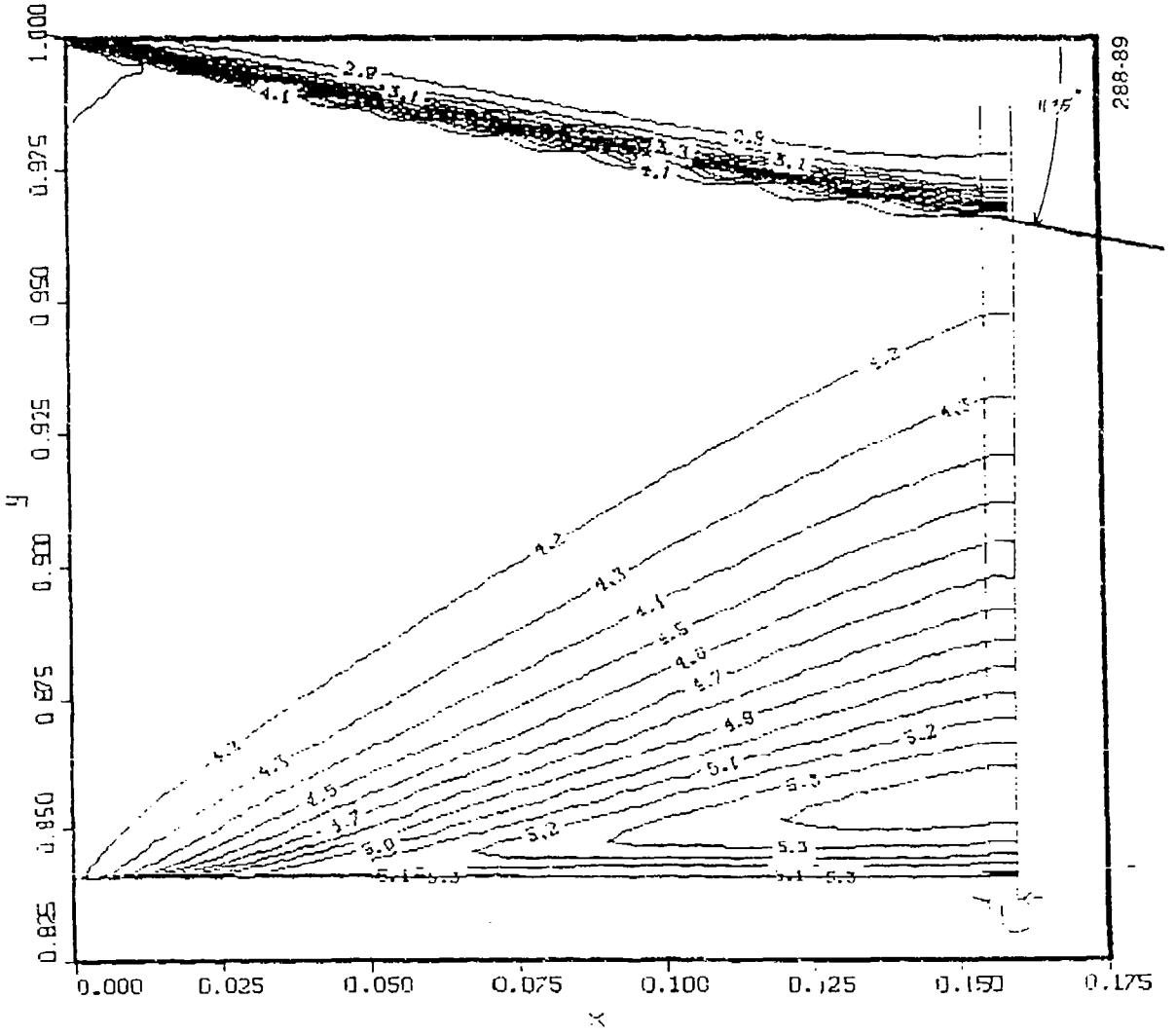

Figure 4-3 Mach Number Contours for Test Problem

expansion wave in each cell as a single discontinuity, not the true expansion fan; again the limits of a finite difference solution. A true Riemann solver such as the well-known Godonov method may help in this instance, but there too the exact nature of the solution is lost since averages must be taken over the cell boundary.

Woodward and Colella [4.8] addressed the problem of the numerical error at the corner of a step by applying an additional boundary condition near the corner of the step. In computational cells in the neighborhood of the shoulder they "reset the density so that the entropy has the same value as in the [cell] just to the left and below the corner of the step," and also "reset the magnitudes of the velocities, not their directions, so that the sum of enthalpy and kinetic energy per unit mass has the same value as in the same [cell] used to set the entropy." While this may have given "consistent" results for the various schemes being compared, it is not apparent that it gives the correct results.

To correct the shoulder expansion problem in the present solution, the shoulder region was treated as a separate zone where the Prandtl-Meyer solution was imposed in place of the finite difference solution. Again, other than the assumption of locally two-dimensional flow, this is an exact solution. The modified zone map is shown in Figure 4-4. The solution with the added Prandtl-Meyer zone is given in Figure 4-5.

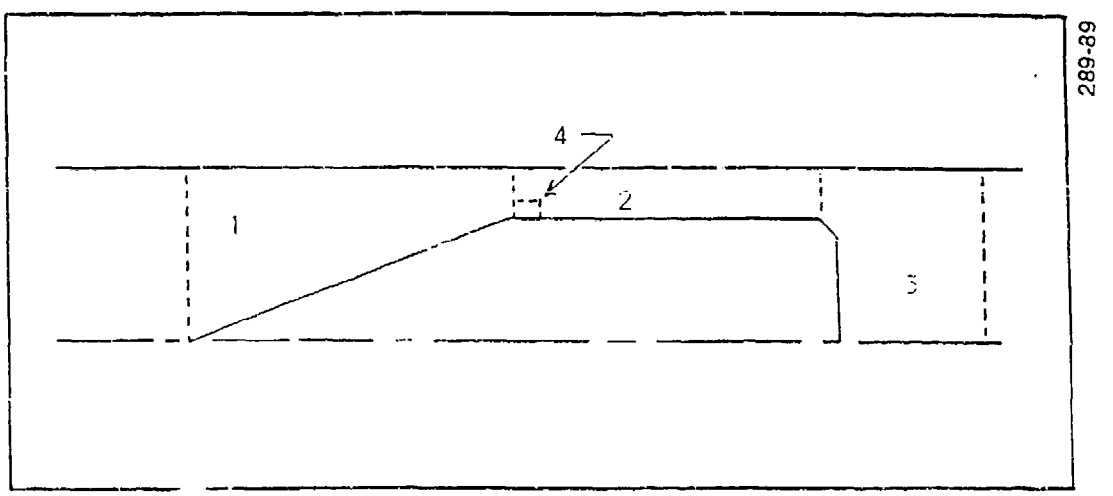

Figure 4-4 Prandtl-Meyer Solution Imposed in Zone 4

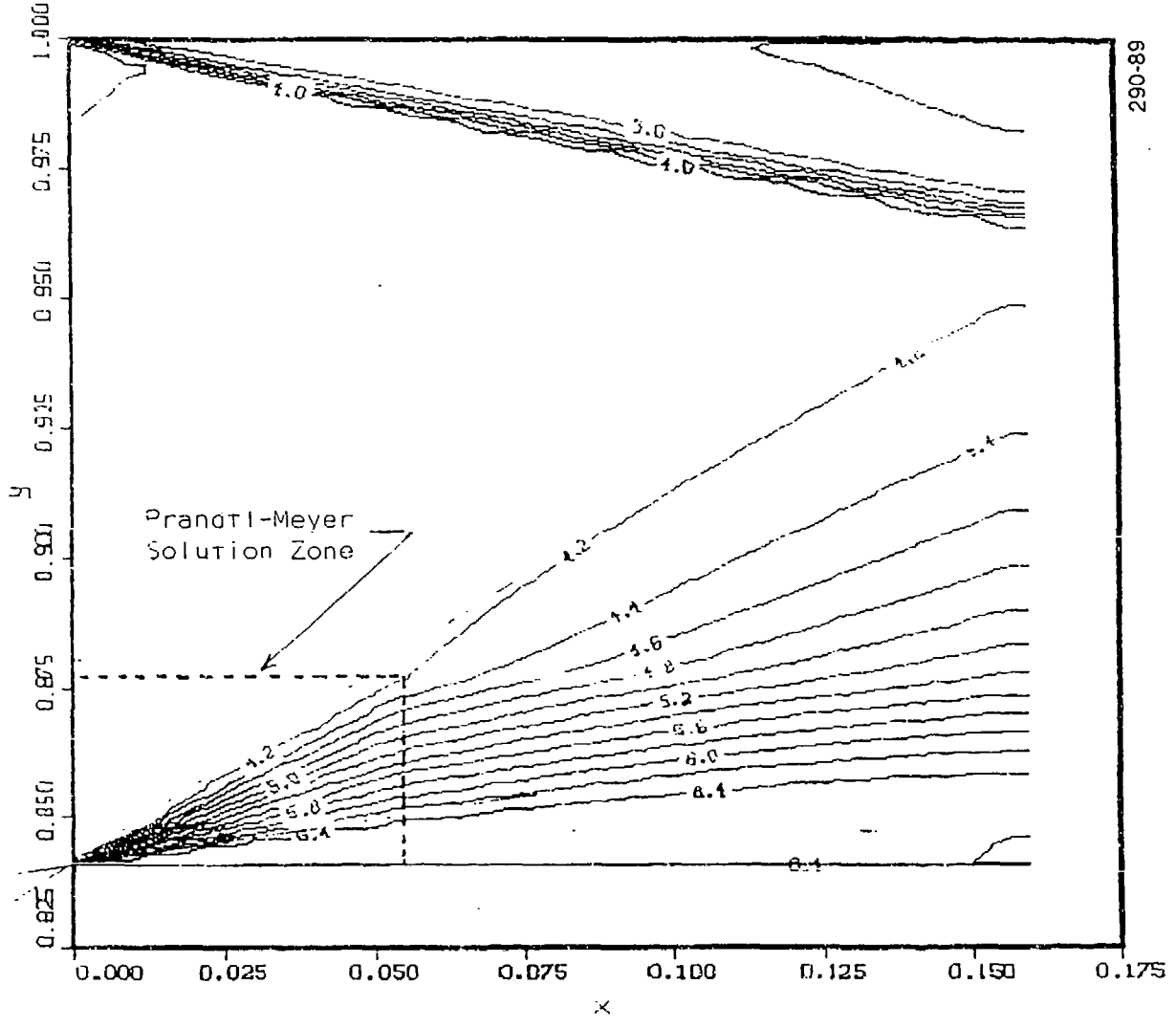

Figure 4-5 Result with Prandtl-Meyer Solution Applied in Shoulder Zone

(The points treated with the analytical solution are noted in the figure.) While the portion of the expansion fan given by the numerical solution is still less than ideal, it represents a vast improvement over the previous result (Figure 4-3).

Static and stagnation pressure contours for the improved solution are shown in Figures 4.6 and 4.7. The static pressure contours look plausible, but there is an obvious problem with the stagnation pressure downstream of the Prandtl-Meyer solution zone. Since expansion waves are isentropic, stagnation pressure should be preserved. The nonphysical decrease in stagnation pressure observed in the solution is apparently related to the poor treatment of expansion waves by the solution algorithm. A solution to this problem has not yet been identified. Harten [4.9] has demonstrated a high degree of "entropy enforcement" in his second-order scheme. Comparison tests between Harten's scheme and the present first-order scheme should be performed.

Finally, with no further change to the solution algorithm or run parameters, a run was made with an annular aspect ratio of 5. The converged solution results are given in Figures 4-8 and 4-9 for Mach number and static pressure contours, respectively. The interaction of the expansion wave and reflected bow shock results in the expected curvature in the shock wave. The shock waves are well defined and the use of the Prandtl-Meyer solution gives a well-represented expansion wave. The residual norm is shown plotted in Figure 4-10. Convergence to a steady solution was achieved with approximately 1300 iterations with a time step of 2.E-4. This required just under 7 hours of execution time on a DEC VAXstation 3200 computer.

4.3.2 Preliminary Results with RPLUS2D

Results are presented for the identical case investigated with the E2D code (Table 4-1). A single run using viscous terms and associated wall boundary conditions is included for comparison. A gaseous flow of air was specified through a small value for the fuel/air equivalence ratio (phi = 0.01) and the reacting flow option was not used. This is not very efficient since all the species equations must be carried along without being changed. Nonetheless, this gives the desired comparison between the two codes. As before, initial runs were made for a 1:1 aspect ratio, though in this case limiting the grid resolution to a 39 x 39 computational mesh. The results in Figures 4-11 through 4-13 present results for Mach number, static pressure and stagnation pressure, respectively.

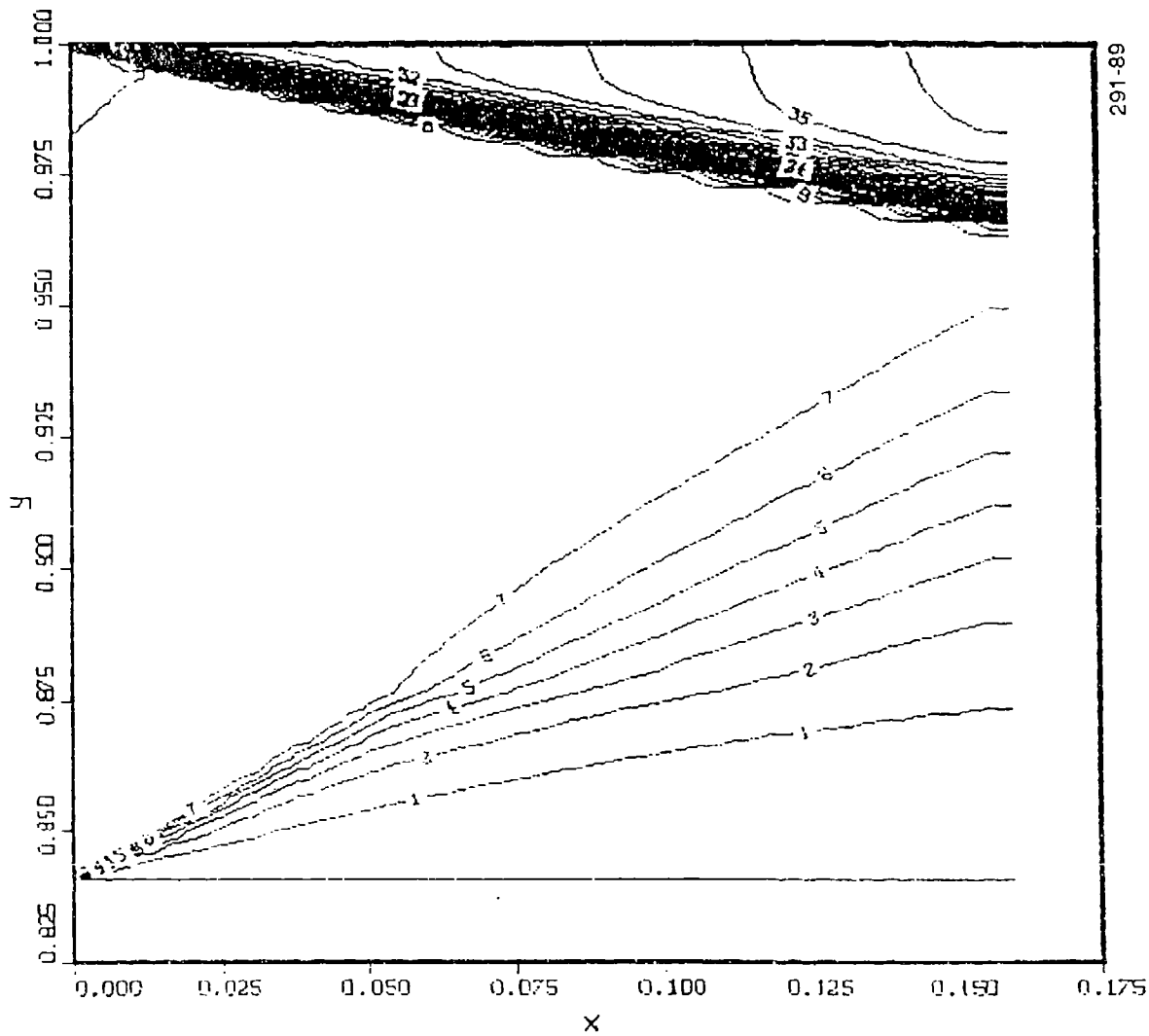

Figure 4-6 Static Pressure Contours

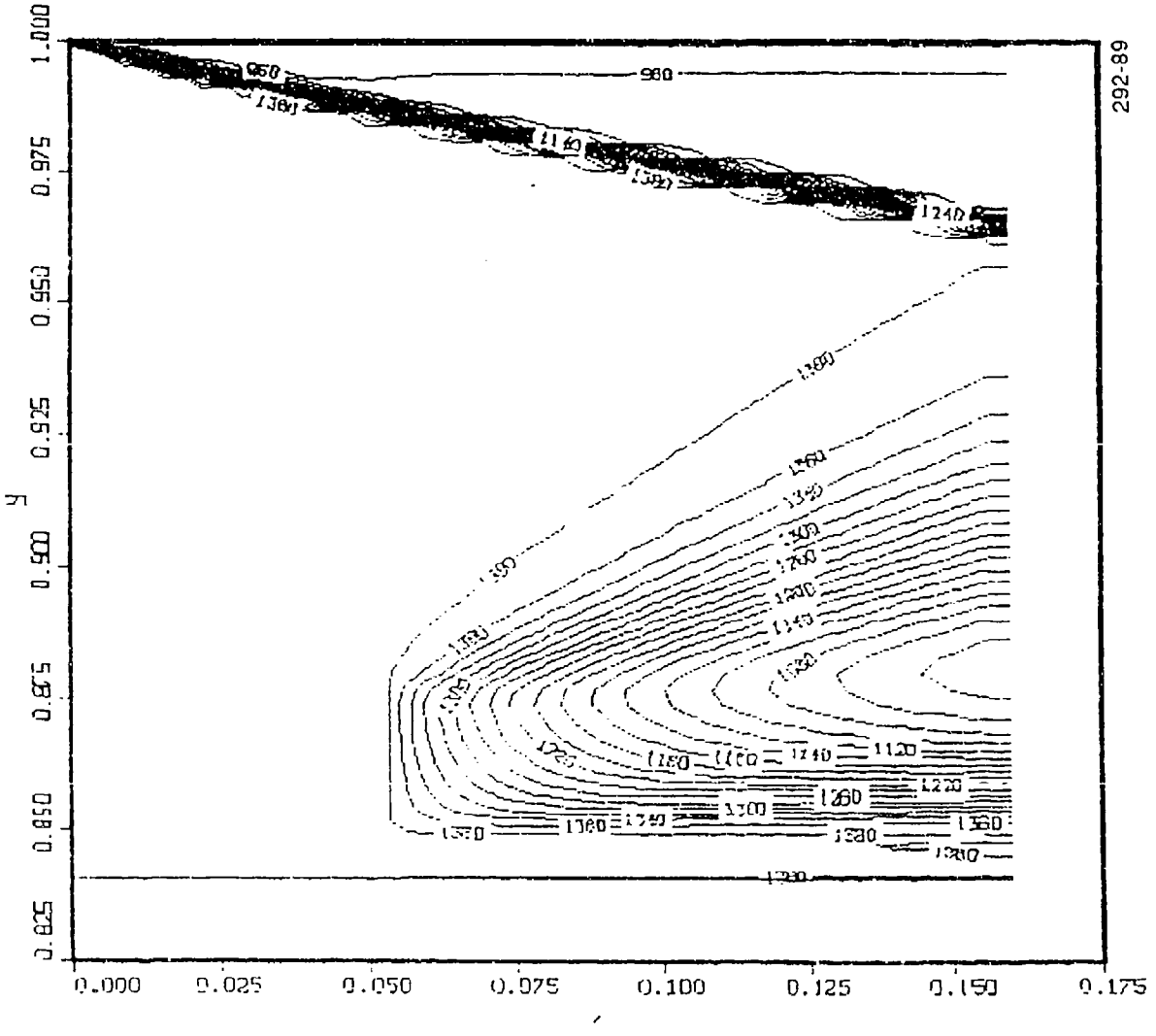

Figure 4-7 Stagnation Pressure Contours

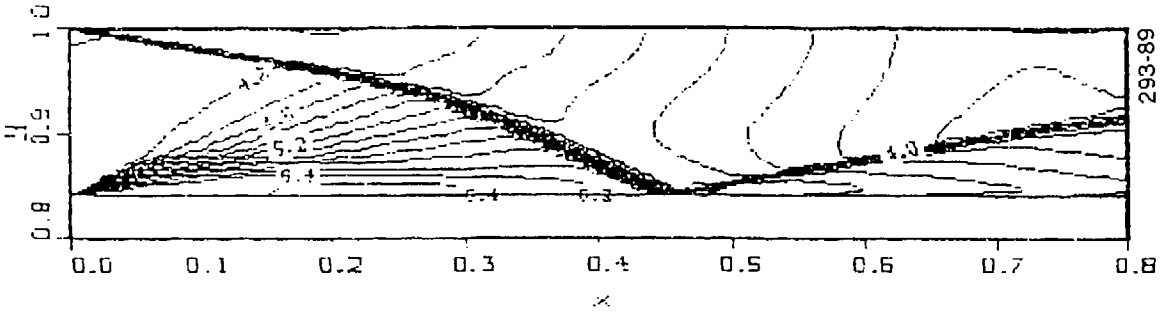

Figure 4-8 Mach Number Contours for 5:1 Aspect Ratio

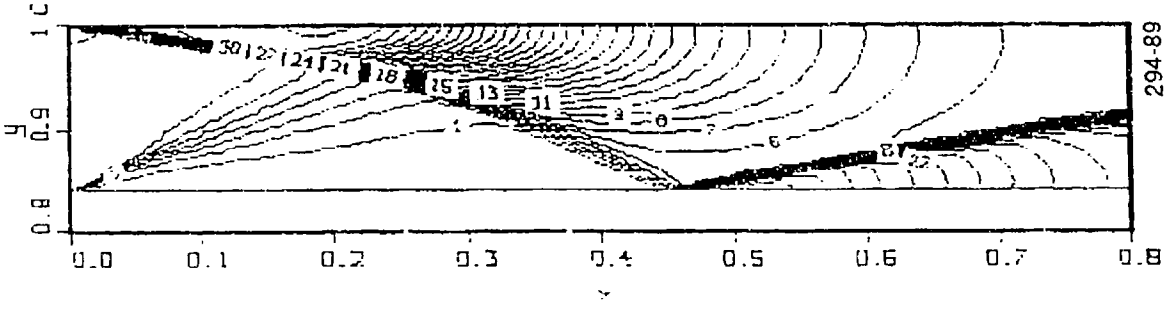

Figure 4-9 Static Pressure Contours for 5:1 Aspect Ratio

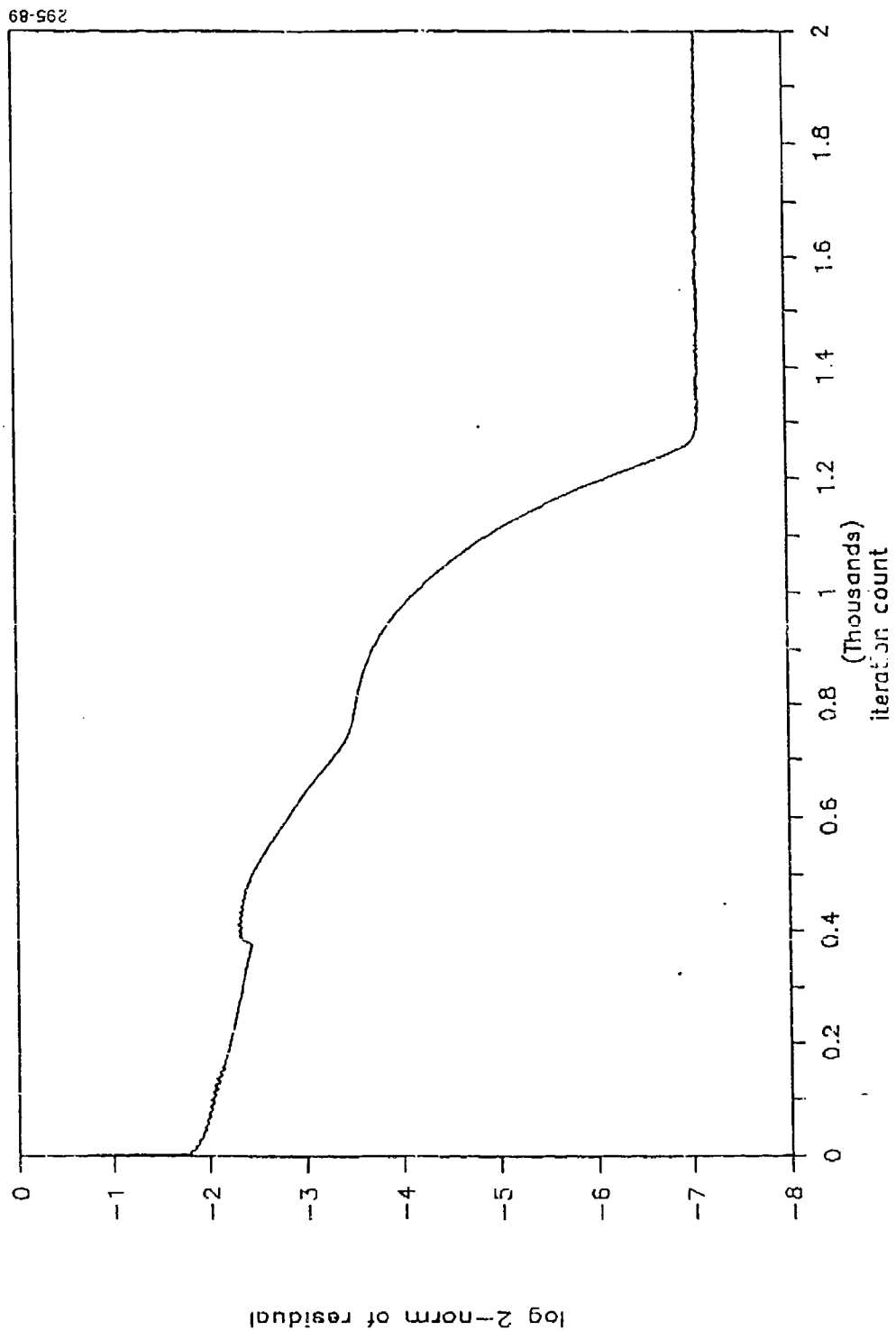

Figure 4-10 Convergence History, Annular Flow Field, Reflective b.c.

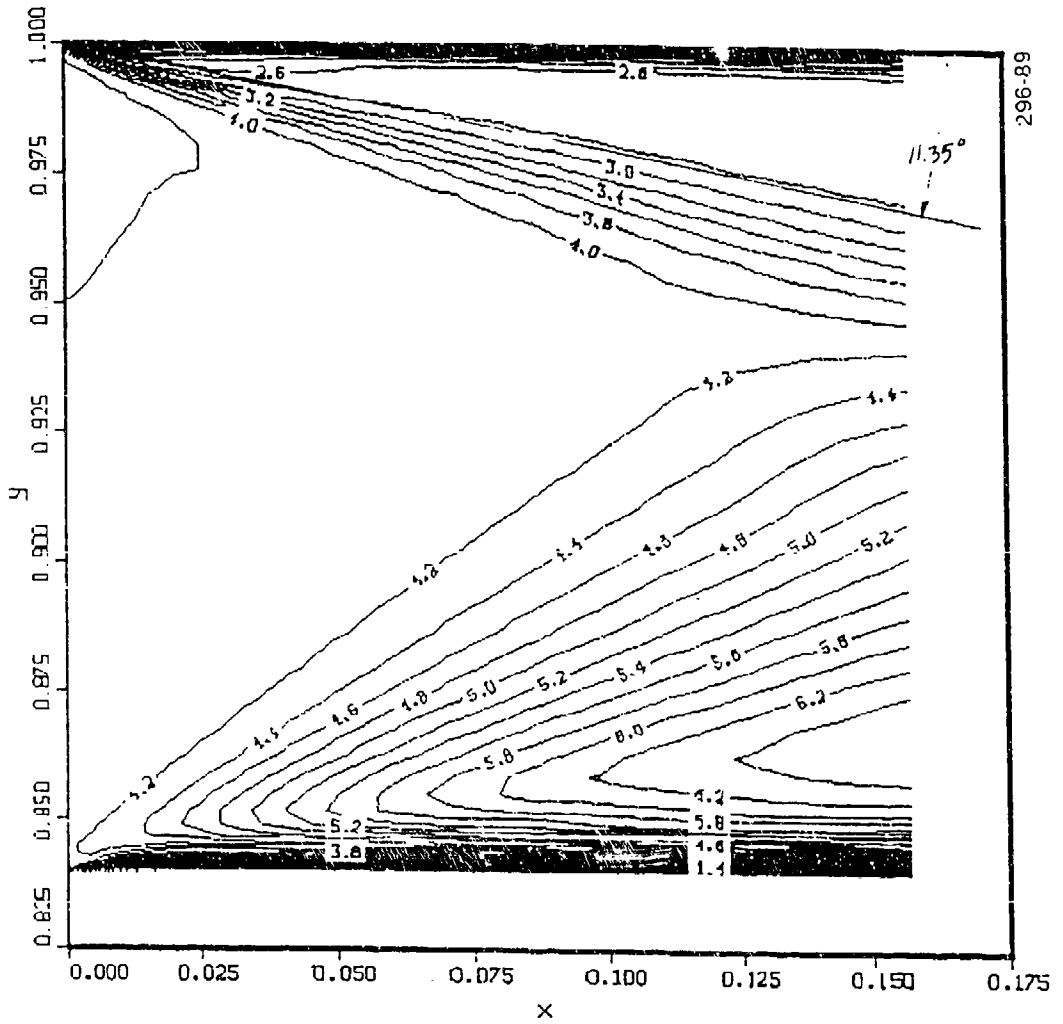

Figure 4-11 Mach Number Contours
(inviscid, RPLUS2D)

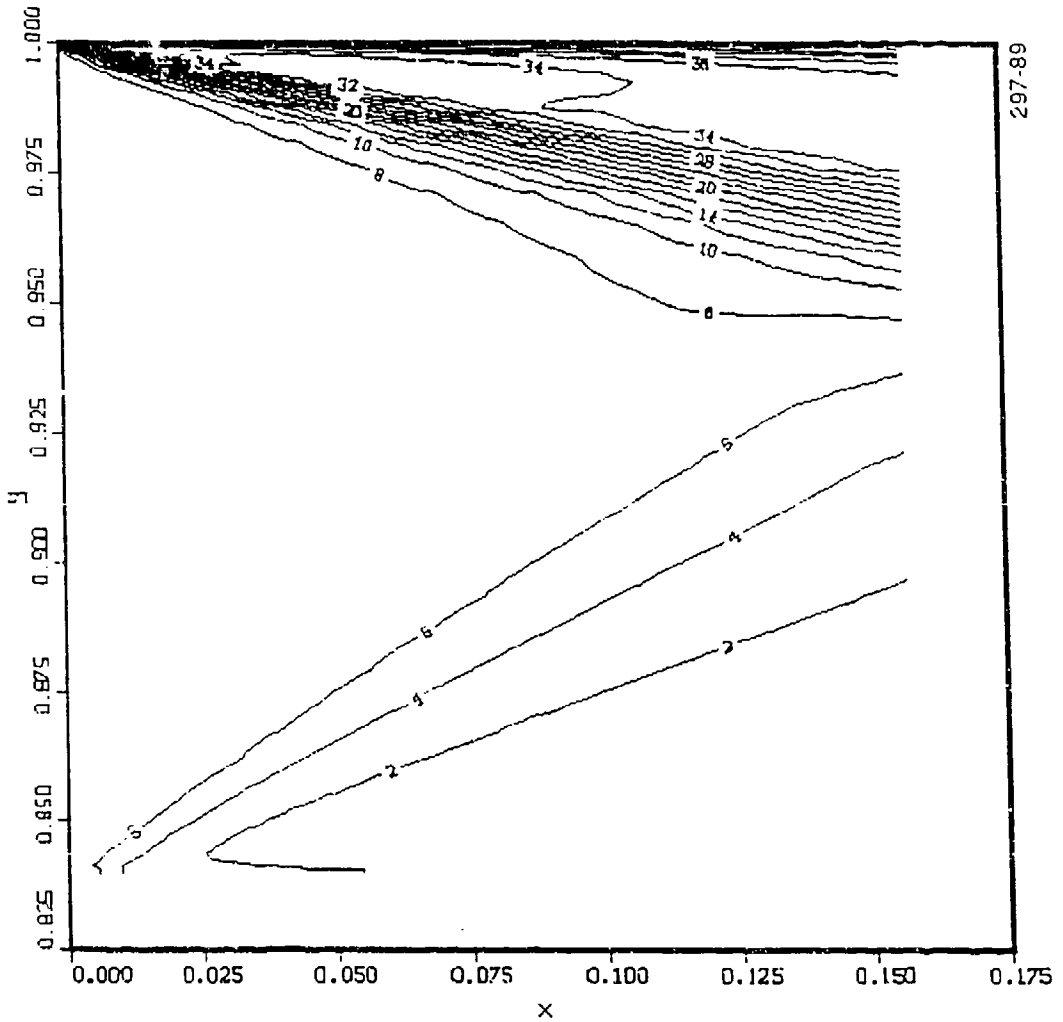

Figure 4-12 Static Pressure Contours
(inviscid, RPLUS2D)

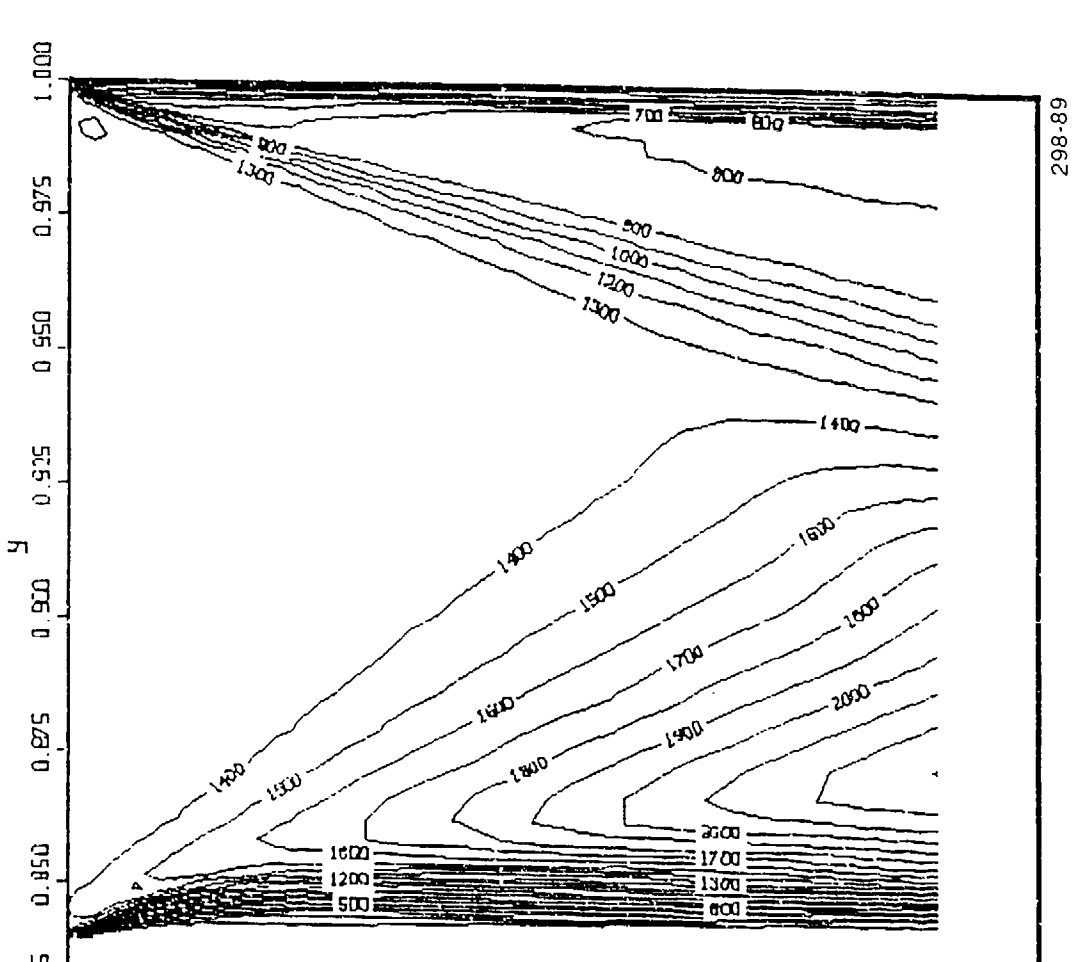

Figure 4-13 Stagnation Pressure Contours
(inviscid, RPLUS2D)

Figure 4-11 can be compared directly with results from E2D in Figure 4-3. Several observations can be made. First, the shock predicted by RPLUS2D is significantly more smeared, even if one allows for the coarser mesh. Furthermore, the shock angle is not well predicted as is evidenced by the exact value shown in Figure 4-11 (11.35° from horizontal). Only the final contour matches this value in the RPLUS2D solution, whereas the E2D predicted shock is smeared nearly equally to both sides of this value. The second observation is the overall poor representation of the expansion fans given by both codes. The RPLUS2D result is, however, much better in terms of the degree of expansion predicted (RPLUS2D giving the exact value of Mach 6.4 versus Mach 5.4 for E2D). The expansion fan problem was addressed with E2D by imposing the analytical solution in the shoulder region. This "fix" has not been made in RPLUS2D. Another observation is that of the thick numerical boundary layer present on both wall boundaries of the RPLUS2D solution. This behavior is present in all of the inviscid solution results with this code and is apparently a problem with the boundary condition, as will be shown directly.

First, however, consider Figure 4-13 which shows contours of stagnation pressure. As in the E2D solution, stagnation pressure (thus entropy) is not preserved through the expansion fan. One great difference is that stagnation pressure is seen to increase in the RPLUS2D solution. Although neither an increase nor a decrease is acceptable, the increase does seem more unsettling. A decrease might be explained through arguments of numerical dissipation, but an easy explanation for an increase is not immediately apparent. Magnitudes of change are significant in both cases and are of the same order.

Addressing the problem of the inviscid boundary condition, the same solution was repeated for the viscous case and results are shown in Figure 4-14. When compared with the inviscid case (Figure 4-11), there is a difference between the two, albeit a very small one. Noting that the boundary layer should be very thin since the upstream solution is inviscid, this is not a very conclusive comparison. A substantial comparison is given using the test problem provided with RPLUS2D, uniform Mach 4 flow over a 10° ramp. The grid is illustrated in Figure 4-15. Mach number contours for the viscous and inviscid cases (both nonreacting) are given in Figures 4-16 and 4-17, respectively. Both walls are initially parallel to the flow. While weak shocks off the developing boundary layer are expected in the viscous solution, there should be none in the inviscid case. Figure 4-16 shows the expected behavior for the viscous case, but the inviscid result in Figure 4-17 is clearly incorrect. A close examination of the code is required to see why this is occurring.

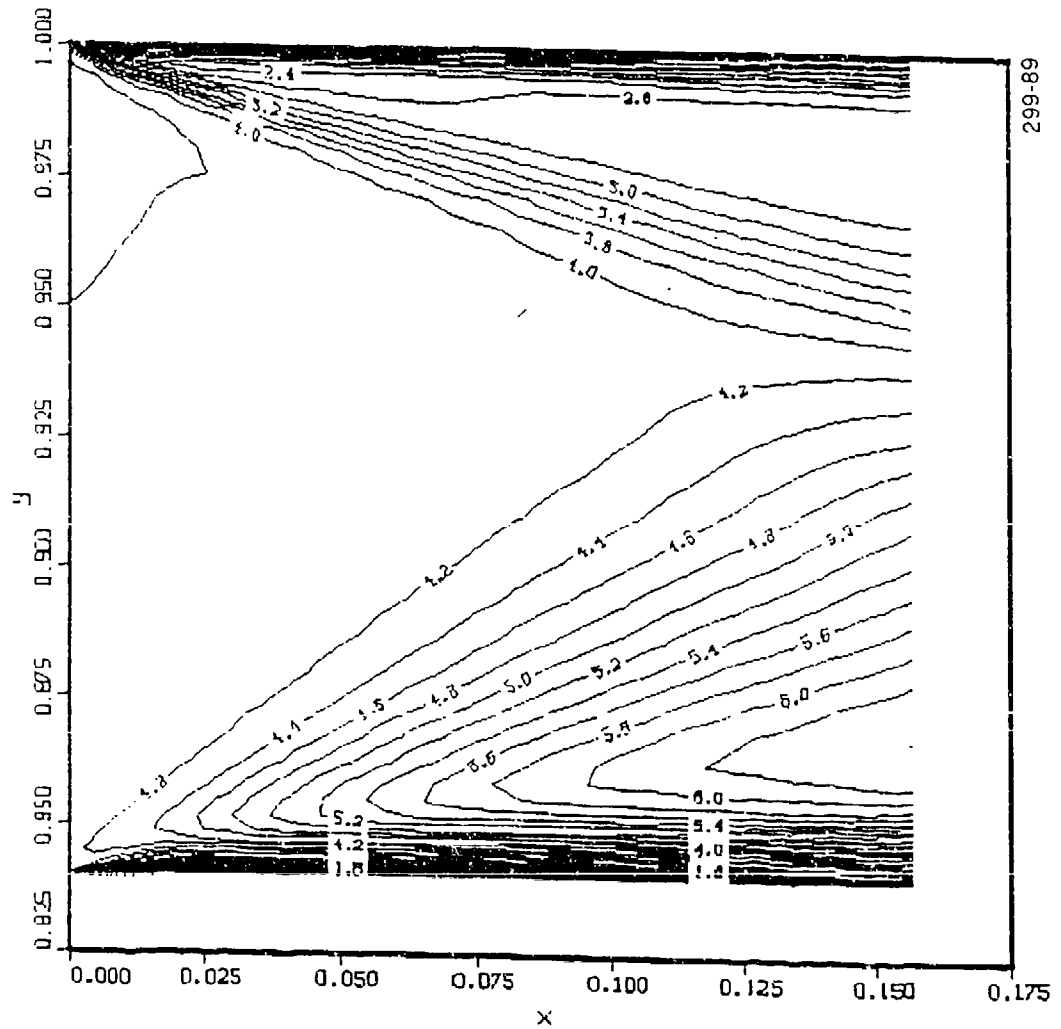

Figure 4-14 Mach Number Contours
(viscous, RPLUS2D)

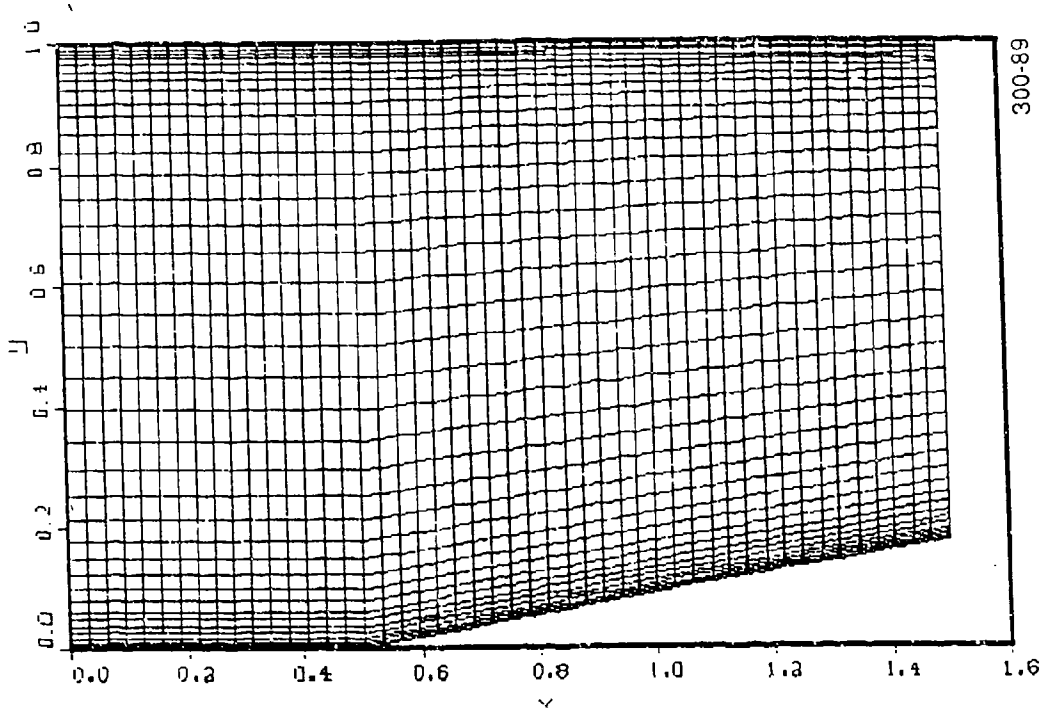

Figure 4-15 Grid for RPLUS2D Test Problem
(49 x 39, 10 deg. ramp)

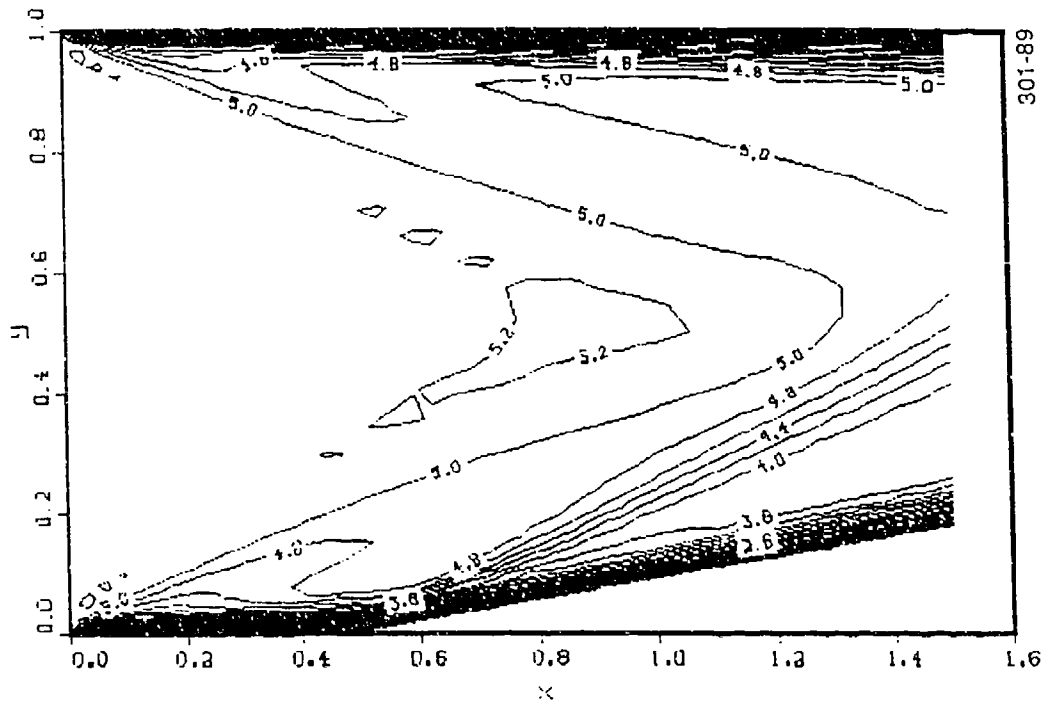

Figure 4-16 Mach Number Contours for Test Problem
(Mach 4 inflow, viscous nonreacting)

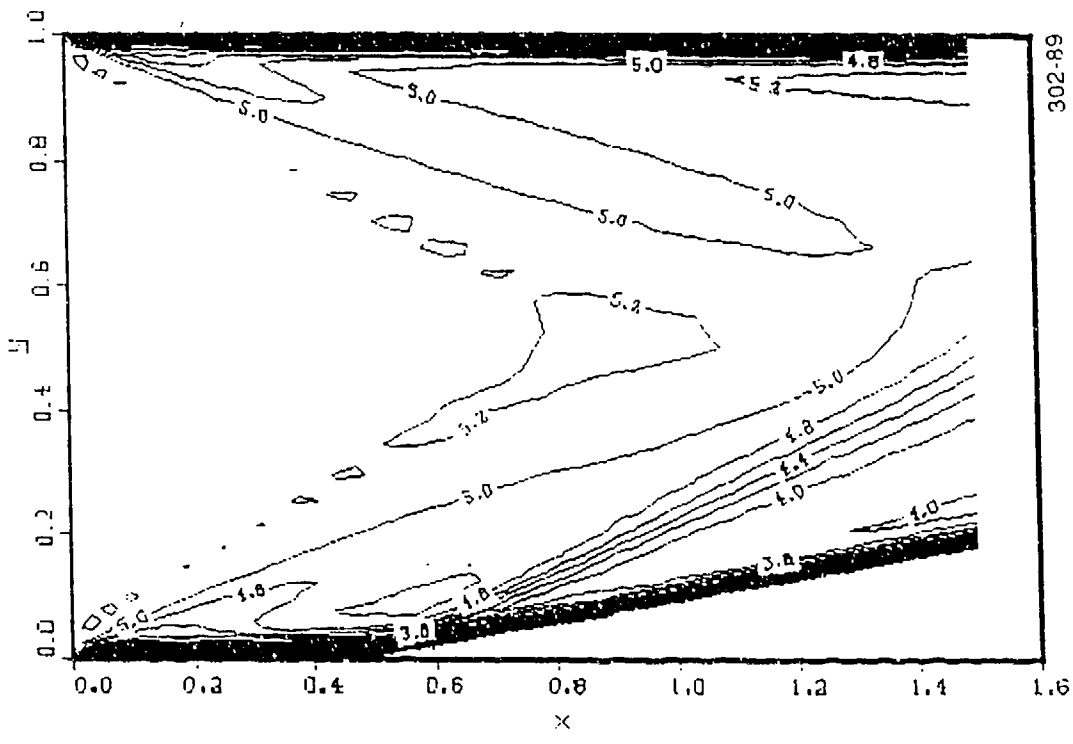

Figure 4-17 Mach Number Contours for Test Problem (Mach 4 inflow, inviscid, non-reacting)

4.4 CONCLUSIONS FROM CFD ANALYSIS

Numerical solutions were performed for inviscid, supersonic, nonreactive flow over a cone-cylinder projectile located axisymmetrically within a uniform radius circular duct. A zonal solution approach allowed for the most efficient treatment of various parts of the flowfield. Two CFD codes were used. In the E2D code, numerical errors in the shoulder region were eliminated by imposing an analytical solution in that region. The result shows an accurately represented and well-defined series of reflected shocks in the annulus. Preliminary results for the RPLUS2D code show a more smeared and less accurate shock than predicted. This is most likely due to the 2D algorithm being based on a more accurate total variation diminishing (TVD) numerical scheme. In both codes, stagnation pressure (therefore entropy) was not preserved through the expansion fan. RPLUS2D gave an increase in stagnation pressure as opposed to a decrease of similar magnitude using E2D. Finally, a problem was noted with the inviscid boundary condition in RPLUS2D since parallel flow to a planar wall resulted in shocks.

4.5 PLANS FOR FUTURE WORK

As described previously, the use of the time-steady code RPLUS2D is proposed for the bulk of the experimental design and analysis. The inviscid boundary condition problem must be resolved and a couple of modifications must be made before the code is put to work. These modifications include the addition of axisymmetric terms and the addition of generalized gaseous fuels capability.

Development of the transient code will continue for use in later investigation and analysis of nonsteady phenomena. For the non-reactive case, the first task is the search for and testing of an alternative solution algorithm to improve the treatment of expansion waves. Harten's second order scheme has been identified as one option. The second task is the addition of viscous terms to investigate the influence of boundary layers.

For the reactive case, a two-stage investigation is proposed. The first stage will follow the approach taken in a related computer simulation of a ram accelerator as described in [4.2]. In that simulation, a one-parameter induction time model due to Oran et al. [4.10] was used to determine the onset of chemical heat release following the induction or ignition delay reactions, following which the gases were assumed to instantaneously achieve chemical equilibrium. To minimize the computational burden of computing the fully detailed finite-rate chemical kinetics in the computational flowfield, the next stage will employ a two-regime model due to Korobeinikov [4.11], as recently used in a related problem by Fujiwara [4.12].

References

[4.1] Bogdanoff, D.W., and D.C. Brackett, "A Computational Fluid Dynamics Code for the Investigation of Ramjet-in-Tube Concepts," Paper No. AIAA-87-1978, AIAA/ASME/SAE 23rd Joint Propulsion Conference, San Diego, California, 29 June-2 July 1987.

[4.2] Glenn, D.E., and D.T. Pratt, "Numerical Modeling of Standing Oblique Detonation Waves," Paper No. AIAA-88-0440, AIAA 26th Aerospace Sciences Meeting, Reno, Nevada, 11-14 January 1988.

[4.3] Yungster, S., S. Eberhardt, and A.P. Bruckner, "Numerical Simulation of Shock-Induced Combustion Generated by High-Speed Projectiles in Detonable Gas Mixtures," Paper No. AIAA-89-0673, AIAA 27th Aerospace Sciences Meeting, Reno, Nevada, 9-12 January 1989.

[4.4] Fort, J.A., and D.T. Pratt, "Supersonic Flow Over a Cone-Cylinder Projectile Confined Within a Circular Duct, Part I - Non-Reacting Flow Over the Forebody and Annulus," University of Washington, 10 January 1989.

[4.5] Shuen, J.S., and S. Yoon, "Numerical Study of Chemically Reacting Flow Using an LU Scheme," NASA TM 180882, and AIAA-88-0436, 1988.

[4.6] Yu, S.T. et al., "Three-Dimensional Calculation of Supersonic Reacting Flows Using an LU Scheme", Paper No. AIAA-89-0391, 1989.

[4.7] Jameson, A. and E. Turkel, "Implicit Schemes and LU Decompositions," Math. Comp. 37, 156, pp. 385-402, October 1981.

[4.8] Woodward, P. and P. Colella, "The Numerical Simulation of Two-Dimensional Fluid Flow with Strong Shocks," J.Comp.Phys., vol. 54, pp. 115-173, 1984.

[4.9] Harten, A., "High Resolution Schemes for Hyperbolic Conservation Laws", J.Comp.Phys., vol. 49, pp. 357-393, 1983.

[4.10] Oran, E. et al., "Numerical Simulations of Detonations in Hydrogen Air Mixtures," in Proceedings of the Eighteenth International Symposium on Combustion, 1981.

[4.11] Korobeinikov, V.P. et al., "Propagation of Blast Waves in a Combustible Gas," Astronautica Acta, 17, pp. 529-537, 1972.

[4.12] Fujiwara, T., and Matsuo, A., "A Two-Dimensional Detonation Supported by a Blunt Body or Wedge," AIAA-88-0098.

SECTION 5 - DESIGN OF TEST FACILITY

We have designed in concept an experimental assembly that will allow confirmation of the establishment of a stable oblique detonation wave (ODW). Because the experiment involves the use of hydrogen, and because some of the processes are experimental, we have designed the apparatus in the expectation that it will be installed in an outdoor, remote facility. For descriptive purposes the apparatus may be divided into six subassemblies:

1. The Wave Gun
2. The propelling gas dump section
3. The sabot strip section
4. The stripping gas and combustion products dump section
5. The oblique detonation wave section
6. The recovery section

Items 2, 3, and 4 are physically combined into a single unit, so they are discussed together. The function and some design parameters of each of these assemblies are discussed in the sections that follow. Figure 5-1 shows a conceptual design of the experimental assembly.

5.1 WAVE GUN

The Wave Gun is a variation of a two-stage light-gas gun that has been developed by Astron as a hypervelocity launcher. The characteristics of the gun are suitable for accelerating a projectile to a velocity appropriate for study of the ODW phenomenon. The theory and some experimental results of Wave Gun development are given in Reference [5.1, 5.2]. Our description of the function of Wave Gun in this report will be cursory; the reader is referred to one of these references for a more complete discussion.

Figure 5-2 is an engineering assembly of the 30-mm Wave Gun proposed for use in the ODW experiments. It shows in detail the component parts of this device. Near the breech end of the assembly is a volume known as the powder chamber. This volume is filled with a cannon powder such as is typically used in artillery applications. The downstream end of this region is closed by a plastic piston that is threaded into the chamber. The piston serves to separate the chamber from a volume of pressurized light gas and to confine the burning powder to the chamber until the

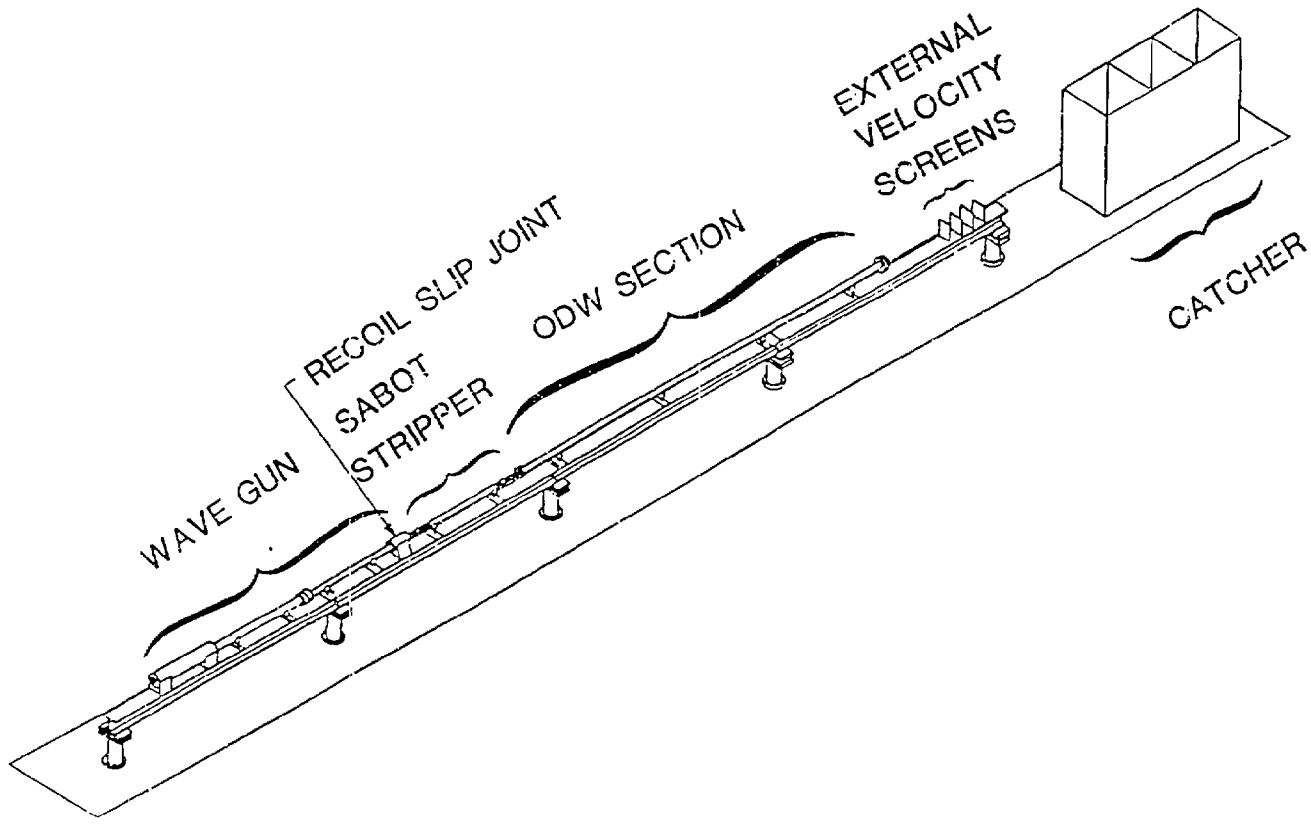

Figure 5-1 Schematic Depiction of the Major Facility Components

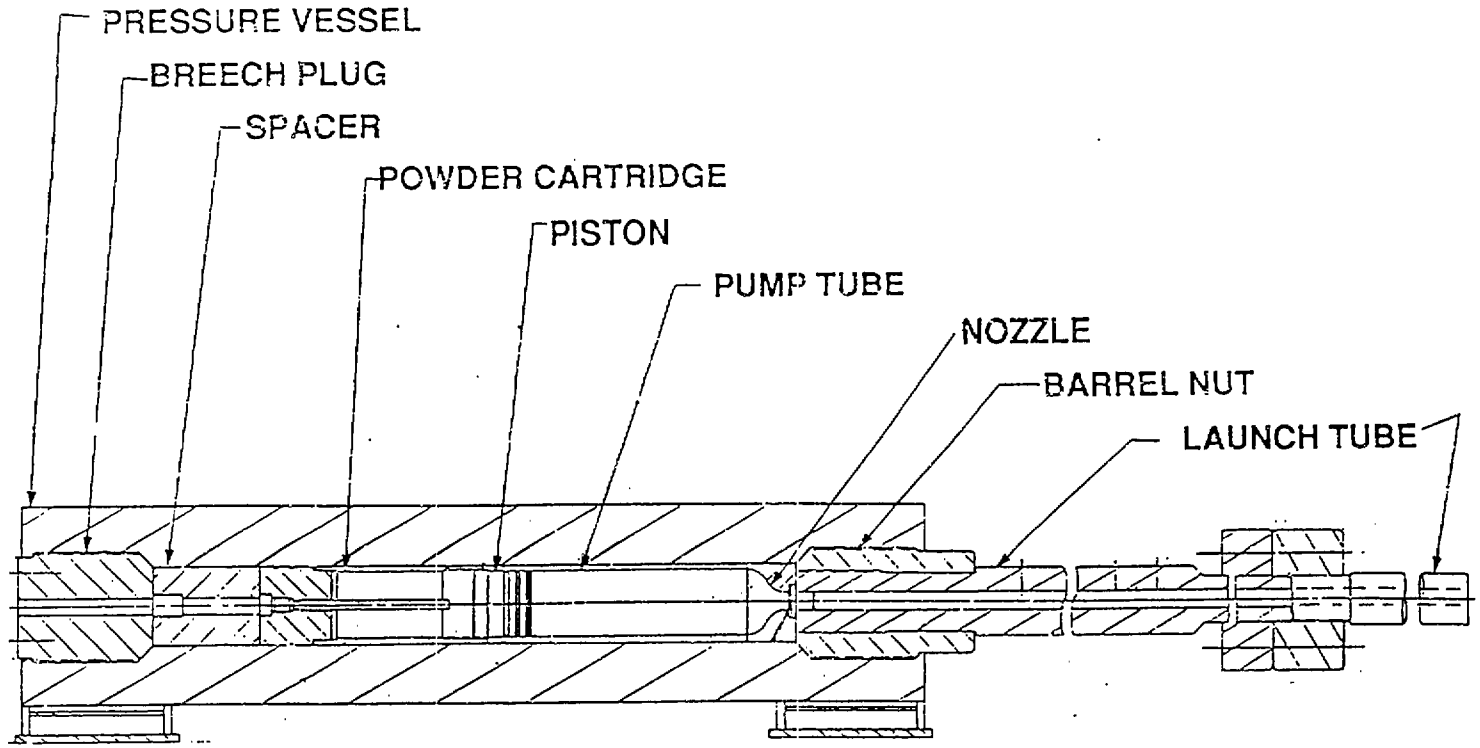

Figure 5-2 Wave Gun Assembly

pressure has risen sufficiently to shear the threads restraining it. In our experiments to date, the light gas has been helium, although, for some purposes hydrogen will be more effective. When the piston threads have been sheared, the piston begins to move thereby compressing the light gas and, since the piston is quite light and moves out quickly, the pressure in the powder chamber is reduced. Ultimately, the pressure in the light gas becomes high enough to stop and reverse piston motion thereby increasing pressure and, consequently, burn velocity in the propellant powder.

At some time in this process the pressure in the light gas becomes high enough to break a restraint which is retaining the projectile. The oscillatory piston motion continues until the powder is fully consumed and/or all of the light gas is forced from the pump tube into the launch tube. For the proposed experiment, this device will accelerate a projectile package to about 2.5 km/s.

5.2 RECOIL ABSORBING JOINT

The joint between the Wave Gun launch tube and the dump and strip tube is designed to isolate recoil of the Wave Gun from the remainder of the experimental assembly. Figure 5-3 shows a conceptual drawing of the joint. Several functions are accomplished within this unit. First, the diaphragm that separates the evacuated launch tube from the atmospheric dump tube is mounted within this unit. Second, the connection to the vacuum system is made in the assembly. Third, the unit is firmly attached to the mounting beam to provide a fixed anchor for all of the downstream hardware, and fourth, the piece provides a means for maintaining an alignment between the bore of the launch tube and the bore of the dump/strip tube to which it abuts. The design allows a recoil of several inches to occur before the sealing and the alignment functions are lost.

5.3 SABOT SEPARATION

The projectile will be launched with a sabot as described in Section 3. The sabot must be separated from the projectile before it enters the test section so that the sabot will not disrupt the flowfield in the test section. The projectile and sabot will experience the following flight history. They will be accelerated in the evacuated Wave Gun barrel by a helium driver gas. The projectile and sabot will pass through a diaphragm located at the end of the Wave Gun barrel, and driver gas will be vented in the driver gas venting section. The sabot will be separated from the projectile as they pass through an axial gasdynamic sabot separation section. The axial gasdynamic sabot separation section gas will be vented in the sabot separation venting section. The projectile will burst through a diaphragm and enter the test section where it will be accelerated. Then it will exit the test section through a diaphragm and be stopped in the catcher section.

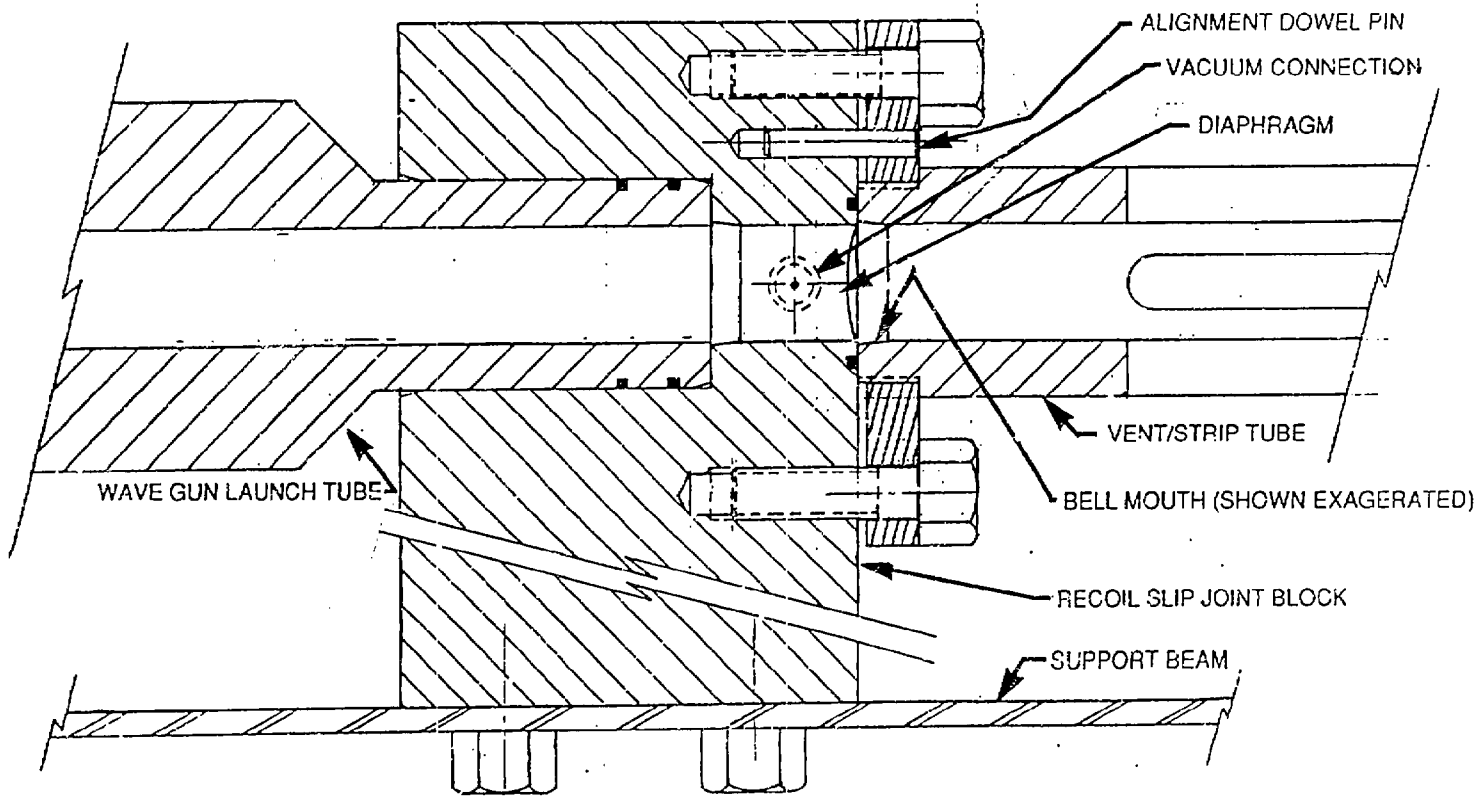

Figure 5-3 Recoil Slip Joint Detail

The helium driver gas will still be at a high pressure as it forces the projectile and sabot into the driver gas venting section. This high pressure must be reduced by venting for the axial gasdynamic sabot separator to work. The axial gasdynamic sabot separator section consists of a straight piece of pipe filled with air at atmospheric pressure. The sabot and projectile will force a normal shock to form in front of them as they pass through this section. The pressure behind the shock and in front of the projectile will be substantially higher than the pressure behind the sabot. This compressed air will not be constrained by the projectile so it will move past and surround the projectile while not slowing it. The pressure difference between the front and rear of the sabot will slow it as it moves down the sabot stripping section. At the end of the sabot stripping section, the stripping gas will be vented. The stripping gas must be vented so that it will not force a shock to form in the test section and disrupt the flow.

The following sections will discuss how the helium driver gas and gasdynamic sabot separation section gas will be vented and how the sabot will be separated from the projectile.

5.3.1 Gas Venting

The gas will be vented through slots in the side of the tube wall in the two 0.5m venting sections as shown in Figure 5-4. The vents will represent 50 percent of the surface area of the pipe in the vent sections. A first-order analysis of the venting is made by assuming that the gas flowing out of the vents is choked, the gas remaining in the tube expands isentropically, and the gas flows out the vent for a time equal to its residence time in the vent section. The integral form of the continuity equation

$$\frac{\partial}{\partial t}\int\int\int_{c.v.} \rho \, dv + \int\int_{s} \rho \vec{V} \cdot \vec{dA} = 0 \qquad (5.1)$$

along with the isentropic relations is used to derive Equation 5.2, which gives the pressure in the vent section as a function of time, geometry, and the initial conditions:

$$P_{vented} = P_{initial}\left[\beta t + 1\right]^{\frac{-2\gamma}{\gamma-1}} \qquad (5.2)$$

where

$$\beta = \frac{A_{vent}}{Vol_{stripper\ section}} \frac{\gamma-1}{2}\left(\frac{2}{\gamma+1}\right)^{\frac{1}{\gamma-1}} \sqrt{\frac{2\gamma}{\gamma+1} R T_{initial}} \qquad (5.3)$$

For the helium driver gas venting section, $T_{initial} = 300\,\mathrm{K}$, $P_{initial} = 200\,\mathrm{atm}$, and the residence time in the venting section is $\frac{.5\ \mathrm{m}}{2500\ \mathrm{m/sec}} = 200\,\mu\mathrm{sec}$.

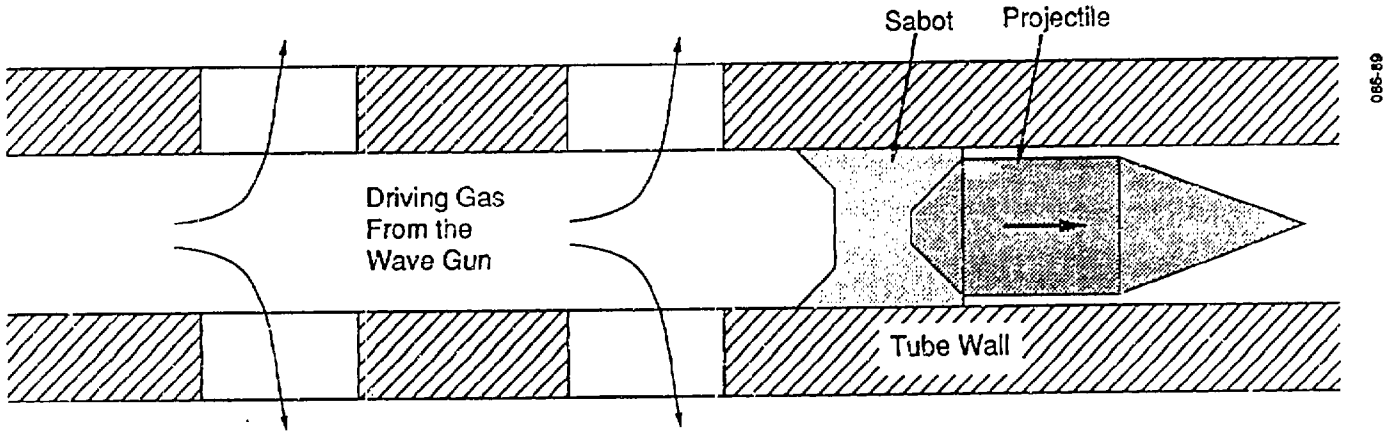

Figure 5-4 Gas Venting

This gives a pressure of 0.36 atm behind the sabot as it enters the sabot stripping section. A pressure of at least $\left(\frac{2}{\gamma+1}\right)^{\frac{-\gamma}{\gamma-1}}$ atm is required in the gas for the flow to be choked. Therefore, Equation 5.2 is not valid below this value and the pressure will actually be somewhere between 1 atm and $\left(\frac{2}{\gamma+1}\right)^{\frac{-\gamma}{\gamma-1}}$ atm. For helium, $\left(\frac{2}{\gamma+1}\right)^{\frac{-\gamma}{\gamma-1}}$ atm equals 2.05 atm which is more than acceptable for the entry into the sabot separator section.

5.3.2 Sabot Separation Section

The sabot will be separated from the projectile by an axial gasdynamic sabot separator. The projectile and sabot will enter this separator at a velocity of 2.5 km/sec which gives a Mach number of 7.2 in air at 300 K. As the projectile and sabot move through the sabot separation section, a shock wave will precede them as shown in Figure 5-5. This separation technique has been analyzed in detail by Swift and Strange [5.4]. Their paper gives the pressure ratio across this shock as

$$\frac{P_{shock}}{P_{initial}} = 1 + \frac{\gamma M}{4}\left[(\gamma+1)M + \sqrt{(\gamma+1)^2 M^2 + 16}\ \right] \tag{5.4}$$

where M is the Mach number for the sabot's velocity in the undisturbed fluid before the shock. The separation between the sabot and the projectile is given to first order by

$$\delta x = \frac{1}{2}\frac{\Delta P\, A_{bore}}{m_{sabot}}\frac{L^2}{V^2} \tag{5.5}$$

where ΔP is the pressure across the sabot. ΔP is calculated by using Equation 5.4 to calculate the pressure in front of the sabot and the maximum of the pressure calculated from Equation 5.2 or $\left(\frac{2}{\gamma+1}\right)^{\frac{-\gamma}{\gamma-1}}$ atm for the pressure behind the sabot. Equation 5.5 over-predicts the separation distance because the pressure ratio across the shock decreases as the sabot travels down the tube. Equation 5.4 shows that the pressure ratio across the shock decreases with decreasing Mach number, which is the reason the pressure ratio decreases as the projectile slows. Swift and Strange [5.4] have performed an iterative analysis that accounts for the changing pressure ratio. Their analysis shows that Equation 5.5 over-predicts the separation by 3 to 4 percent. Therefore Equation 5.5 can be rewritten as

$$\delta x = \frac{.96}{2}\frac{\Delta P\, A_{bore}}{m_{sabot}}\frac{L^2}{V^2} \tag{5.6}$$

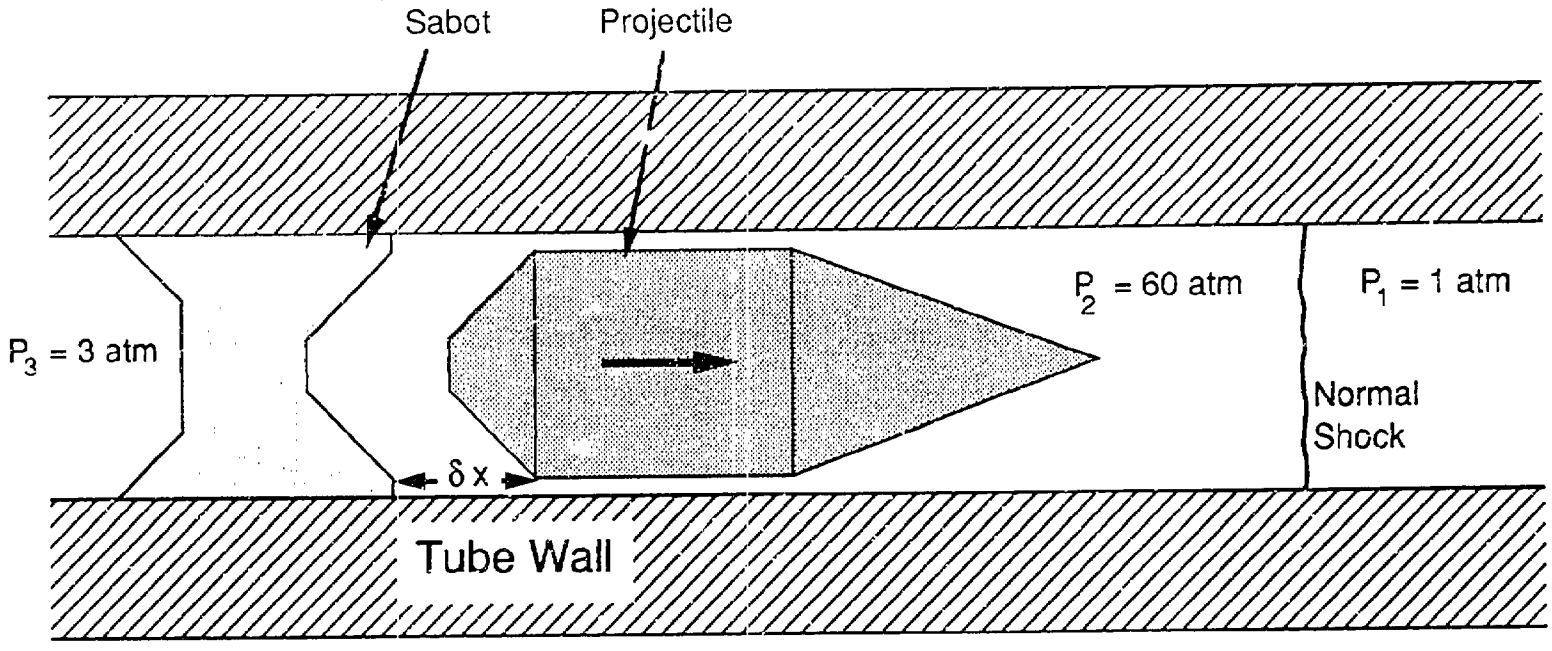

Figure 5-5 Sabot Separation

The velocity of the sabot at the end of the sabot separator section can be approximated by

$$V_{sabot_{exit}} = V_{sabot_{inlet}} - .96 \frac{\Delta P A_{bore}}{m_{sabot}} \frac{L}{V} \tag{5.7}$$

From Shapiro [5.3], the temperature of the gas between the shock and the sabot is given by the Rankine-Hugoniot equation as

$$\frac{T_{shock}}{T_{initial}} = \frac{\frac{P_{shock}}{P_{initial}}\left[1 + \left(\frac{\gamma - 1}{\gamma + 1}\right)\frac{P_{shock}}{P_{initial}}\right]}{\frac{P_{shock}}{P_{initial}} + \frac{\gamma - 1}{\gamma + 1}} \tag{5.8}$$

where the pressure ratio is taken from Equation 5.4. The distance between the shock and the sabot is given by

$$\delta x_{shock} = \frac{\rho_{initial}}{\rho_{shock}} L_{Separator} \tag{5.9}$$

where from Shapiro [5.3],

$$\frac{\rho_{initial}}{\rho_{shock}} = \frac{\frac{P_{shock}}{P_{initial}} + \frac{\gamma + 1}{\gamma - 1}}{\left(\frac{\gamma + 1}{\gamma - 1}\right)\frac{P_{shock}}{P_{initial}} + 1} \tag{5.10}$$

Using Equations 5.6 and 5.9, the conditions at the end of the 2m-long axial gasdynamic sabot separator section can now be calculated. For a pressure of $\left(\frac{2}{\gamma+1}\right)^{\frac{-\gamma}{\gamma-1}}$ atm behind the sabot as it exits the helium driver gas venting section and T = 300 K and P = 1 atm in the sabot separator section the distance between a 20g sabot and the 50g projectile will be 95 mm. The distance between the shock and the sabot is calculated to be 360 mm using the velocity at the end of the separator section as given by Equation 5.7 and Equation 5.9. The temperature behind the shock will be 4750 K at the entrance and 3970 K at the exit of the sabot separator section. Equations 5.2 to 5.3 give a pressure of 0.038 atm at the end of the 0.5m-long axial sabot stripping gas venting section. The pressure will not drop below 1 atm but should drop to or below $\left(\frac{2}{\gamma+1}\right)^{\frac{-\gamma}{\gamma-1}}$ atm which is 1.9 atm for air.

5.3.3 Venting/Stripping Tube Construction

This component will be built using commercially available alloy steel tubing. A likely candidate is stock tubing of 4130 steel cold drawn and stress relieved with an outside diameter

(O.D.) of 60.3 mm (2.38 inches) by 28.6 mm (1.12 inch) inside diameter (I.D.) honed to the desired bore of 30.0 mm. This heavy wall section is considerably stronger than required from the standpoint of resisting the internal pressure, but we have selected the thick wall to provide rigidity and sufficient stock for mounting pressure gages and other diagnostic components. A single section of the tube will form this component. The venting slits at each end of the tube will be made by milling slots 12 mm (0.47 inch) in diameter through the wall in four places equally spaced around the circumference to provide venting area equal to half of the tube surface area. There will be two sets of these slots at each end of the tube each about 200 mm (8 inches) long separated by about 50 mm (2 inches) of unperforated tube. Figure 5-6 illustrates the construction of this component.

5.4 OBLIQUE DETONATION WAVE TEST SECTION

The same basic tubing stock will be used for fabricating this unit as was described for the dump/strip section, i.e., 60.3 mm O.D. by 28.6 mm I.D. honed out to 30.0 mm I.D. The full test section will consist of four individual identical sections each 2.5m long. Each section will be tapped for mounting one or more pressure transducers.

The joints between the individual sections of the test section will utilize universal flanged connections that will also serve to mount diaphragms and to connect the ODW test section to the strip/dump section. A schematic representation of one of these joints is shown in Figure 5-7. The method used to prepare and align the joints is a simplified version of one described by Swift and Strange [5.5]. The flanges are manufactured in upstream/downstream pairs. The alignment of each pair is controlled by three asymmetrically placed dowel pins; the asymmetry is used to preclude misalignment by rotation about the axis to an improper orientation. Location of the pins to ensure alignment is achieved in the following manner. The flanges are first threaded onto the ends of the tube section until they stop against a shoulder. The threads are sealed by the use of a high-strength cyanoacrylate thread-sealing cement to preclude accidental loss of alignment. A specialized and precisely manufactured drilling jig with a bolt circle identical to that of the flanges is loosely bolted to one of the flanges. The jig has a central hole of precisely the same diameter as the bore and three hardened precision drilling jigs representing the three dowel pin locations. The central hole and the bore are then precisely aligned by inserting an aligning tool consisting of a hydraulically expanded tubing into the assembly and expanding it to precisely align the two bores. The clamping bolts are then securely clamped and holes are drilled and reamed to accept the pins. The drilling fixture is then removed, reversed and bolted to the mating flange. The alignment process is repeated and matching holes are drilled and reamed in the mating flange. The

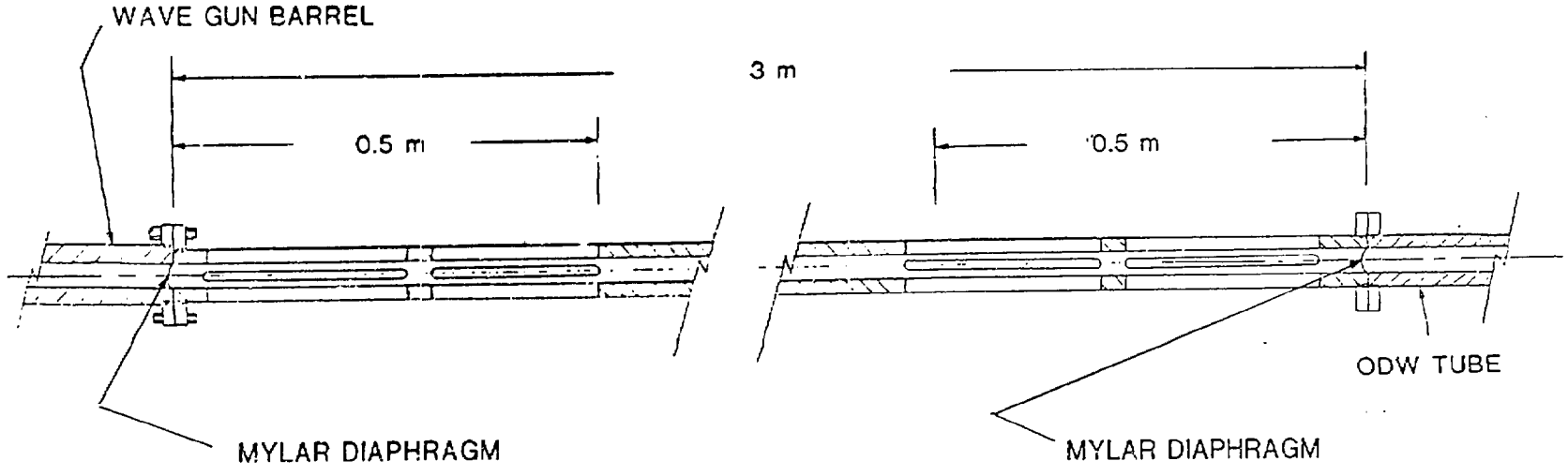

Figure 5-6 Gas Vent/Sabot Separation Section

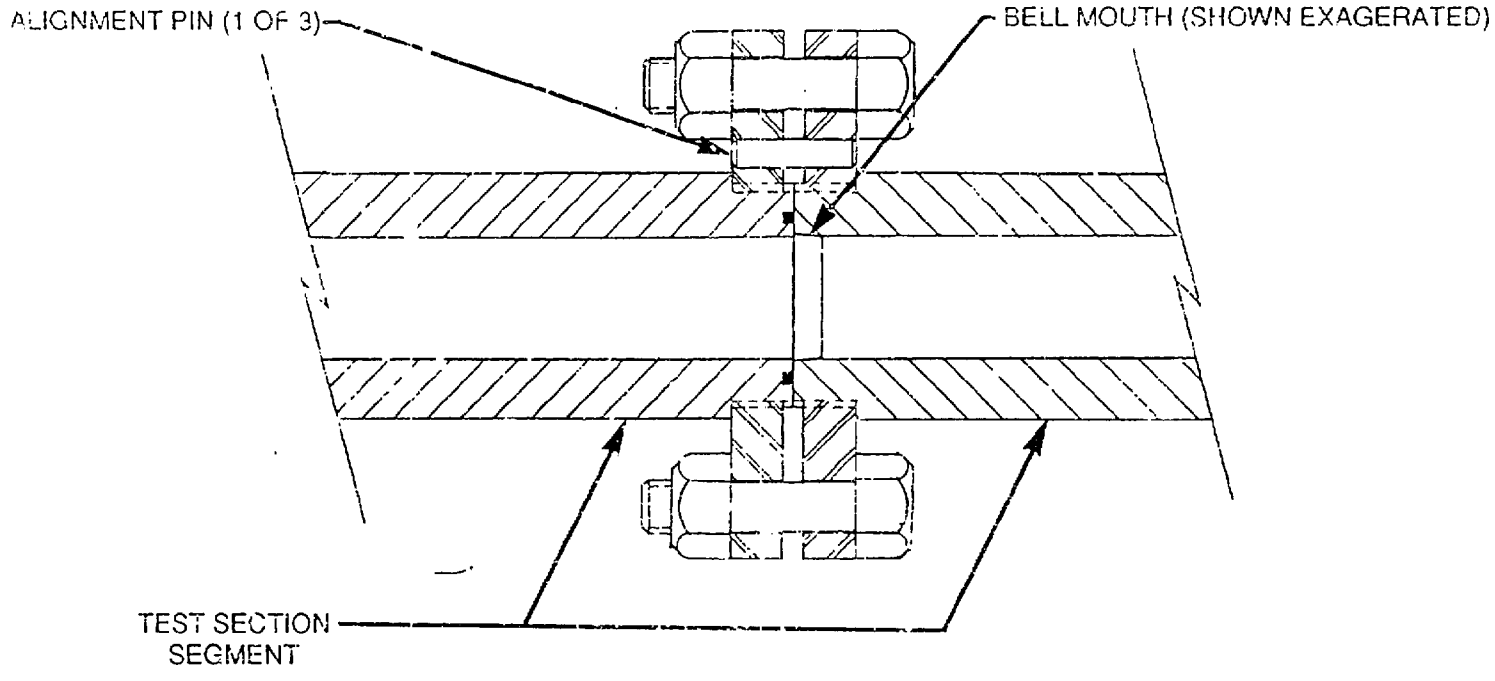

Figure 5-7 ODW Test Section Joint Detail

quality and reproducibility of the alignment that can be produced by this technique is estimated to be about 25 μm. Any residual misalignment within this range is accommodated by honing a slight "bell mouth" at the entrance of the downstream portion of each joint. This method will preclude the possibility of the projectile encountering a step as it proceeds across the joint. Such encounters must be strictly avoided as they will always produce a phenomenon known as "gouging" at this velocity [5.6, 5.7]. The bell mouth technique has been shown to produce satisfactory results in our own laboratory as well as in others [5.5].

Each of the 2.5m-long units of the test section will have two ports for connecting to the gas fill system. Each of these will consist of a pipe tapped port for accepting a compression type tubing fitting and a very small (about 1 mm) hole drilled through to the bore. This connecting hole will be oriented so as to be neither normal to the bore axis nor directed toward it to promote a helical swirl pattern as the section is filled with gas. We have examined the question of achieving a homogeneous gas mixture presuming the introduction of gas at discrete locations along the length of the tube. The basis for the analysis is that of binary diffusion of gasses initially distinct and is derived from a discussion by Bird, Stewart and Lightfoot [5.8]. They give the diffusion coefficient of a binary gas system as:

$$D_{AB}=0.0018583\frac{\sqrt{T^3\left(\frac{1}{M_A}+\frac{1}{M_B}\right)}}{P\sigma_{AB}^2\Omega_{AB}} \qquad (5.11)$$

where: T is the temperature in degrees Kelvin,

M_A and M_B are the molecular weights of the gases,

P is the pressure in atmospheres,

σ_{AB} is the mean molecular diameter in angstrom units, and

Ω_{AB} is an empirical constant related to the collision frequency.

For air and hydrogen at 298K and 10 atm, the diffusion coefficient evaluates to 0.077 cm^2/s. The time for a binary gas system to diffuse to a given degree of uniformity is given by:

$$t = -(\ln F)\frac{L^2}{D\pi^2} \qquad (5.12)$$

where: F is the residual nonuniformity (taken as 0.01 for this calculation),

D is the diffusion coefficient as calculated by eq. 5.11, and

L is the length of the gas column.

We guess that the characteristic unmixed length of gases after filling the column by the described technique will be 10 cm or less. Using this value for L we compute a time of about 600 sec for the diffusion process to give a 99 percent uniformity to the mix.

5.5 GAS PRESSURE INTERFACES

In Section 5.3 mention was made of pressure interfaces through which the projectile must pass in the course of the experiment. In a Stage I test there is one of these interfaces between the vent section and the ODW test section. For Stage II tests another interface will be needed between the vent/strip section and the evacuated Wave Gun barrel.

By far the simplest and most direct method for providing these separations is by using a plastic diaphragm clamped in a special fixture such as shown in Figure 5.3. The projectile simply pierces the diaphragm when it reaches the station. There is some concern that collision of the projectile with even a very thin plastic film may cause some distortion of the tip of the conical nose section. The nature of the shock structure is highly dependent on the configuration of the tip, so even a minor distortion can have a profound effect on results. For this reason we have formulated a conceptual design for a fast acting valve that will open a clear path for the projectile in an acceptably short time. It is expected that the diaphragm separation will prove to be adequate, but it is also prudent to have a backup approach.

A conceptual design of the valve is shown in Figure 5-8. The driving force will be provided by a pneumatic cylinder precharged to a high pressure with nitrogen. A connecting rod in tension is connected to a shutter strip that passes through a slide sandwiched between the ends of the two tube sections. Gas sealing is provided by lubricated "O" rings. The strip is restrained by an explosive bolt which, when actuated, releases the valving strip.

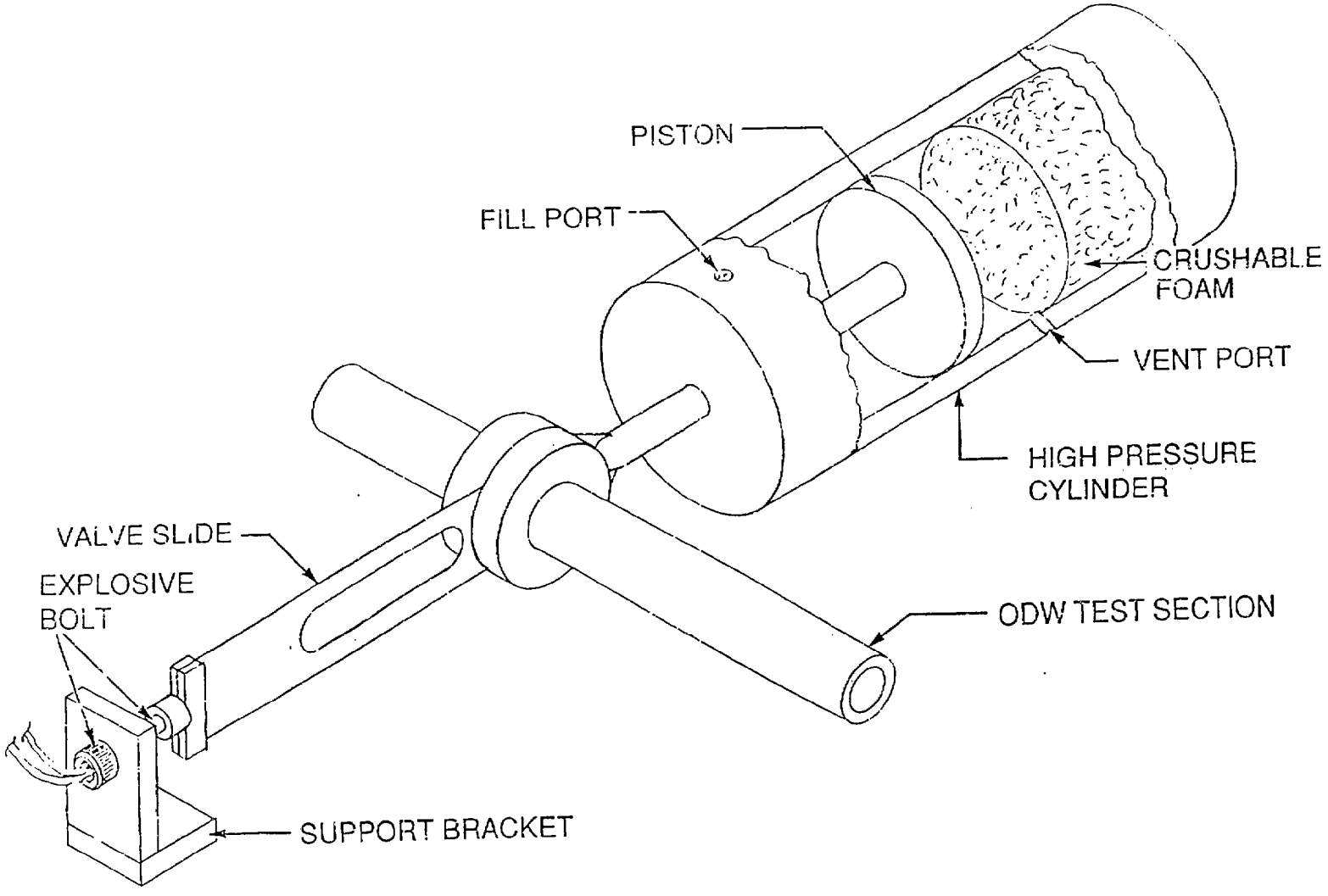

Figure 5-8 Conceptual Design of Fast Acting Valve

A preliminary estimate indicates that a 10 cm diameter cylinder charged to 2000 psi can move a slide mechanism through a distance of 9 cm in 1 msec. In this time span, a rarefaction wave will move into the higher pressure region a distance of about 30 cm. From this point on, the projectile will fly through still gas at initial conditions. Achievement of proper synchronism between the actuation of the valve and the flight of the projectile will require careful calibration of the function time of the various components and a sophisticated timing circuit to control their initiation. It is hoped and expected that the simpler, more direct diaphragm separation technique will serve the required function well, but we are confident that the fast acting valve can be successfully applied if required.

5.6 STOPPER ASSEMBLY

As its name implies, the function of this element is to provide a means for bringing the projectile to a stop in a relatively short distance so that it can be located and examined for evidence as to its experience during flight. We will not attempt to make the recovery "soft" enough to permit reuse of the projectile, but it will be very valuable if damage is sufficiently limited to permit an estimate of whether or not surface melting or other forms of ablation occurred during the test. The requirements for this component have not been fully established at this time, but we expect that the unit will consist of an open framework that will hold weak walls in position to contain quantities of bulk material in three or four bins of increasing density. Such materials as sawdust, sawdust mixed with sand, and sand are under consideration as candidates. The details of the design of this element will be modified as a result of empirical observation in the course of the experimental program.

5.7 GENERAL ASSEMBLY

The unit that will provide for support and alignment of all of the elements will be a wide-flange structural beam as shown in Figure 5.1. This beam will, in turn, be supported by sections of pipe attached to a support slab and to the beam by standard flanges. The Wave Gun is already provided with a mount designed to support the gun on a beam with a flange that is 8.5 in wide. For simplicity, a beam with this width will be used. The full length of the test assembly will be about 20 m. Some additional length of beam will be needed to accommodate recoil, recoil absorbing apparatus, the external velocity measuring switch assembly and some room for axial movement to accommodate assembly and disassembly. The full beam length requirement will be about 25 meters or about 80 ft. The maximum length of beam that can be obtained and delivered to the test site is not known, but clearly at least two, and more probably four, beam sections will be required. The beam support will need to be designed so that there

is a mechanism for supporting the joints between sections and aligning them with precision both laterally and in elevation.

The tubing sections themselves will be supported on rollers and frames that are constructed entirely of commercially available units that are part of a modular construction system known as "Unistrut." This system offers a rich variety of components that can serve a selection of functions and are quite reasonably priced. Each of the support structures will include a roller device that constrains the tube to a fixed transverse position but permits free axial motion. Such flexibility is essential to permit efficient disassembly, inspection, refurbishment and reassembly of the apparatus. The joining techniques that are inherent to the modular system permit all necessary adjustments without the fabrication of any special parts. An optical alignment telescope will be used to align each of the roller assemblies with the range centerline.

REFERENCES

[5.1] Dahm, T.J. and Randall, D.S.; "The Wave Gun Concept for a Hypervelocity Rapid-Fire Weapon." Presented at the 1984 JANNAF Propulsion Meeting, New Orleans, LA, February 1984.

[5.2] Dahm, T.J., Randall, D.S. and Sullivan, J.D.; "Wave Gun Performance through Evaluation and Analysis, Volume I, Summary of Program and Results." Astron Research and Engineering Report No. FR-7045-01, June 1987.

[5.3] Shapiro, Ascher H., The Dynamics and Thermodynamics of Compressible Fluid Flow, Volume I, The Ronald Press Company, New York, 1953.

[5.4] Swift, H.F., and Strange, D.E.; "Sabot Discard Technology," 38th Meeting of the Aeroballistic Range Association, Tokyo, Japan, October 1987.

[5.5] Swift, H.F. and Strange, D.E., "Coupling Tube Segments for High-Performance Launchers," 36th Meeting of the Aeroballistic Range Association, San Antonio, TX, October 1985.

[5.6] Barker, L.M., Trucano, T.G. and Susoeff, A.R., "Gun Barrel Gouging by Sliding Metal Contact at Very High Velocities." 39th Meeting of the Aeroballistic Range Association, Albuquerque, NM, October 1988.

[5.7] Personal Communication with L.M. Barker, Sandia National Laboratories, Albuquerque, NM, January 1989.

[5.8] Bird, R.B., Stuart, W.E. and Lightfoot, E.N., Transport Phenomena, John Wiley and Sons, Inc., 1960.

SECTION 6. DIAGNOSTIC METHODS AND INSTRUMENTATION

The objectives of the diagnostic effort are to identify, confirm and analyze the formation and stability of an oblique detonation wave. We have designed a variety of diagnostic techniques by which the success in achieving this goal can be evaluated. In this section we discuss an overview of diagnostic methods to be employed for specific measurements in Section 6.1. More detailed discussions of each of the diagnostic techniques are given in Sections 6.2, 6.3 and 6.4.

6.1 OVERVIEW OF DIAGNOSTIC METHODS

In order to obtain data for in-depth characterization of the ODW phenomena the following quantities will be measured:

- Projectile velocity
- Structure of the shock waves in the region surrounding the projectile
- Gas pressure history at the wall of the ODW tube
- Gas temperature in the various thermodynamic regions of the event
- Optical signatures of various chemical species as evidenced by spectral emission lines

In addition to the measurements listed above there are others that will be included as important design qualification tests:

- Ability of the projectile to survive the Wave Gun acceleration process
- Surface temperature of the projectile body behind the oblique detonation

The environments for the diagnostic measurements and the instrumentation are extreme: the projectile geometry is small and the velocity is high; the transit time of the entire event is small even though the test section has a substantial length (10 meters) due to the extremely high velocity of the projectile.

Another consequence of the nature of the ODW event is the extreme rapidity with which the environment changes. Pressures and temperatures increase virtually instantaneously as the reactant gases cross the detonation boundary. Resolution of the nature and location of this singular event requires transducers

with excellent time response. It also requires recording devices with similar time resolution and with absolute time correlation between the recording channels.

To understand the oblique detonation wave phenomena it is essential to obtain two-dimensional optical visualization. The measurement in this instance is complicated by the fact that the internal geometry of the test section must be maintained and that the event must be enclosed within a pressure vessel of considerable strength. We plan to utilize an approach that minimizes the complications imposed by these challenges. The approach is discussed in Section 6.4.

The following paragraphs contain more detail on each of the techniques to be applied for the measurement of each of the quantities mentioned above.

Projectile Velocity

We will measure projectile velocity by determinig the time of arrival of the projectile at a series of closely spaced points. Arrival will be detected by the eclipsing of a narrow beam of light crossing the tube along a diameter. This technique is covered in detail in Section 6.2.

We will also consider the use of a microwave interferometer to provide a continuous record of velocity as a function of time. Such techniques have been widely used in ballistic work [6.1]. The technique uses the test section tubing as a waveguide and the projectile as a moving reflector to generate a continuous history of velocity versus time. This technique could be especially useful if there appears to be any instability in the ODW under certain conditions.

As a backup means of measuring the velocity after the projectile has exited the ODW test section we will install a set of four switches that will be actuated by contact of the projectile. The switches will be placed just downstream of the tube exit.

Shock Structure Visualization

Two-dimensional photographs of the event will be made using a technique known as synchroballistic photography coupled with shadowgraphic illumination. The recording instrument will be an electronically controlled camera referred to as an image converter camera. The methodology and the instrumentation is more fully described in Section 6.4.

Gas Pressure Measurements

Time resolved pressure measurements will be made at several points within the Wave Gun structure for confirmation of proper function. Similar measurements will be made at several points along the ODW test section to record the nature of the pressure field associated with the passage of the projectile. The pressure records will also provide confirmation of the arrival time measurements made using the fiberoptic detectors.

Gas Temperature Measurements

The methodology for determining the time-resolved gas temperature profile will be the use of spectrally discrete measurements of the gray body radiation from the gas behind the detonation. An instrument is already in our inventory that is ideally suited to make such observations simultaneously at several wavelengths. Light is conducted into the instrument through a large diameter optical fiber that is divided into several individual fibers each of which becomes a separate channel which can be individually filtered and recorded. A full description of the instrument and of the proposed application is given in Section 6.3.

Signatures of Significant Chemical Species

The apparatus to be used in these measurements will be the same as for the gas temperature measurements. Refer to Section 6.3 for a more complete description of the instrument and its application to these measurements. We give particular attention to two emission lines: the line characteristic of the hydroxyl radical produced in hydrogen/oxygen combustion; and the lines representing any of several molecules in the family of oxides of nitrogen (NO_x).

Projectile Structural Integrity and Sabot Separation

It will be very important to determine that the projectile has maintained its structural integrity through the process of acceleration by the Wave Gun. As mentioned in Section 3, the acceleration loads are extreme and the design includes delicate internal structure. Despite careful design and analysis, the success of the projectile in surviving the loadings must be confirmed. In the initial experiment or experiments the test apparatus will be configured with only the Wave Gun and the vent/strip assembly installed. A flash x-ray system will be be positioned such that an exposure will be made just after the projectile exits the tube. This will reveal both the condition of the projectile and the separation of the sabot.

Projectile Body Temperature

We will obtain measurements of the temperature of the surface of the projectile body using the multicolor optical pyrometer mentioned in the gas temperature measurements section and described in Section 6.3. The projectile body surface temperature reflects the gas temperature and the heat transfer phenomena in the ODW region. Success of the measurement will depend on the degree of transparency of the gases in the annulus that separates the projectile body from the tube wall. The analysis of the optical thickness will need to be addressed in more detail to assess the prospects for success in this measurement.

6.2 TIME OF ARRIVAL MEASUREMENTS

Arrival detectors will be placed at regularly spaced intervals along the Wave Gun launch tube, the vent/strip assembly and the ODW test section. The detector stations will consist of two diametrically opposed optical fibers inserted through the wall of the tube and secured with a compression-type fitting as shown in Figure 6-1. A laser diode will produce light continuously at a near infrared wavelength. A bundle of fibers will be optically coupled to the diode so that each fiber carries a steady optical flux. Another fiber will be placed directly opposite each of these input fibers. These receiver fibers will transmit the light to a phototransistor unique to the particular station. This photodetector will be in the "on" state until the transmitted light is obscured by arrival of the projectile. The outputs of all of these detectors will be routed to a conditioning/multiplexing circuit which will form a pulse with a width uniquely characteristic of the station at which the arrival was detected. The resulting pulse train will be recorded on a single channel sampling the input at a 10 MHz rate. About twenty such stations will be installed. This series of time/distance data points will provide an excellent record of the velocity history of the projectile.

6.3 DYNAMIC PRESSURE MEASUREMENTS

A very important part of our diagnostic scheme will be the use of piezoelectric pressure transducers. The reliance on this method as an important technique stems, in large part, from our considerable experience and success in using these devices in diagnosing the function of the Wave Gun during development phases on this device from 1983 to 1988. It seem sensible to use the devices to monitor the oblique detonation wave because of our familiarity with the gages, and because we have a substantial inventory of them. We also have instruments ideally suited to

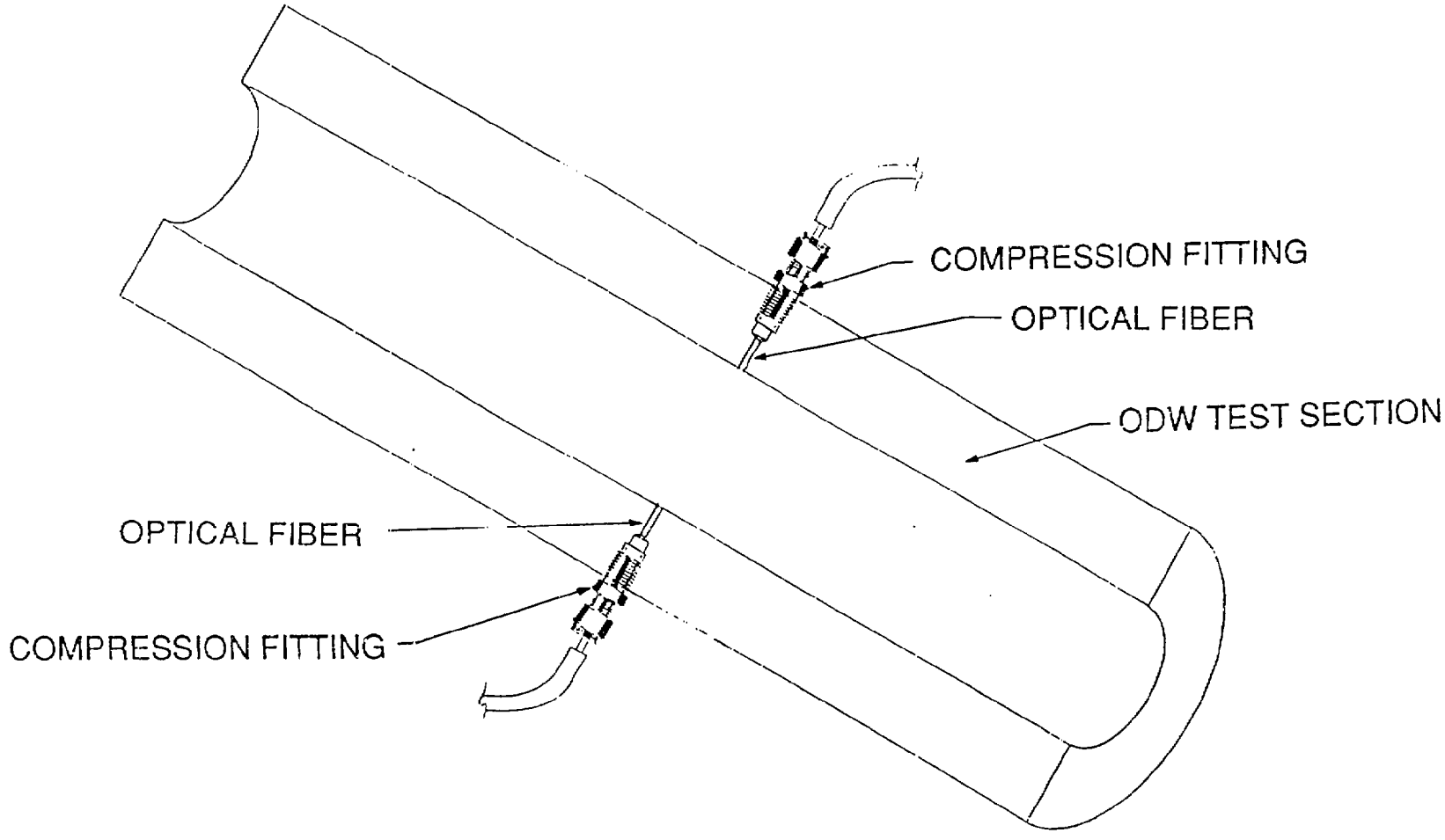

Figure 6-1 Time of Arrival Probe

record the outputs in digital form. These gages will be used to monitor Wave Gun function and the ODW phenomena during the course of this program. Figure 6-2 illustrates a typical gage installation.

We believe that interpretation of pressure records pertaining to the projectile velocity can in themselves be definitive as to the presence or absence of an ODW. First, if a stable ODW is developed, the projectile will accelerate. An acceleration of more than 9800 g (96 km/s^2) will be experienced for the sample case we have calculated. For the expected residence time of 3.7 ms in the test section, the velocity will increase by about 358 m/s. This represents an increase of about 14 percent, an amount that will be very clearly resolvable. The sampling interval of the waveform recorder to be used is 2 μs and the decrease in transit time for a 2.5 m interval will be about 67 μs, many times the minimum time resolution of the system. On the other hand, the absence of a detonation wave will result in the projectile decelerating significantly as a result of the substantial pressure (about 70 atm) behind the bow shock impressed on the face of the projectile. Thus the projectile arrival time inferred by the pressure signal should, of itself, be an indication of the presence (or absence) of either an ODW or shock-induced combustion.

The amplitude of the pressure rise at the time of shock arrival comprises another definitive indication of ODW presence. If the reflected shock achieves detonation, the pressure should rise virtually instantaneously to about 600 atm, and remain essentially constant until passage of the confined annulus region. In the absence of a detonation, however, the immediate pressure increase at shock arrival will be only that of a reflected, non-reactive shock wave, about 275 atm. If little or no combustion occurs, the pressure will remain essentially constant until passage of the annular region, followed by a rapid decrease and quite obviously accompanied by deceleration of the projectile. If shock-induced combustion results, the static pressure will rise continuously along the annulus. The maximum pressure which will be achieved prior to expansion over the projectile afterbody depends on the degree of completion of the combustion reaction, can approach or even exceed the 600 atm ODW peak pressure, and consequently may result in thrust comparable to that of oblique detonation. Consequently, measurement of thrust and/or acceleration does not constitute a suitable discriminant for whether ODW or shock-induced combustion occurs. However, the measurement of pressure-time history during passage of the projectile constitutes a clear diagnostic method for discriminating between shock-induced combustion and oblique detonation.

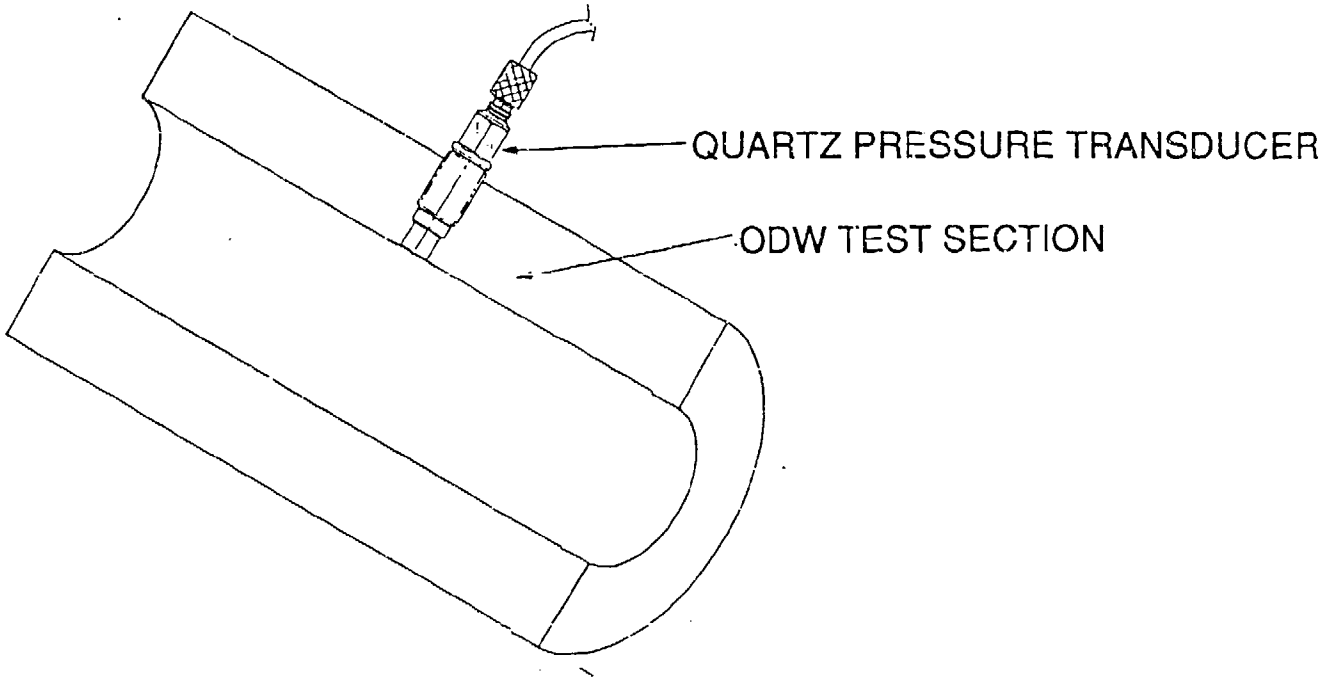

Figure 6-2 Typical Pressure Transducer Installation

6.4 SPECTRALLY RESOLVED OPTICAL OBSERVATIONS

The rapid combustion of hydrogen in air will produce many chemical species, some of them transient. This will be especially true if the combustion is in the form of a detonation with the associated extremely large values of temperature and pressure inherent in this process. Many of these species will radiate in some characteristic emission line. One of these lines is representative of the formation of the hydroxyl (OH) radical and should always be present in hydrogen/oxygen combustion. When nitrogen is present as in air, quantities of various oxides of nitrogen (NO_x) should be formed and radiate with their own characteristic wavelengths. All of these emission lines will be broadened in conditions of high pressure. We have not evaluated at this time whether this line broadening will be sufficiently extreme to obscure the desired results under the conditions expected in this experiment. The projectile body heated to high temperatures by the thermodynamic processes will radiate a broadband radiation with a spectral content dependent on their temperature and emissivity. Instrumentation will be provided for investigating each of these phenomena so as to permit interpretation of the resulting data as to its implications regarding the presence and nature of the combustion reactions that might be present.

The basic instrument to be used for all of these measurements is one that has been constructed originally as an multi-color optical pyrometer. Figure 6-3 is a photograph of the interior of the instrument. Optical flux enters the enclosure through a large (1.5 mm) optical fiber which is terminated just inside. The output end of the fiber is imaged on a cluster of seven smaller fibers each of which carries the full spectral content of the input. Each individual fiber then passes to a station at which it terminates at another pair of lenses between which an interference filter is placed. The spectrally limited output of the station is imaged on a photodiode the output of which is conditioned so that it will be suitable for recording.

The optical flux passes through several materials each with its own spectral transmissivity characteristics and through several lenses which will have certain residual chromatic aberrations. For this reason, it will be necessary to calibrate the instrument at each wavelength being monitored by exposure of the system to an optical source with known spectral content.

As presently configured, the instrument monitors four wavelengths chosen for their ability to define the temperature of resistively heated carbon. These wavelengths are 350, 410, 470 and 650 nm. It may be desirable to substitute filters passing